

Bernhard Gerl

A flexible, low-cost solar simulator for automated CPV cell and
module testing

Master of Science

Mechanical Engineering

Graz University of Technology

Faculty of Mechanical Engineering and Economic Sciences

Institute of Electrical Measurement and Measurement Signal Processing

Director:

Univ.-Prof. Dipl.-Ing. Dr.techn. Georg Brasseur

Supervisors:

Ass.Prof. Priv.-Doz. Dipl.-Ing. Dr.techn. Hannes Wegleiter

Dipl.-Ing. Dr.techn. Armin Buchroithner

Graz, 12 July 2018

Acknowledgement

An dieser Stelle möchte ich mich bei all jenen bedanken, welche mich bei dieser Diplomarbeit unterstützt, mir weitergeholfen und dadurch einen Beitrag zum Gelingen dieser Arbeit geleistet haben.

Ganz besonders bedanken möchte ich mich bei Dipl.-Ing. Richard the Rock Felsberger und Dr.techn. Armin Buchroithner für die Unterstützung bei der Erstellung meiner Diplomarbeit. Weiters möchte ich auch Herrn Stefan Veitsberger danken, der stets eine große Unterstützung bei den praktischen Arbeiten war. Vielen Dank für die hilfreichen Anregungen, sowie die Chance diese Arbeit zu verfassen.

Zudem möchte ich meinen Eltern danken, die mir mein Studium ermöglichen und mich stets auch moralisch immer unterstützen.

Herzlich bedanken möchte ich mich auch bei meiner nun ehemaligen Mitbewohnerin Anna, die mir mit ihren Kenntnissen stets zur Seite gestanden ist und die englische Sprache mehr liebt als ich es je tun werde.

Statutory Declaration

Ich erkläre an Eides statt, dass ich die vorliegende Arbeit selbstständig verfasst, andere als die angegebenen Quellen/Hilfsmittel nicht benutzt, und die den benutzten Quellen wörtlich und inhaltlich entnommenen Stellen als solche kenntlich gemacht habe.

Graz, am

(Unterschrift)

I declare that I have authored this thesis independently, that I have not used other than the declared sources/resources, and I have explicitly marked all material which has been quoted either literally or by content from used sources.

.....

(Date)

(Signature)

Abstract

Within the Nexus of Electricity and Water Supply for Urban Needs (NEWSUN) project, which deals with the thermal desalination of seawater, a solar simulator was needed for the simulation of concentrated solar radiation. These simulators are not available as an off-the-shelf product, which made it necessary to design and build this test rig. Therefore, this thesis deals with the analysis of already existing High Flux Solar Simulators, as well as with the design and testing of a custom model for the Institute of Electrical Measurement and Signal Processing. Special emphasis was placed on the minimum requirements, which are a concentration factor of 60 times the sun and a pillbox distribution of the radiation intensity at the test target. Another aspect that was examined in detail during the work was the possibility of cost reduction for the most expensive components, which were identified as the reflector, the lamps and their ballasts. Low-cost alternatives were examined and selected, which reduced the overall costs of the simulator significantly. Furthermore, the influence of different reflective materials, which change the light spectrum of the lamps due to their reflective properties, is assessed.

Kurzfassung

Im Rahmen des NEWSUN Projekts, welches sich mit der thermischen Entsalzung von Meerwasser beschäftigt wurde ein Solar Simulator für Anwendungen mit konzentrierter Sonnenenergie benötigt. Diese Simulatoren sind jedoch nicht als fertige Produkt zu kaufen, was es notwendig machte diesen Prüfstand selbst zu konstruieren und zu bauen. Die vorliegende Arbeit befasst sich mit der Analyse von bereits am Markt befindlichen Hochleistungsstrahlern, sowie mit der Konstruktion und dem Bau eines maßgeschneiderten Solarsimulators für das Institut für Elektrische Messtechnik und Messsignalverarbeitung. Dabei wurde besonderer Wert auf die Mindestanforderung von 60-facher Sonnenkonzentration und eine gleichmäßige Verteilung der Strahlungsintensität auf der Testebene gelegt. Ein weiterer Punkt der im Rahmen der Arbeit genauer untersucht wurde war die Möglichkeit der Kostenreduktion für die teuersten Bauteile, welche als der Reflektor, die Lampen und deren Vorschaltgeräte identifiziert wurden. Kostengünstige Alternativen wurden dabei genauer untersucht und ausgewählt. Weiters wird in der Arbeit der Einfluss von verschiedenen reflektierenden Materialien, welche das Lichtspektrum der Lampen aufgrund deren Reflexionseigenschaften verändern, erläutert.

Contents

- Acknowledgement..... i
- Statutory Declaration..... ii
- Abstract iii
- Kurzfassung..... iii
- Contents..... iv
- Structure of the thesis 7
- 1 Introduction and Motivation..... 8
 - 1.1 The “Nexus of Electricity and Water Supply for Urban Needs” (NEWSUN) project..... 8
 - 1.1.1 Solar irradiance, water scarcity and population density 10
 - 1.2 Goals of this work 12
 - 1.2.1 Requirements for GigiONE..... 13
- 2 Physical Background..... 15
 - 2.1 Simulating the sun 15
 - 2.2 Properties of sunlight..... 15
 - 2.3 Influence of the atmosphere 16
 - 2.3.1 Air mass..... 16
 - 2.4 Guiding the light..... 18
 - 2.4.1 Lenses for HFSS applications 18
 - 2.4.2 Reflectors for HFSS 18
 - 2.5 Reflectivity of the surface 21
- 3 State of the Art 23
 - 3.1 Common architectures / topologies:..... 25
 - 3.1.1 Arrangement of reflector and lamps..... 25
 - 3.2 Lamp types 26
- 4 Numerical Design and Simulation of the HFSS “GigiONE” 27
 - 4.1 *Comsol* Multiphysics simulation 27
 - 4.2 Overview of the HFSS parts..... 27
 - 4.3 The simulation..... 28
 - 4.3.1 Geometric layout / Simulation setup 28
 - 4.3.2 Optical simulation of the arc diameter 29

| | | |
|-------|---|----|
| 4.3.3 | Optical simulation case studies | 29 |
| 4.4 | Ansys Multiphysics | 39 |
| 4.4.1 | Air stream in casing..... | 39 |
| 4.4.2 | Temperature analysis of the clamp..... | 40 |
| 5 | Component Selection | 42 |
| 5.1 | Lamps | 42 |
| 5.1.1 | Lamp types utility analysis..... | 43 |
| 5.2 | Ballasts for metal-halide lamps | 44 |
| 5.2.1 | Different producers..... | 44 |
| 5.3 | Reflectors..... | 44 |
| 5.3.1 | Material selection for the reflector | 45 |
| 6 | Final Design of the GigiONE..... | 46 |
| 6.1 | The 3D concepts..... | 46 |
| 6.2 | Safety considerations..... | 48 |
| 6.3 | System costs | 48 |
| 7 | Component Testing | 49 |
| 7.1 | Measurement of <i>Osram HMI 1200</i> metal-halide lamp..... | 49 |
| 7.1.1 | First testing..... | 49 |
| 7.1.2 | Second testing..... | 57 |
| 7.2 | Reflectivity of aluminum..... | 59 |
| 7.2.1 | Setup..... | 59 |
| 7.2.2 | Results | 59 |
| 7.3 | Component temperature testing..... | 67 |
| 7.3.1 | First setup temperature test..... | 67 |
| 7.3.2 | First results temperature test..... | 67 |
| 7.3.3 | Second setup temperature test | 68 |
| 7.3.4 | Second results temperature test | 68 |
| 7.3.5 | Third setup temperature test | 69 |
| 7.3.6 | Third results temperature test | 69 |
| 7.4 | Air stream test of the casing | 70 |
| 8 | Manufacturing and Assembly of Components | 71 |
| 8.1 | Clamp unit | 71 |
| 8.2 | Lamp socket | 71 |
| 8.3 | Frame with measuring table | 72 |
| 8.4 | Lamp unit casing | 73 |
| 8.5 | Mounting plates..... | 73 |

| | | |
|-------|---|----|
| 8.6 | Reflector | 74 |
| 8.6.1 | Reflector 3D scanning | 75 |
| 8.7 | Tunnel..... | 76 |
| 8.8 | Linear guide..... | 76 |
| 8.9 | Fan..... | 76 |
| 8.10 | The HFSS | 77 |
| 9 | Final Validation and Verification | 78 |
| 9.1 | First commissioning test of the solar simulator..... | 78 |
| | First test setup..... | 78 |
| 9.1.1 | Results of the first test | 79 |
| 9.2 | Second testing of the Solar Simulator | 80 |
| 9.2.1 | Second test setup | 80 |
| 9.2.2 | Results of the second test | 80 |
| 9.3 | Testing the flux distribution in the focal point plane..... | 81 |
| 9.3.1 | Irradiance for 1 lamp (Lamp 1) at 50 percent power..... | 81 |
| 9.3.2 | Irradiance for 1 lamp (Lamp 1) at 100 percent power..... | 82 |
| 9.3.3 | Irradiance for 4 lamps at 50 percent power | 82 |
| 9.3.4 | Irradiance for 4 lamps at 100 percent power | 83 |
| 10 | Conclusion, Summary and Outlook | 84 |
| 10.1 | Conclusion..... | 84 |
| 10.2 | Summary | 84 |
| 10.3 | Outlook..... | 85 |
| | List of Figures | I |
| | List of Tables..... | IV |
| | Bibliography..... | V |

Structure of the thesis

Chapter 1 gives a brief introduction in the Nexus of Electricity and Water Supply for Urban Needs (NEWSUN) project. It describes some facts of other desalination processes and why desalination gets more important right now and how the NEWSUN technology can be used beneficially. Furthermore, the targets that must be achieved with the High Flux Solar Simulator (HFSS) are described.

Chapter 2 describes the physical background, such as the properties of the sun and how the atmosphere influences the solar spectrum on the earth. This chapter also describes the different possibilities of guiding the emitted light of the lamps into the desired direction. It also deals with material properties for the reflector material and how different manufacturing process influence the reflection.

Chapter 3 benchmarks different Solar Simulators on the market and HFSS built by different research institutes. The most common architecture of HFSS were discussed and some lamp types that are used in the field of solar research are mentioned.

Chapter 4 elaborates on the optical ray tracing simulation, the computational fluid dynamics simulation and the thermal simulation of the HFSS

Chapter 5 describes the component selection of those parts that showed a possibility of reducing the costs because these were the most expensive components in other HFSS. These key components are lamps, ballasts and reflectors.

Chapter 6 shows the design of the new HFSS, talks about some possibly safety hazards of HFSS and gives an overview of the expenses of the HFSS components.

Chapter 7 describes the tests that were performed on the different components such as lamps and the reflector unit and their results. It also shows the reflection test and results of some aluminum specimen, as well as the built prototype of the casing.

Chapter 8 contains an overview of all components used to build the HFSS, how they were assembled and how they interact.

Chapter 9 gives an overview of the performed validation test which are the results of the measured irradiance level and the distribution after the light guide tunnel and in the focal plane.

Chapter 10 contains a conclusion and a summary of the whole thesis and gives an outlook for future improvements and application fields.

1 Introduction and Motivation

1.1 The “Nexus of Electricity and Water Supply for Urban Needs” (NEWSUN) project

The worldwide demand for drinking water is increasing every year about one percent due to population growth and the respective development of the economy and lifestyle. Big shares of this problem can be accounted to industrially and domestic water demands, because the increase in these sectors is much higher than the increase in the agricultural sector. This also intensifies the problem because the need for high quality water is more crucial for industry and domestic use than it is for agriculture. There is no sign that this will change, which means that water scarcity will increase further if no action is taken. The world water report of the *United Natopms* in 2017 says that around a quarter of the world population has no safe source of drinking water and around two-thirds have to deal with water scarcity during the year [1], [2].

Solutions to this problem must be found, otherwise problems will go from bad to worse. One possible solution that could help to reduce this problem is the NEWSUN project. NEWSUN is the idea of an old technology that should be adapted to fit in the 21st century and the current development of the increasing efficiency and usage of renewable energies. To be more specific, the technology of Multiple-effect distillation is used to vaporize water. The process itself is complex but for explanatory purposes it can be broken down to a distillation apparatus as shown in **Figure 1**. The liquid, in case of NEWSUN water with impurities / salty sea water or brackish water, is heated up to its boiling point to extract the fluid of interest as evaporated gas, while other substances still remain in the heating area until they are removed. In the next step the gas is cooled down below boiling point to liquify it again and it subsequently can be collected [3].

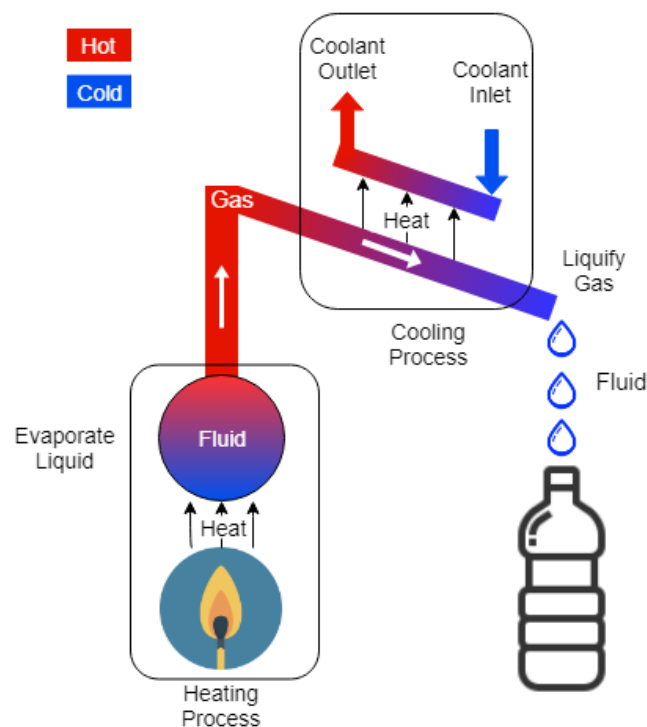


Figure 1: How a distillation process works.

As mentioned before the real process which is described in Figure 2 is more complicated owing to the need increase efficiency but uses the same principle of evaporating water with a subsequent cooling process to liquify the steam again. This process is also called *Multi-effect evaporation* (MEE). The essential idea in the NEWSUN process is that all energy that must be provided to operate the process, is harvested from the sun. This is a key point for NEWSUN, because it is possible to produce clean water without any additional source of energy other than the sun. This is not only an economic but also a big environmental advantage compared to alternative devices that produce water. In Table 1 the costs of some important competitive processes and their energy consumption are described. As shown in Table 1 there is a big spreading between energy consumption and costs for different technologies. This is because *Multi-Stage Flash* (MSF) and MEE are able to use low cost energy as thermal heat and *Reverse Osmosis* (RO) uses mechanical energy which has higher costs compared to thermal energy [4], [3].

Table 1: Energy consumption of different desalination processes according to [4].

| Process | Energy Consumption [kJ/kg _{fresh water}] | Operating Costs [\$/m ³ _{fresh water}] |
|--|---|--|
| Multi-Stage Flash (MSF) | 95-290 | 1,10-1,50 |
| Multi-Effect Evaporation (MEE) | 107-132 | 0,46-0,85 |
| Seawater Reverse Osmosis (RO) (salt concentration dependent) | 15-30 | 0,45-0,92 |
| Brackish water Reverse Osmosis (RO) | 7,2-11 | 0,2-0,35 |

For NEWSUN the costs as shown in Table 1 are to be reduced to zero. In order to achieve this parabolic trough collectors guide the sun beams into the focal point of the collector, where a so called *hybrid-absorber* is placed to harvest the concentrated solar energy. The collector itself is called hybrid absorber because it consists of photovoltaic cells to produce electric energy and a pipe filled with fluid that heats up and is used as storage and transport system for the thermal energy. To gain a better understanding of the system it is depicted in Figure 2.

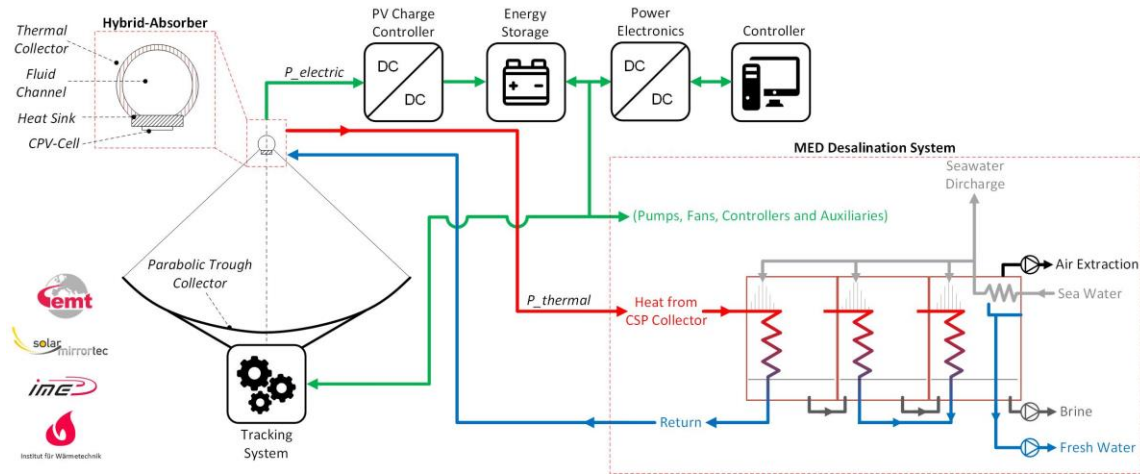


Figure 2: Schematics of the self-sufficient NEWSUN desalination plant [3].

Photovoltaic cells, especially the ones suitable for operation under concentration, have a high conversion efficiency of up to about 40 percent as seen in Figure 3 [5]. Still the excess heat must be ejected through cooling, otherwise the cells would be less efficient or could even be destroyed. The advantage of the hybrid absorber is the combination of converting the sun energy to electric energy and thermal energy, whereby both types of energy are used in NEWSUN.

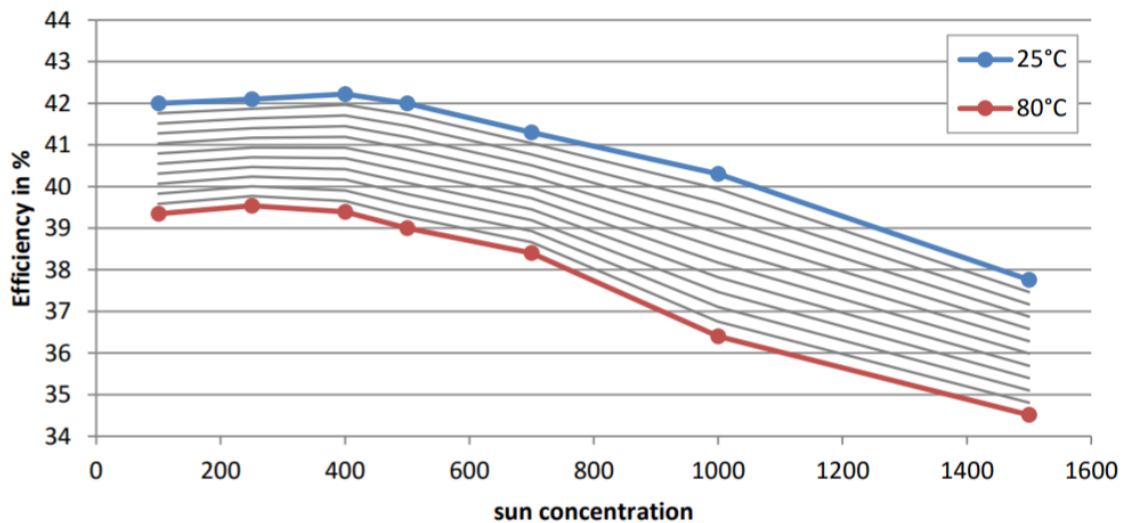


Figure 3: Typical performance over temperature for an AZUR SPACE CPV cell according [5].

1.1.1 Solar irradiance, water scarcity and population density

As mentioned before NEWSUN aims to harvest solar energy to produce fresh water. The sun is a crucial part of this process and has a direct impact on the amount of water that can be produced. Therefore, it can be concluded that areas with higher solar irradiance are able to produce more fresh water since high solar irradiance means more solar energy. Figure 4 shows a world map according to direct solar irradiance. Figure 5 and Figure 6 show world maps illustrating population density and water scarcity to

identify the areas in which fresh water production is needed. According to these maps many parts of the world with a lack of fresh water could profit from a system like NEWSUN because many areas with high solar irradiance are congruent with those of water scarcity and high population density.

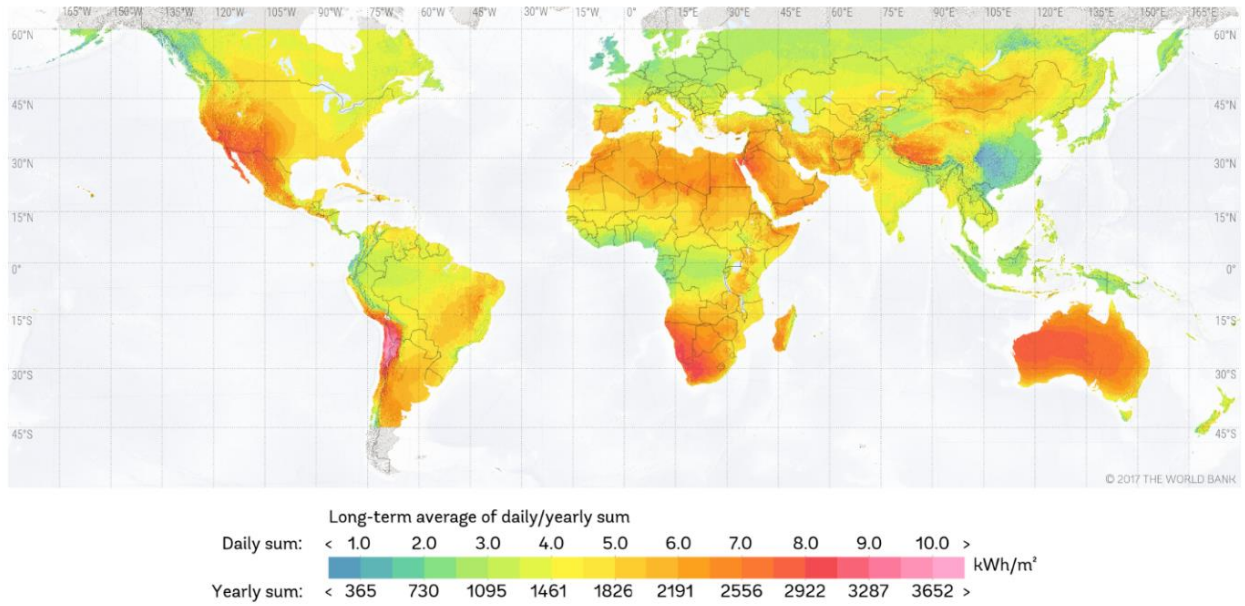


Figure 4: Direct normal solar irradiation modified [6].

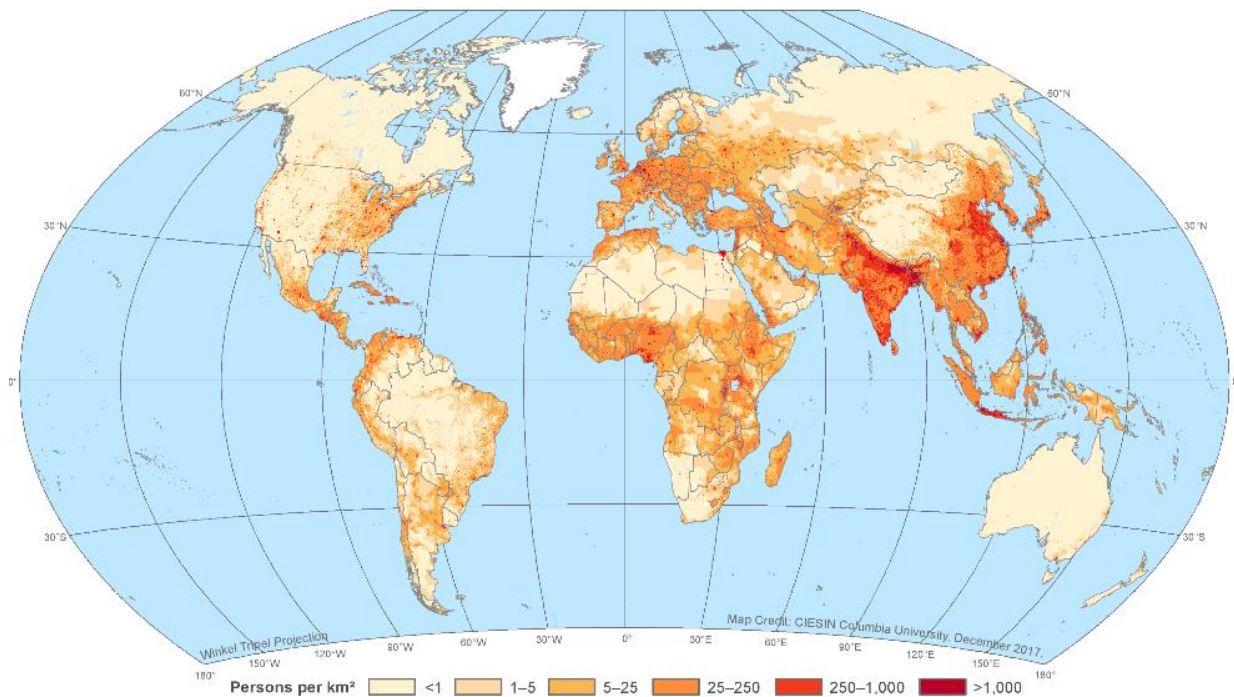


Figure 5: Population density of the world for the year 2015 modified [7].

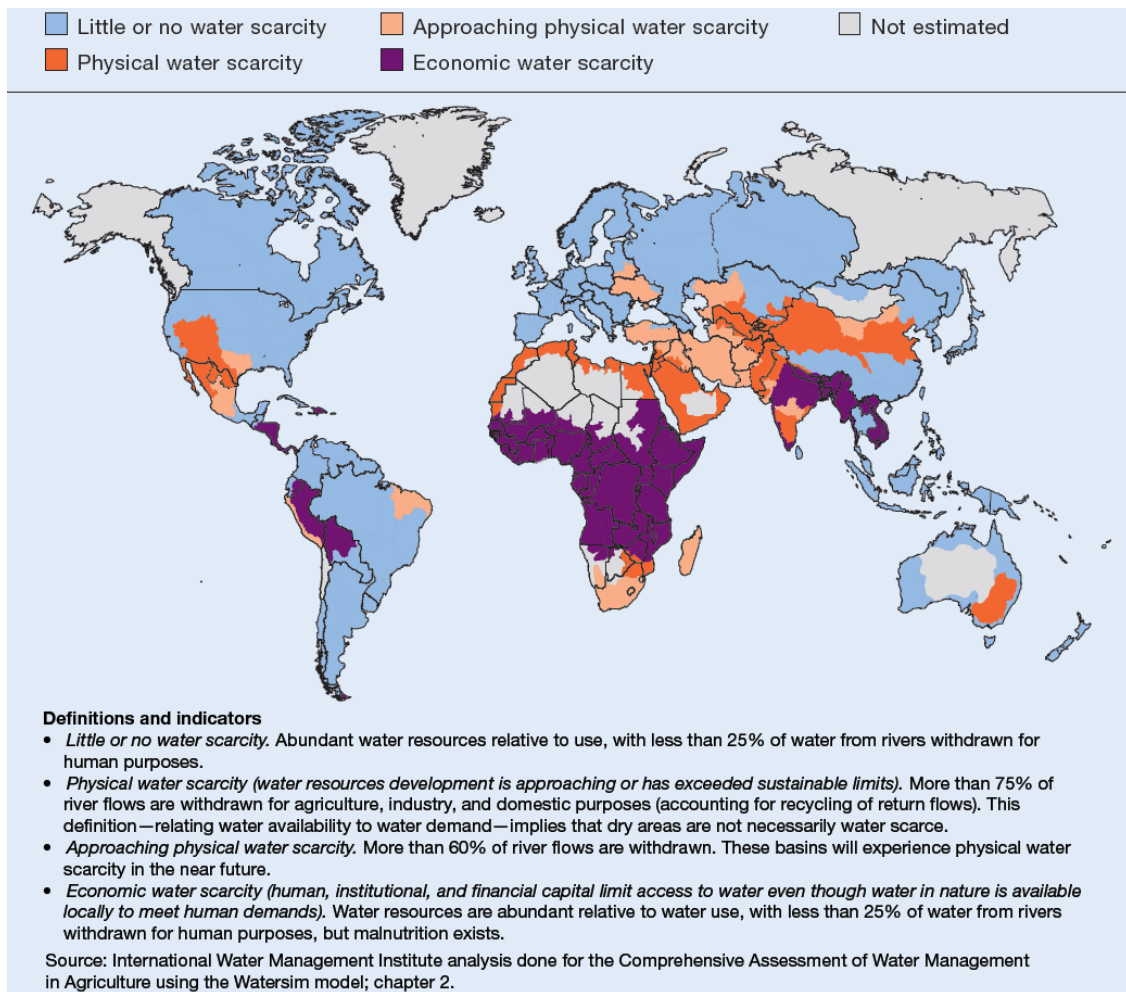


Figure 6: Areas of physical and economic water scarcity according to [8].

1.2 Goals of this work

Part of the NEWSUN project is a test setup for the hybrid absorber and therefore, a light source which simulates the sun is imperative. To serve this exact purpose, a *High Flux Solar Simulator* (HFSS) is built and described in this thesis. The main idea is to have a tool that can test solar cells, such as the *photovoltaic cells* (PV) or *concentrated photovoltaic cells* (CPV) with or without the complete absorber. The advantage of testing components in the HFSS is that test set ups can be conducted under specific reproducible conditions to have reproducible results of test. Under real conditions however, influences like fog and clouds cannot be influenced and therefore the produced results would be incomparable. Additionally, the time of day and year have an impact on the results due to different angles of to sun to the ground and would cause differences in solar flux. All these uncertainties can be eliminated with the usage of the HFSS.

1.2.1 Requirements for GigiONE

To simulate the sun, certain aspects must be considered. These aspects can be split into three categories:

- Solar spectrum
- Concentration ratio
- Flux distribution

The spectrum of the sun as seen in Figure 7, is of great importance. This is because some testing of multi-junction cells as depicted in Figure 8 require a light source that produces wavelengths in the range of ultraviolet light which is below 380-400nm.

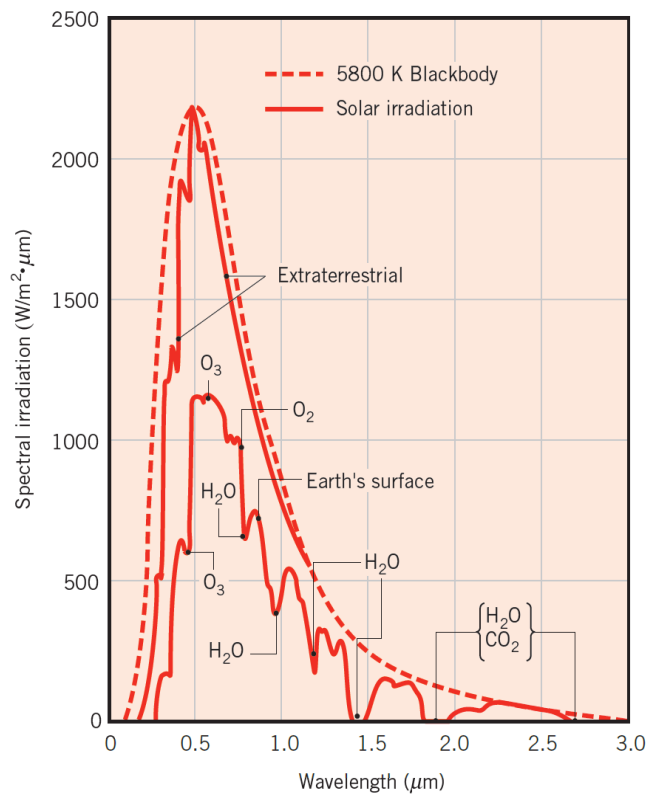


Figure 7: Spectral distribution of downward-propagating short wavelength solar radiation [9].

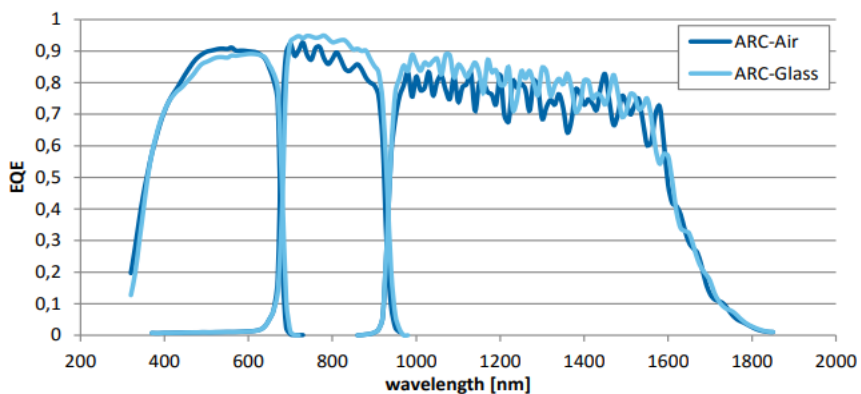


Figure 8: Spectral response of triple-junction cells from Azur Space according to [10].

The geometrical concentration ratio C_{geo} is described in equation (1-1) and visualized in Figure 9, this ratio C_{geo} is from [11]. For the solar simulator a minimum concentration ratio of 60 is required this is equivalent to a radiation power of 60000 W/m^2 .

$$C_{geo} = \frac{\text{area of the aperture}}{\text{area of the receiver}} = \frac{A_a}{A_r} \quad (1-1)$$

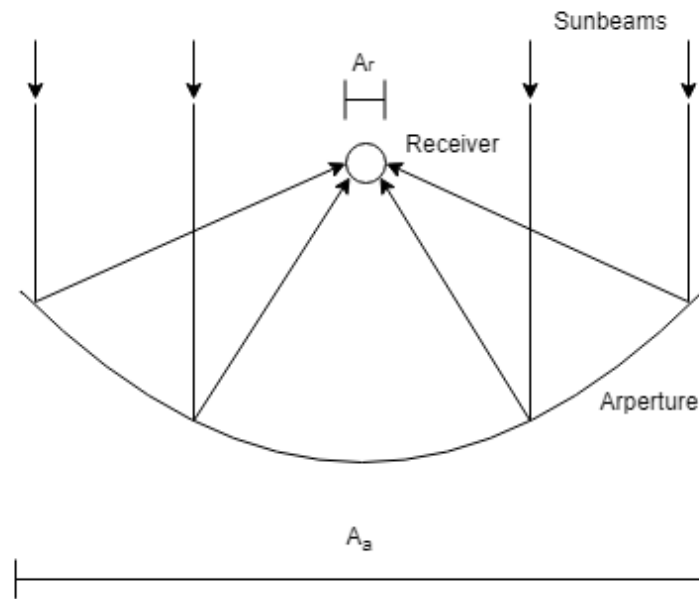


Figure 9: Geometrical concentration ratio described on a parabolic through mirror.

A “flat” flux distribution for the test cell is required. The normal distribution for a focused system is a gaussian distribution. The different distribution can be seen in Figure 10. In this figure the idea of the flat distribution for a PV cell becomes more tangible. A PV cell should be illuminated with the same intensity over the whole area to avoid heat spots and subsequently efficiency losses. Therefore, testing the PV cell under a gaussian distribution is not an ideal test environment [12].

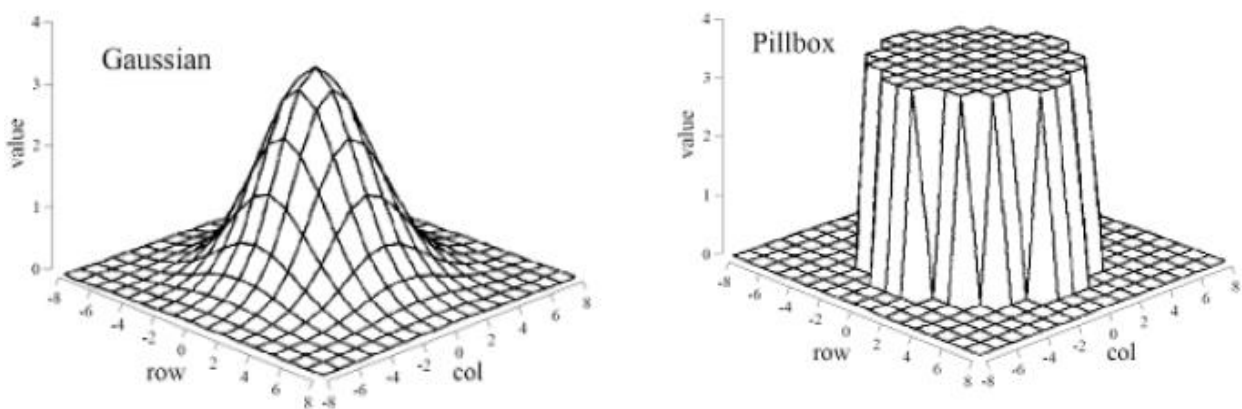


Figure 10: Gaussian(left) and flat, desired distribution (right) [12].

2 Physical Background

2.1 Simulating the sun

The HFSS is a tool to test sun-light-dependent components and devices. To do is under reproducible ambient parameters a HFSS is used, because only in such an environment a comparable test of different devices can be carried out. The primary goal for simulating the sun is to get as close to its real properties as possible and to have the opportunity to repeat the test under the exact same conditions.

2.2 Properties of sunlight

The spectrum of the sunlight is depicted in Figure 7 where the spectrum outside of the earth's atmosphere as well as the spectrum on the surface of the earth is shown. The difference of both curves is described in 2.3. The solar radiation is much higher on earth's surface but to get there it must travel at about $1,5 \times 10^{11}$ m. Since this radiation intensity decreases because of the spherical spread while the light travels through the earth, the value of flux on earth is about 1368 W/m^2 . The light rays that reach the earth are nearly parallel. This is because of the great distance between sun and earth. Figure 11 shows the configuration of these two objects and it also describes the angle of 4,6 mrad which is the geometrical result of the distance between sun and earth.

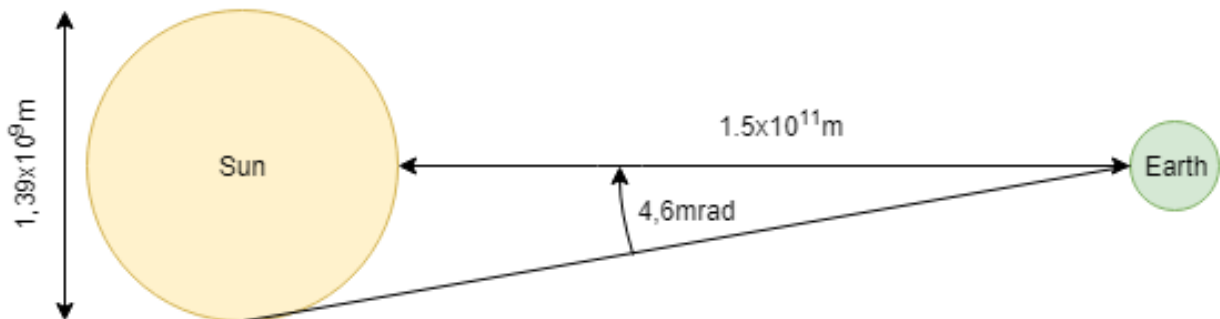


Figure 11: Sun and earth configuration.

Summary of sunlight properties:

- Rays with an angle up to 4,6 mrad seen in Figure 11, which is half of the angular diameter of the sun seen from earth.
- Intensity on edge of the atmosphere 1368 W/m^2 .
- Intensity on earth surface about 1000 W/m^2 (depending on the incident angle).
- Spectrum of Blackbody with 5800K, reduced by earth's atmospheric influences.

2.3 Influence of the atmosphere

The atmosphere mostly consists of nitrogen and oxygen but also contains some trace gases such as carbon dioxide and water vapor. Additionally, dust and aerosols from various sources are part of the atmosphere. Some of these gases have a big influence on the solar spectrum, as depicted in Figure 7, due to *scattering* and *absorption*. Figure 7 also shows which components of earth's atmosphere influence the intensity of specific wavelengths of the sun's spectrum. The overall reduction of irradiation is mostly caused by scattering and sharp declines around specific wavelengths, which are caused by absorption of specific substances such as O₃, O₂, H₂O and CO₂. This also means that if the light must travel a longer distance in the atmosphere the intensity decreases which is described in 2.3.1 [9].

2.3.1 Air mass

The effects described earlier are all subject to various influences, but they do have one thing in common. they reduce the intensity of solar irradiation. Often the individual effects are not as important as their combined effect. This impact of reducing the intensity of solar rays is defined in the term air mass. The air mass describes the path length that the rays must pass before hitting the earth's surface as visualized in Figure 12. The standard air mass values are given in Table 2 [13], [14].

Description of terms according to *Newport* [14]:

- AM 0-extraterrestrial spectrum (edge of the atmosphere).
- AM 1-terrestrial spectrum with shortest possible path through the atmosphere.
- AM 1,5-terrestrial spectrum with longer path through atmosphere than AM 1.
 - AM 1,5G global standard (for photovoltaic testing).
 - AM 1,5D direct standard (for concentrated applications).

The difference between global and direct is described in Figure 13.

Table 2: Standard power densities according to [14].

| Solar Condition | Standard | Total W/m^2 . |
|-----------------|-----------------------------|-----------------|
| | WMO Spectrum | 1367 |
| AM 0 | ASTM E 490 | 1353 |
| AM 1,0D | CIE Publication 85, Table 2 | - |
| AM 1,5D | ASTM E 891 | 768.3 |
| AM 1,5G | ASTM E 892 | 963.8 |
| AM 1,5G | CEI/IEC* 904-3 | 1000 |

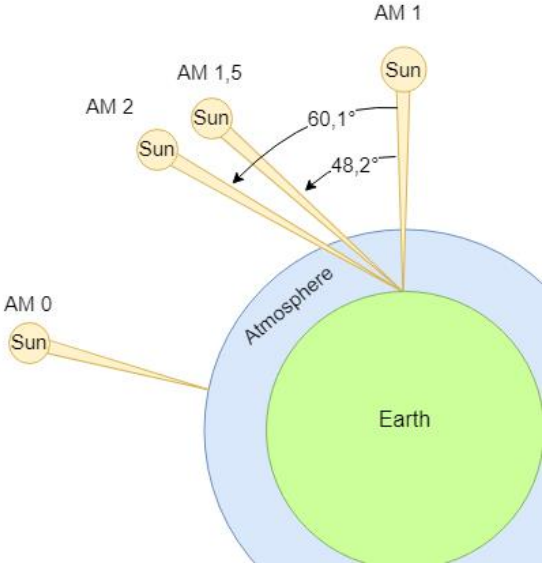


Figure 12: Air mass values according to [13].

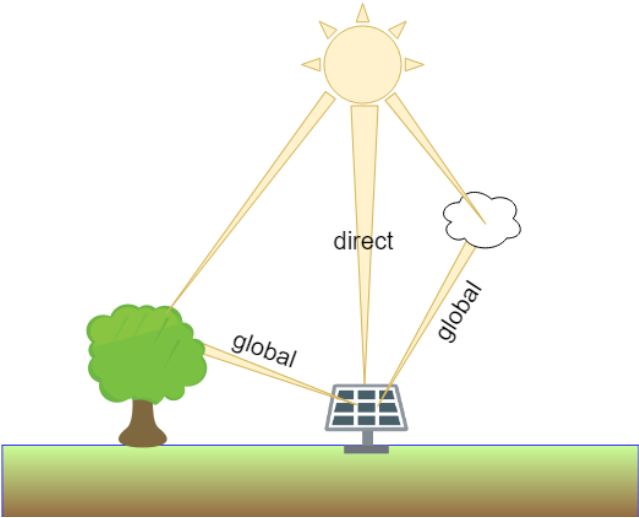


Figure 13: Direct and global radiation according to [13].

2.4 Guiding the light

The practical ways to guide light in a desired direction are by *refraction* or *reflection*. These two principles are used by lenses and mirrors, which are different approaches to guide the light for HFSSs. The way how they are used in HFSS are described in the following chapters.

2.4.1 Lenses for HFSS applications

Lenses use refraction to change the direction of a light ray. The most common ones in the HFSS application are *Fresnel lenses* that use the principle of curved lenses. At a Fresnel lens a lot a material that has minor influence on the light deflection is removed, this makes the lenses cheaper and lighter than conventional curved lenses. Normally they are used in HFSS as a converging lens to focus a collimated light beam into a focal point. Figure 14 visualizes the common shape and usage in a HFSS. [15].

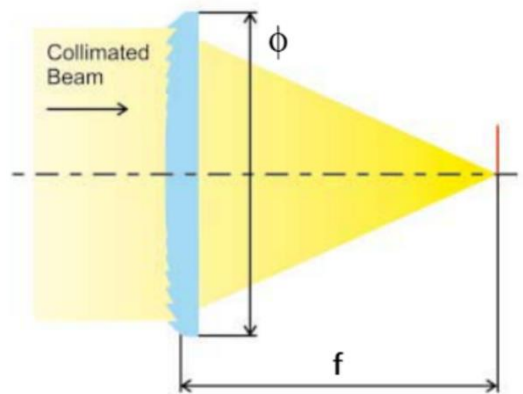


Figure 14: Focusing *Fresnel lens* [15].

2.4.2 Reflectors for HFSS

Reflectors are specially curved mirror surfaces and use their shape to guide the light. Most of the HFSSs use a reflector for the primary reflection. This is sensible, because most of the light from the lamp can be effectively used for the focusing process. This is possible because the focusing points, where the lamps normally are located, are located inside of the reflector and therefore allow coverage of a big portion of the lamp. The common reflectors for HFSS are *elliptical* and *parabolic* shaped reflectors. The position of the focal points can be seen in Figure 15 and Figure 16 and their properties are described below.

2.4.2.1 Elliptical reflector shape

Most of the existing HFSS systems, which are described in more detail in chapter 3, use *elliptical reflectors*. Often this shape is used because of the possibility to already focus the light with the reflector without the need of any further equipment. The way this works is that an ellipsoid has two focal points. In Figure 15 these are called $F1$ and $F2$. The figure also shows how the concentration due to the geometrical shape works. Depending on the shape of the elliptical reflector the distance between the

focal points can be influenced. Smaller simulators can use short focus distances, but bigger ones generally have long focus distances which allow to combine more light sources to increase flux density on the target [16].

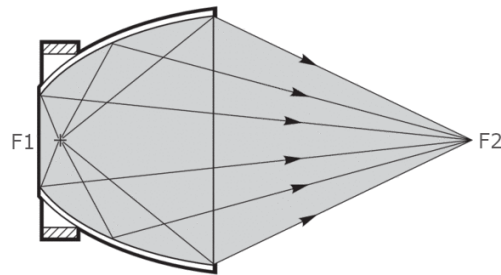


Figure 15: Elliptical reflector with two focal points according to [16].

2.4.2.2 Parabolic reflector shape

Parabolic reflectors are more common for smaller solar simulators that are not used for high concentration applications. This geometry allows the light rays to be collimated. If the simulator is used as an HFSS a lens must be placed into the optical path to concentrate the light rays in a focal point. This was the approach to build a HFSS at the *KTH Royal Institute of Technology* where sky searchlights from the manufacturer *Noyechina*. were used [17]

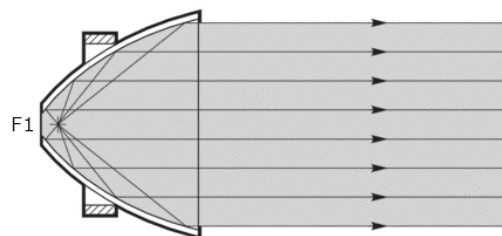


Figure 16: Parabolic Reflector with one focal point according to [16].

2.4.2.3 The problems of non-ideal light sources

When lamp and reflector are combined, some problems regarding the focusing occurs. Practically the geometric correlation as aforementioned is not adaptable. Figure 17 shows an elliptical reflector with the described issue of a real lamp arc. Since *real arcs* are not infinitely small points but have a finite size. The finite *arc length* results in different reflection angles on the reflector surface and causes the subsequent divergence of the light rays. *Ben M Ekman* in [18] calculated the influence of the arc length and the visualized this for two arc lengths and two different focal lengths. He also mentions that a bigger arc and a greater focal length will result in a wider light spread on the target plane. His calculation is shown in Figure 18. A reduction to this problem is possible by using lamps with short arc lengths and a length to width ratio of the ellipsoid close to the value of one, which describes a very spherically shaped ellipsoid.

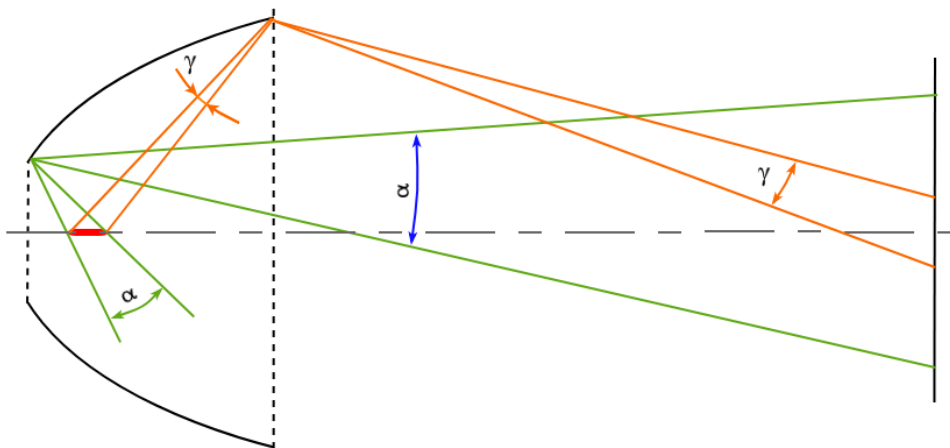


Figure 17: Elliptical reflector with focus widening due to arc length according to [18].

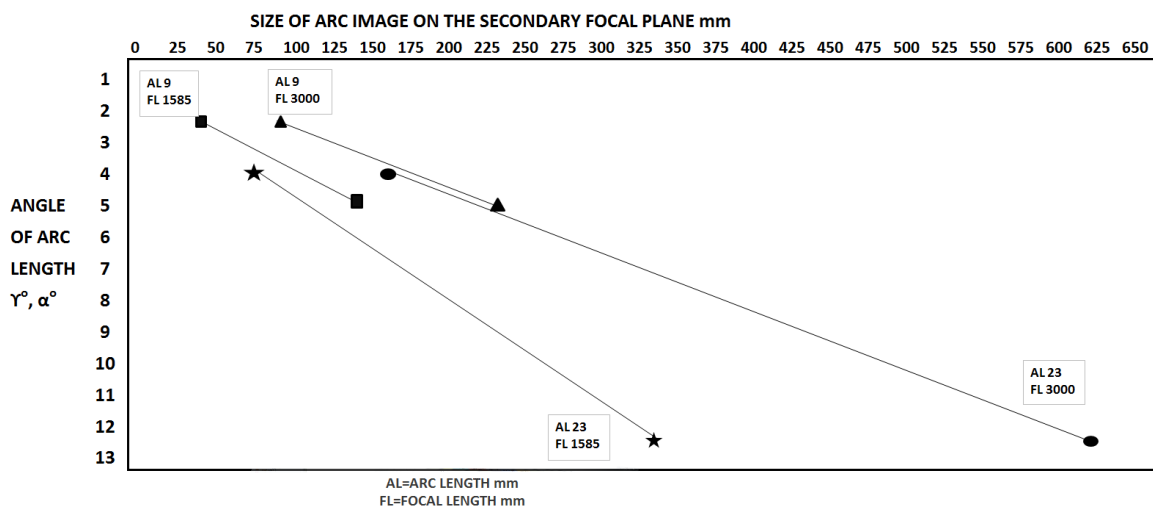


Figure 18: Size of arc image at the secondary focal plane for an arc length of 9 mm and 23 mm and a focal length of 1585 mm and 3000 mm [18].

2.5 Reflectivity of the surface

The most common materials that are used as reflective surfaces are silver and aluminum. Silver has a high reflectivity for the visible light area but has a sharp decrease of reflectivity in the range of UVA. Pure aluminum has a very good reflectance over a far range which also includes the UV spectrum. The negative aspect of those two materials is that they oxidize which decreases the reflectivity of the surfaces. To avoid uncontrolled decrease of reflectivity due to oxidation it is possible to protect the surfaces with coatings. [19]. Since this thesis also deals with the problem of reflecting UV and silver is not able to do so, it will not be discussed further in this thesis.

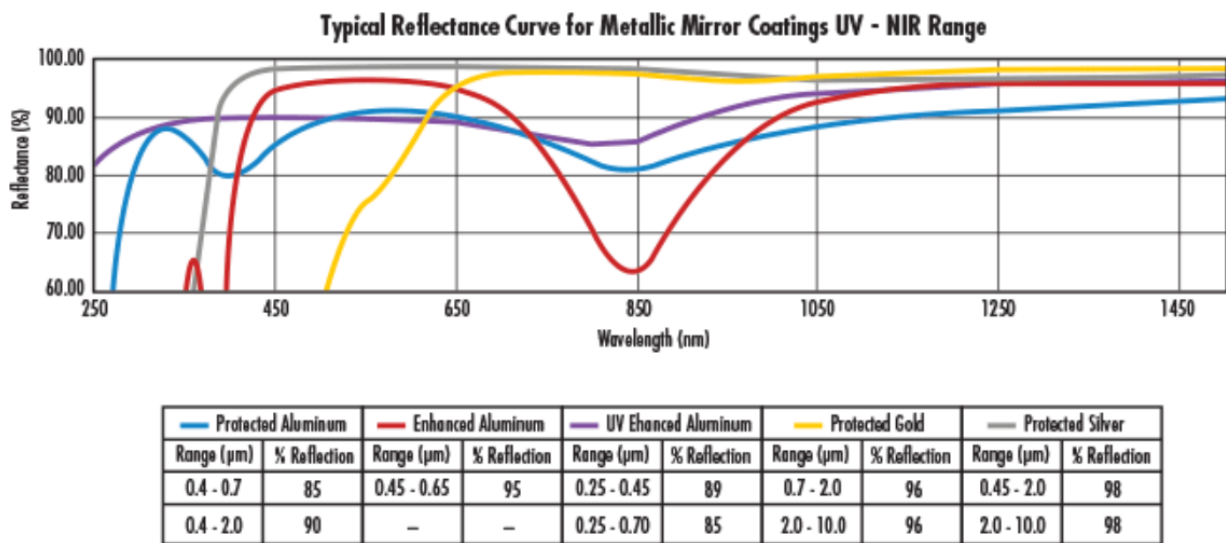


Figure 19: Reflectance of metallic surfaces [20].

2.5.1.1.1 Highly reflective coatings

The reflective coating has two major tasks. One is to protect the surface from unwanted oxidation and the second is to maintain or even increase the reflectivity properties. Coatings that are available are *anodized aluminum*, *protected aluminum*, *enhanced aluminum* and *UV enhanced aluminum*. The problem of some of the coatings are that their manufacturing costs are very high which makes them not to desirable for a low-cost application.

2.5.1.1.2 Anodized aluminum

Anodizing aluminum is a standard way of surface protection which is very similar to the natural process of atmospheric(natural) oxidation. The difference between natural oxidation and anodizing is the thickness of the protective Al_2O_3 layer. A natural layer of Al_2O_3 normally is between 0,1-0,5μm thick. Since this layer is often not thick enough to protect the metal surface against environmental influences, aluminum anodizing was invented to produce a several micrometers thick Al_2O_3 layer to increase corrosion resistance and abrasive withstanding [21].

Using this process for optical surfaces can result in some problems. Charles C. He and *Thomas M. Heslin* researched the issue of occurring cracks in anodize processes in *Preventing Cracking Anodized Coatings* [22]. In their opinion different thermal expansion coefficients of aluminum and oxide coatings lead to stress in the surfaces which let the cracks appear. The major issue seems to be the hot water sealing which is done as a final step to finish the treatment. They also mention that thick anodized layers are more vulnerable than thin layers. Also, humidity plays a role in terms of cracking. He and Heslin also conducted temperature cycle tests to anodized and unsealed specimen where they discovered that the clear coating did not show any cracks and the black unsealed coating showed minor cracks [22].

If anodized aluminum is used for solar simulation only a small layer should be added. Such small layers can be achieved by applying a boric acid process as hard coated films seem to have a low reflectance. Furthermore, the hot water sealing should be avoided because water is stored in the anodic layer which influences the reflectance of the material and as described before produces cracks in the anodic layer [23].

2.5.1.1.3 Pure aluminum and temperature influence on it

Researches from *Lewis Research Center* determined the reflectance of several metallic surfaces (Al, Cu, Au, Mo, Ni, Pt, Ag, stainless steel 304, Ta, Sn, Ti, and V) and investigated the influence of temperature to reflectance of these metal surfaces [24]. They concluded that the influence between 250- 500 K is minor. Nevertheless, they still provided the data which show us the results of highly specular aluminum which are available in Figure 20 [24]. The problem of pure aluminum, which can be polished to increase reflectivity, is that the surface must be handled with tremendous care because scratches can easily occur on the very soft aluminum surface.

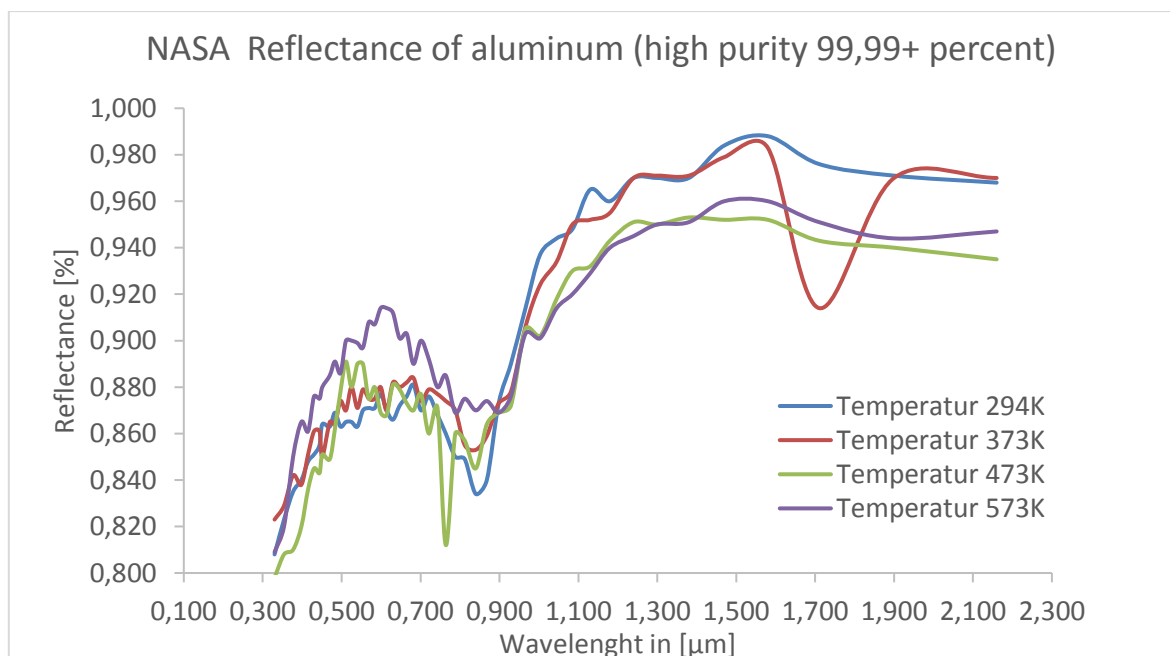


Figure 20: Reflectance of aluminum at different temperatures [24].


3 State of the Art

The following sections describe the different types of solar simulators that are available on the market and the HFSS that are constructed and built by various research institutes. Many of the used ideas in this work is a result of the analysis of the existing HFSS mentioned in Table 4. This benchmark demonstrated that HFSS cannot be purchased as an off-the-shelf product and that certain items of HFSSs are very expensive.

The benchmark of different solar simulator producers in Table 3 showed that the test rigs that are commercially available are generally used for PV cells that are not used for concentrated applications.

Table 3: Solar simulators with costs, available on the market.

| Company | Image | Lamp Type | Concentration [suns] | Power [W] | Price | Ref |
|------------------|---|--------------|----------------------|-----------|---------------|------|
| NEWPORT |  | Xenon-Lamp | 0,1-1 | 450-1600 | - | [16] |
| infinityPV |  | Metal-Halide | 1 | 1200 | - | [25] |
| Photo Emission |  | Xenon Lamp | 1 | 100-7000 | | [26] |
| SCIENCETECH INC. |  | Xenon Lamp | 1 | 150-300 | USD\$6,089.00 | [27] |

| | | | | | | |
|---------------------|---|---------------|---|--------------|-----------------------------------|------|
| SCIENCETECH INC. |  | Xenon Lamp | 1 | 150- 1600 | USD\$11,950.00- USD\$70,125.00 | [27] |
|---------------------|---|---------------|---|--------------|-----------------------------------|------|

The list in Table 4 is showing some of the HFSS built since 2015. Many of them are equipped with xenon arc lamps to achieve high peak fluxes. Lots of the ideas regarding the shapes of the reflector and their assembly configuration are extracted from these HFSSs.

Table 4: List of high flux solar simulators since 2015.

| High-Flux-Solar-Simulator | Started | Solar power [kW] | Lamps | Peak flux [MW/m ²] | Ref |
|--|---------|-------------------|--------------|--------------------------------|------|
| Swinburne University, Melbourne | 2015 | 12 | Metal-Halide | 0,9 | [28] |
| EPFL Lausanne, LRESE | 2015 | 15 | Xenon | 21,7 | [28] |
| Australian National Univ., Canberra | 2015 | 15 | Xenon | 9,5 | [28] |
| North China Electric Power University, Beijing | 2016 | 20 | Xenon | 4 | [28] |
| University of Colorado, Boulder | 2016 | 10 | Xenon | (n.a.) | [28] |
| DLR, Synlight, Jülich | 2017 | 310 240 240 | Xenon | 12,5 10 10 | [28] |

In Table 5 two research institutes offered a deep insight to the construction process of their HFSSs with occurring costs available. Thereby, these institutes offer a guide for a smart approach of building a HFSS at reasonable costs.

Table 5: HFSS with expenses.

| High-Flux Simulator | Solar | Started | Solar power [kW] (estimated) | Lamps | Price | Ref |
|---------------------------------------|----------|---------|------------------------------|--------------|----------|------|
| Massachusetts Institute of Technology | | 2013 | 3 | Metal-Halide | \$6,105 | [29] |
| Sandia Laboratories | National | 2018 | 2 | Metal-Halide | \$14,300 | [30] |

3.1 Common architectures / topologies:

Based on the findings summarized in Table 4 and Table 5, the most common architectures are summarized below. It also mentions the final arrangement of the lamp units and its purpose.

3.1.1 Arrangement of reflector and lamps

The *ETH Zurich (Swiss Federal Institute of Technology in Zurich)* as one of the first research centers to build their own HFSS has already gained some experience in developing and constructing these test benches. One of their first approaches showed a 75 kW HFSS with a cooled long arc xenon lamp. This lamp was put in an elliptical trough reflector as seen in Figure 21 [31]. This way they obtained a high concentration factor and the design seems quite simple, but it has limited possibilities regarding parameter variation.

Their next development was the nowadays mostly used approach for the reflector configuration. In this approach the lamp and the reflector form a unit. Then several copies of the same unit are arranged in a spherical shape. Since most of the used reflectors for HFSS are elliptical ones these units may also have the same focal length. To obtain a high concentration factor the radius of the previously mentioned spherical arrangement must be the same as the focal length of the reflector as visualized in Figure 22. Otherwise the laterally placed units would already defocus again and therefore would not deliver the same flux density on the heat spot as a center arranged unit. [32]

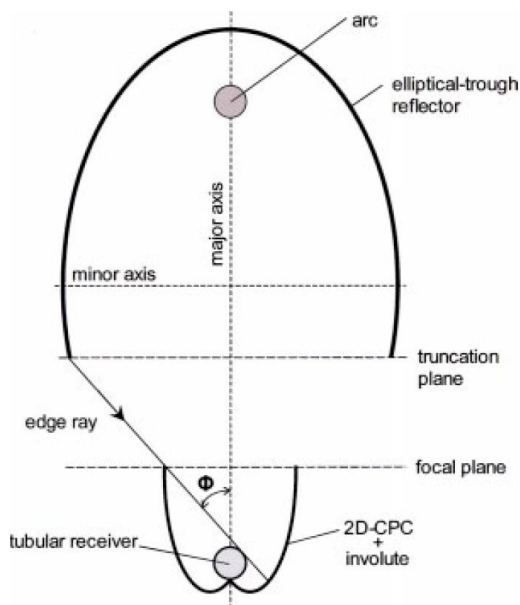


Figure 21: Arrangement of 75 kW lamp and reflector [31].

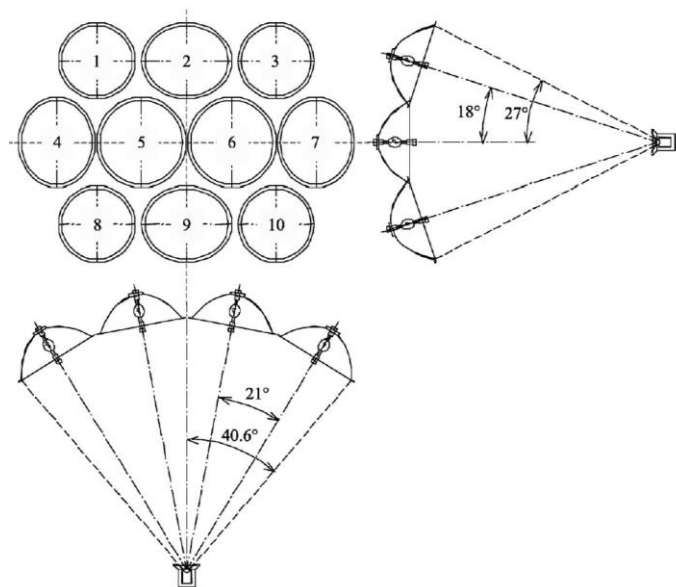


Figure 22: Arrangement of several reflector and lamp units [32].

3.2 Lamp types

A literature review of *Wujun Wang* in “Simulate a ‘sun’ for Solar Research” [33] showed a wide variation of lamps that were already used for solar simulation.

- Carbon arc lamp
- Quartz tungsten halogen lamp
- Mercury xenon lamp
- Xenon arc lamp
- Argon arc lamp
- Metal-halid Lamp
- Light-emitting diode lamp „LED „

For HFSS nowadays most simulators work with *xenon arc lamps* followed by *metal-halide lamps* and only a low number of HFSSs use *argon arc lamps*. An overview of the spectrum of these are shown in Figure 23, Figure 24 and Figure 25. All of them are emitting a useful spectrum for solar simulation [34].

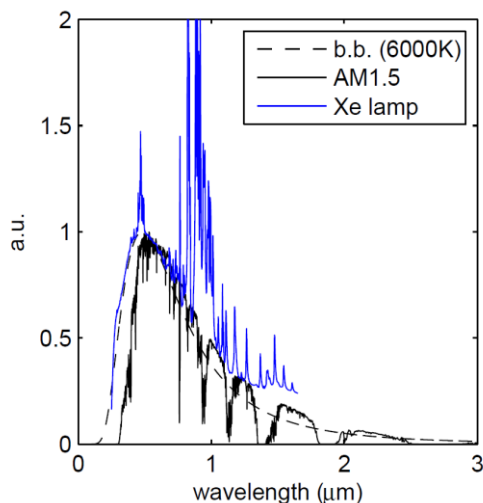


Figure 23: Spectrum of xenon arc lamp [34].

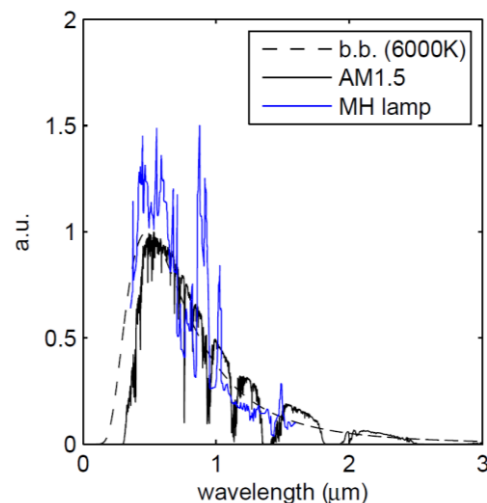


Figure 24: Spectrum of metal-halide lamp [34].

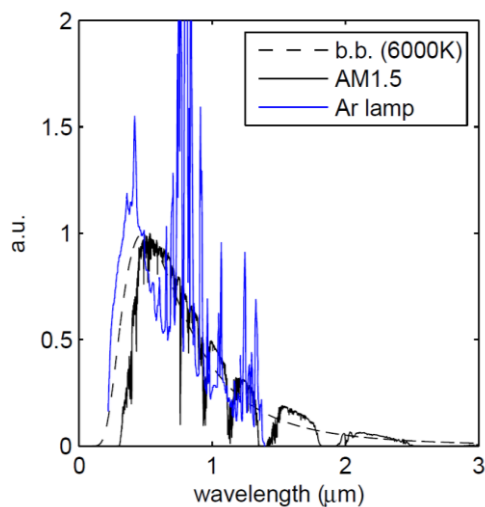


Figure 25: Spectrum of argon arc lamp [34].

4 Numerical Design and Simulation of the HFSS “GigiONE”

4.1 COMSOL multiphysics simulation

The targets for the HFSS are mentioned in Table 6 but only the concentration factor and the pillbox distribution could be simulated. Therefore, these two targets are part of the ray tracing simulation process.

Table 6: Targets for the final HFSS.

| Target |
|---|
| Minimum concentration factor of 60 suns (equal to $60000 W/m^2$) |
| Pillbox distribution of the light flux |
| Delivering a spectrum that is close to the solar spectrum |

4.2 Overview of the HFSS parts

Figure 26 depicts the HFSS in Catia V5 where all four lamps are targeting at the same point in front of the tunnel to concentrate big shares of the light energy in the light guide tunnel. Figure 27 gives a close view of the reflector unit.

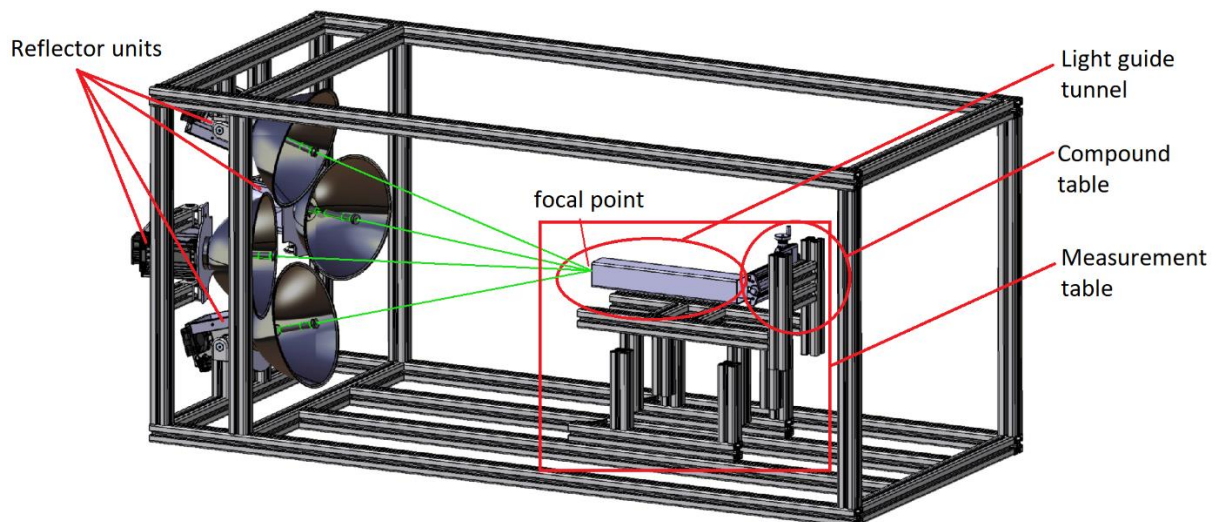


Figure 26: HFSS parts with elliptical axis.

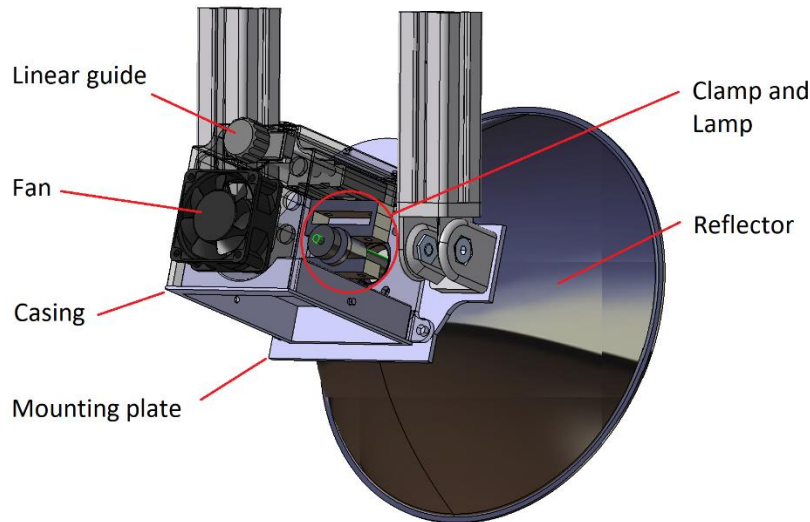


Figure 27: Reflector unit parts.

4.3 The simulation

The simulation approach was chosen based on different scientific papers that already used ray tracing tools to simulate their test bench before constructing it. The arc diameter had a big influence on the simulation. Therefore, different arc diameters were simulated and validated with the results of *Boubault et al.* [30]

Various reflector geometries were simulated to see, if it is possible to get a flat distribution without any further equipment. After several attempts of varying the position of the arc and the geometry of the reflector this idea was discarded. The idea of the team of the *German Aerospace Center (DLR)* who used a tunnel was tested and within only a few variations the results were very satisfying regarding the flux distribution. [12]

4.3.1 Geometric layout / simulation setup

1. The arc was set as a release with a total source power of 1200W
2. The reflector was used as a mirror boundary with an *absorption coefficient* of 0,1
3. The tunnel was a mirror boundary with an *absorption coefficient* of 0,1 and could be varied in length and position

As mentioned in 4.3 we used the experimental data of *Boubault et al.* [30] to validate the arc diameter of our lamp. Therefore, we used the same geometric set up as *Boubault et al.* and varied the arc diameter. The different results can be seen in Figure 28 in the next section.

4.3.2 Optical simulation of the arc diameter

To get as close as possible to *Beaboults* results we set up the simulation as similar as possible to those of *Beaboults*. To achieve this, we took the same reflector geometry and the same target length. After that we tested several arc lengths and chose the same diameter with the only difference that we used our lamp power. Finally, it was chosen to use a 5 mm arc for the following simulations.

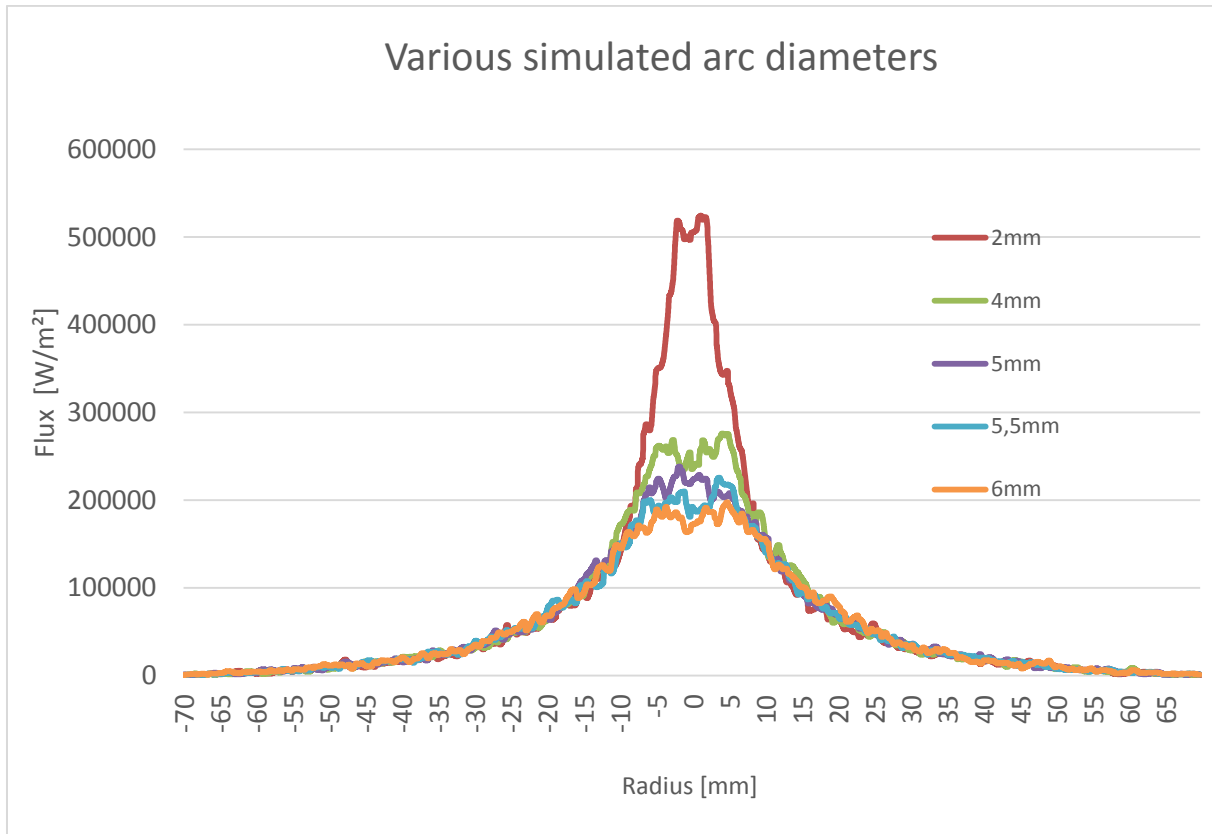


Figure 28: Arc diameter variation in simulation.

4.3.3 Optical simulation case studies

After some test simulation with different amounts of reflectors and a several reflector geometries. A set up with four reflectors in a spherical arrangement was used. This composition was used because simulations showed, when using a square tunnel to generate a pillbox distribution (Figure 10) it showed the best results with four reflectors. The setup for the simulation is shown in Figure 29 and Figure 30. The used geometry for the reflector is shown in Figure 65.

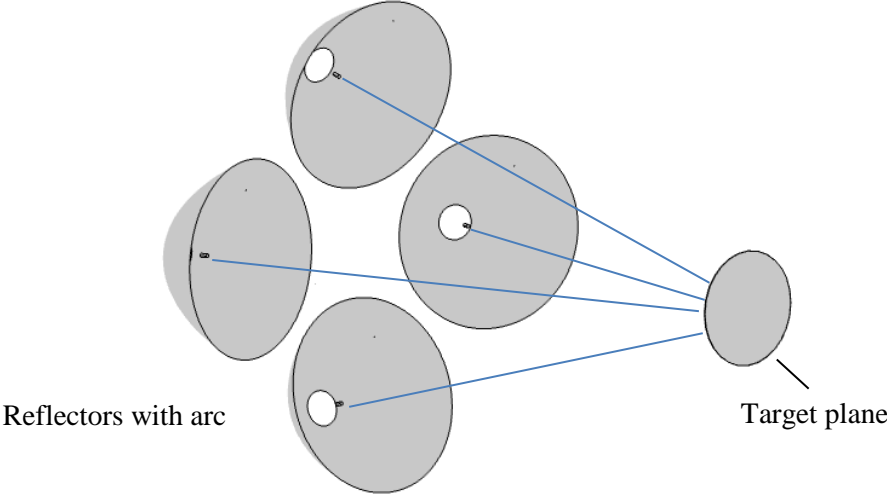


Figure 29: Geometric layout without tunnel.

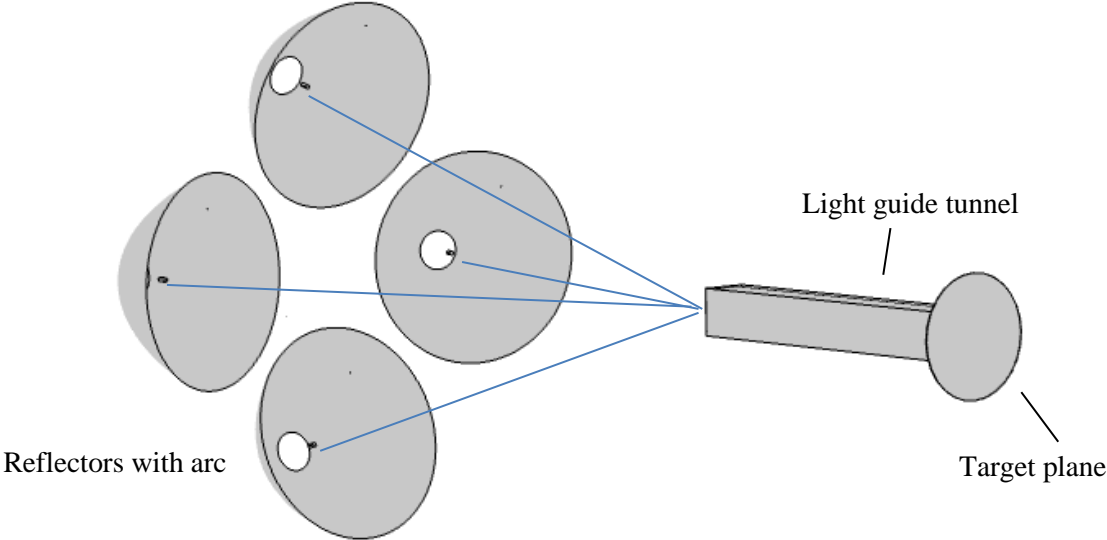


Figure 30: Geometric layout with tunnel.

The simulation of Figure 31 and Figure 32 shows the distribution of the four reflectors in a configuration shown in Figure 29 below the pictures information regarding the arc (arc length/diameter and axial displacement) and target distance. Figure 31 has a lot of parameters varied to get sense for the variation of the parameters and how they behave. Getting a flatter distribution is possible by putting the target away from the focal point and varying the arc position.

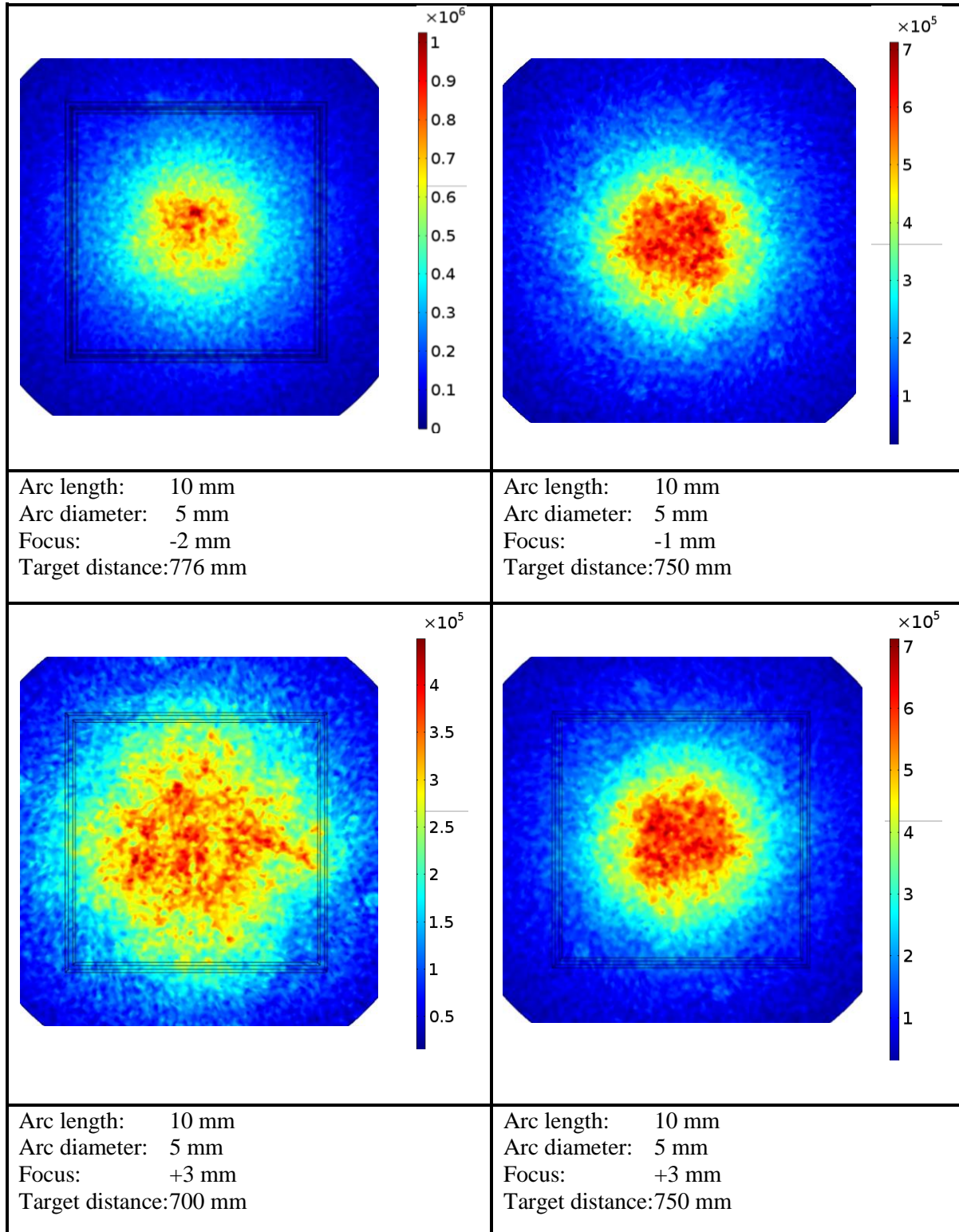


Figure 31: Ray tracing simulation using all lamps without light guide tunnel varying distance and arc position.

Figure 32 shows the simulation only varying the target distance, the focal point is at distance of about 770mm. Putting the target close to the focal point results in a high flux as shown in the right bottom picture on Figure 32. Putting the target closer to the light sources flattens the flux distribution and even seems to produce a square *flat distribution*.

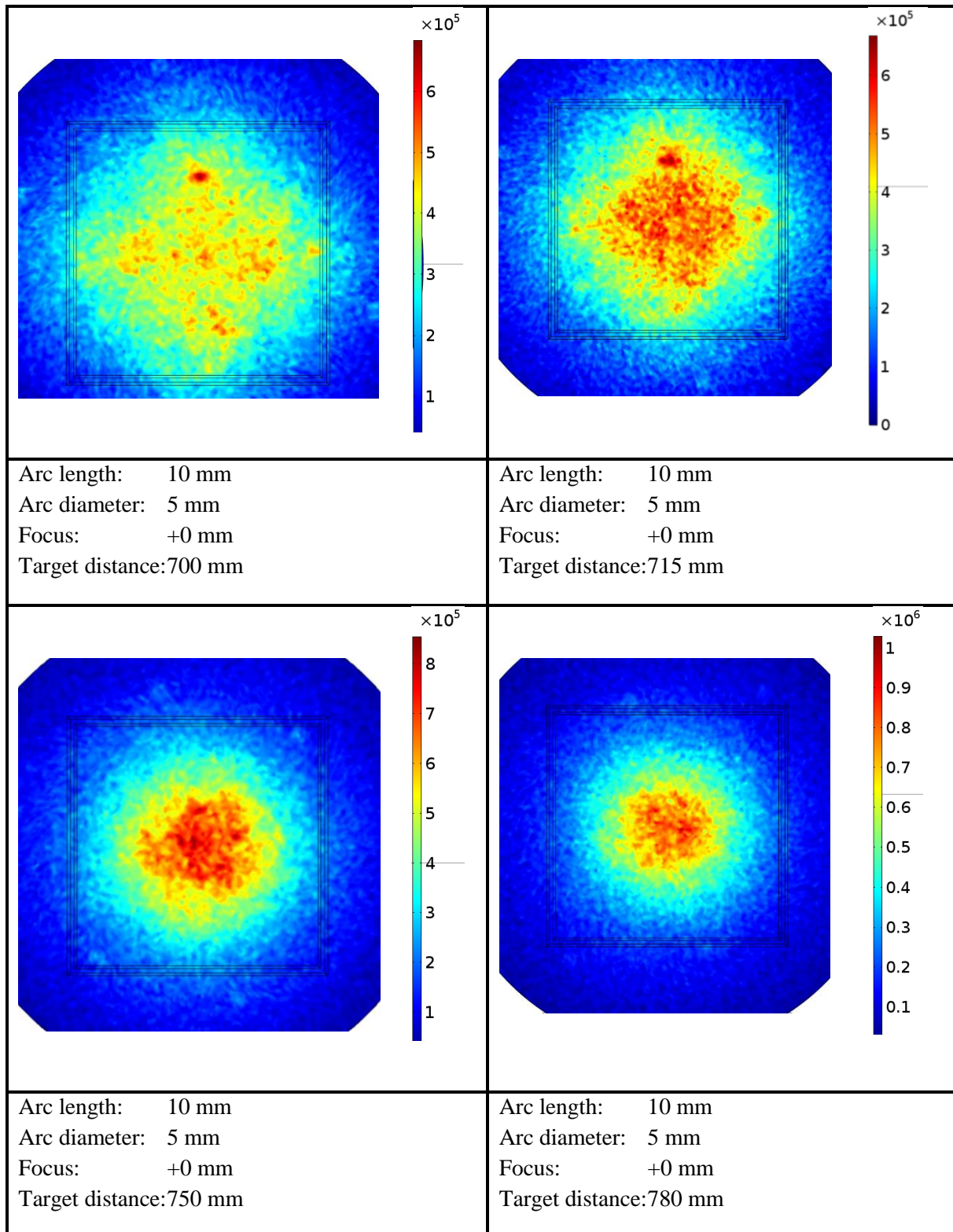


Figure 32: Ray tracing simulation using all lamps without light guide tunnel varying distance and arc position.

Figure 33 depicts the target plane of the simulation with only two arcs releasing light rays. These are the upper and the lower arcs. The results show that a longer light guide tunnel is beneficial for a *pillbox distribution* on the target. Furthermore, it shows that when a lower irradiation is wanted the HFSS can also work with only two lamps switched on.

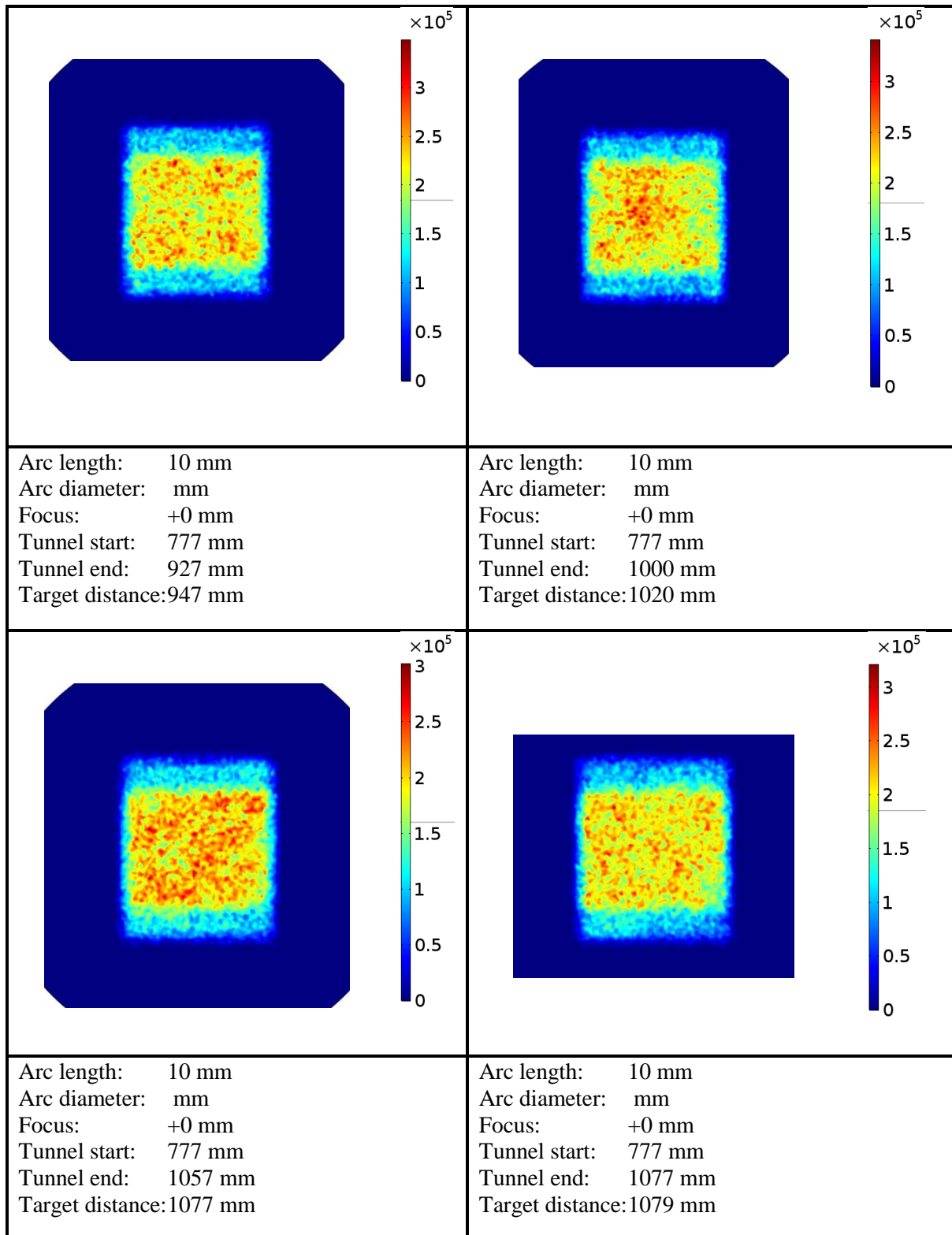


Figure 33: Ray tracing simulation using two lamps with light guide tunnel varying tunnel length and target distance.

Figure 34 and Figure 35 depict the target plane with all four arcs releasing light rays. The pictures of the irradiance on the target plane shown in Figure 34 show that a tunnel with about 120 mm length is not enough to smooth the irradiance distribution. Figure 35 shows that the shortest useful length for the tunnel lies between 150-200mm to reach desirable distribution. It also shows that longer light guide tunnels have more losses than shorter ones.

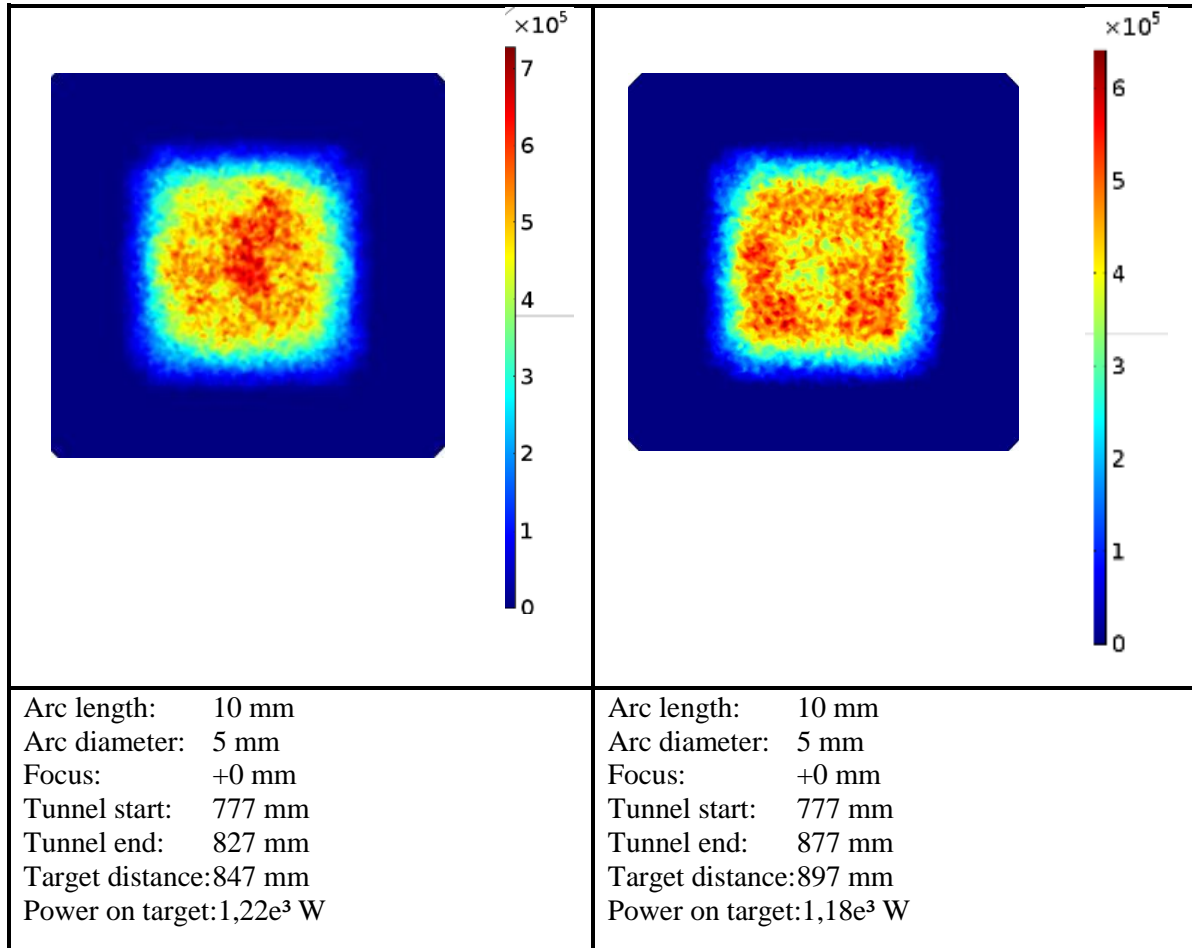


Figure 34: Ray tracing simulation using all lamps with light guide tunnel varying tunnel length and target distance.

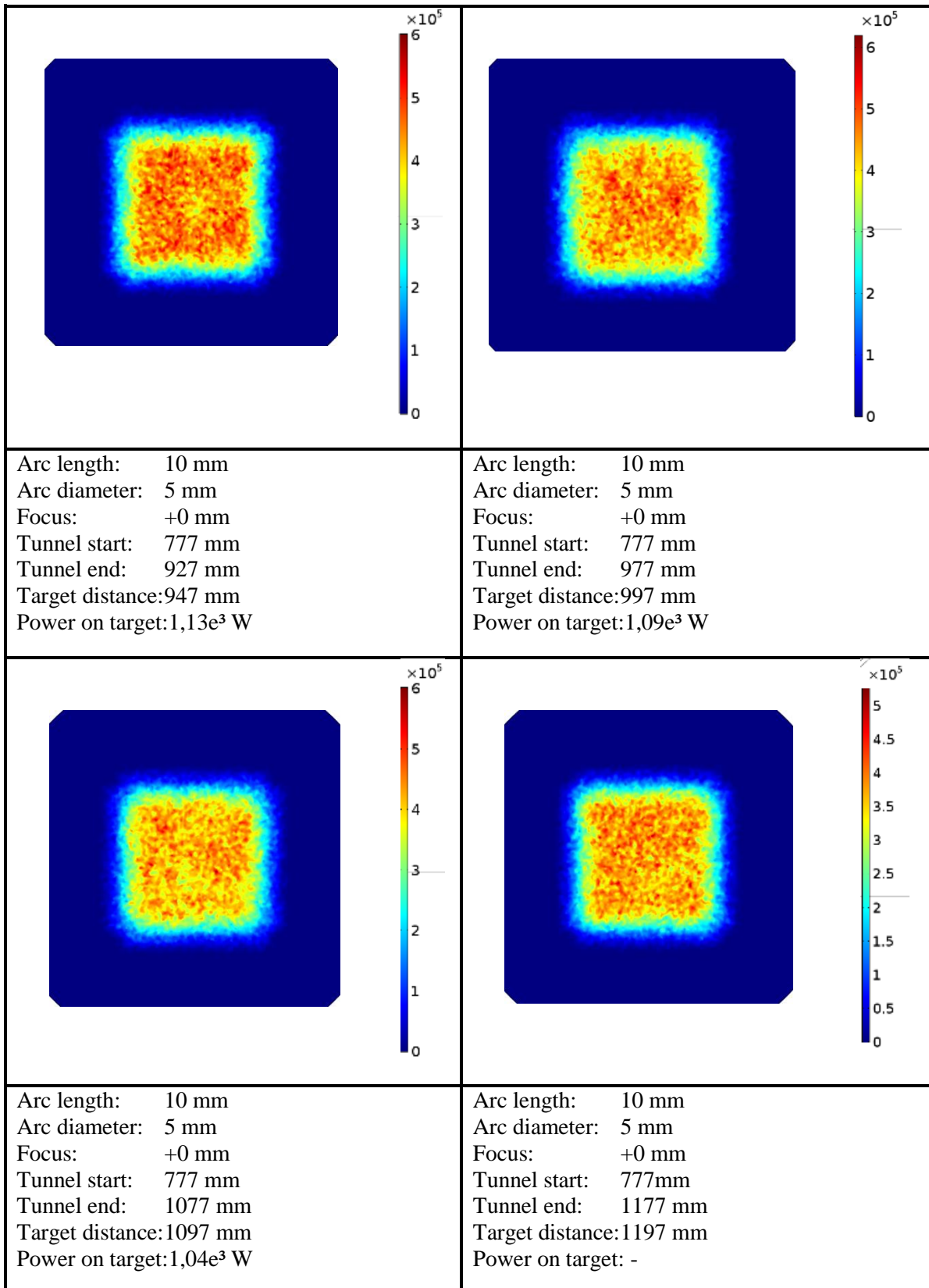


Figure 35: Ray tracing simulation using all lamps with light guide tunnel varying tunnel length and target distance.

Figure 36 and Figure 37 depict the target plane with all four arcs releasing light rays. The light guide tunnel has undergone a rotation of 45°. The pictures of the irradiance on the target plane show that a short tunnel has not enough length to transform the distribution to a smooth pillbox distribution. On the other hand, some shorter tunnel lengths showed a very interesting distribution of a “positive” and “negative” cross on the target plane. A long tunnel has similar behavior on the distribution as a non-rotated one.

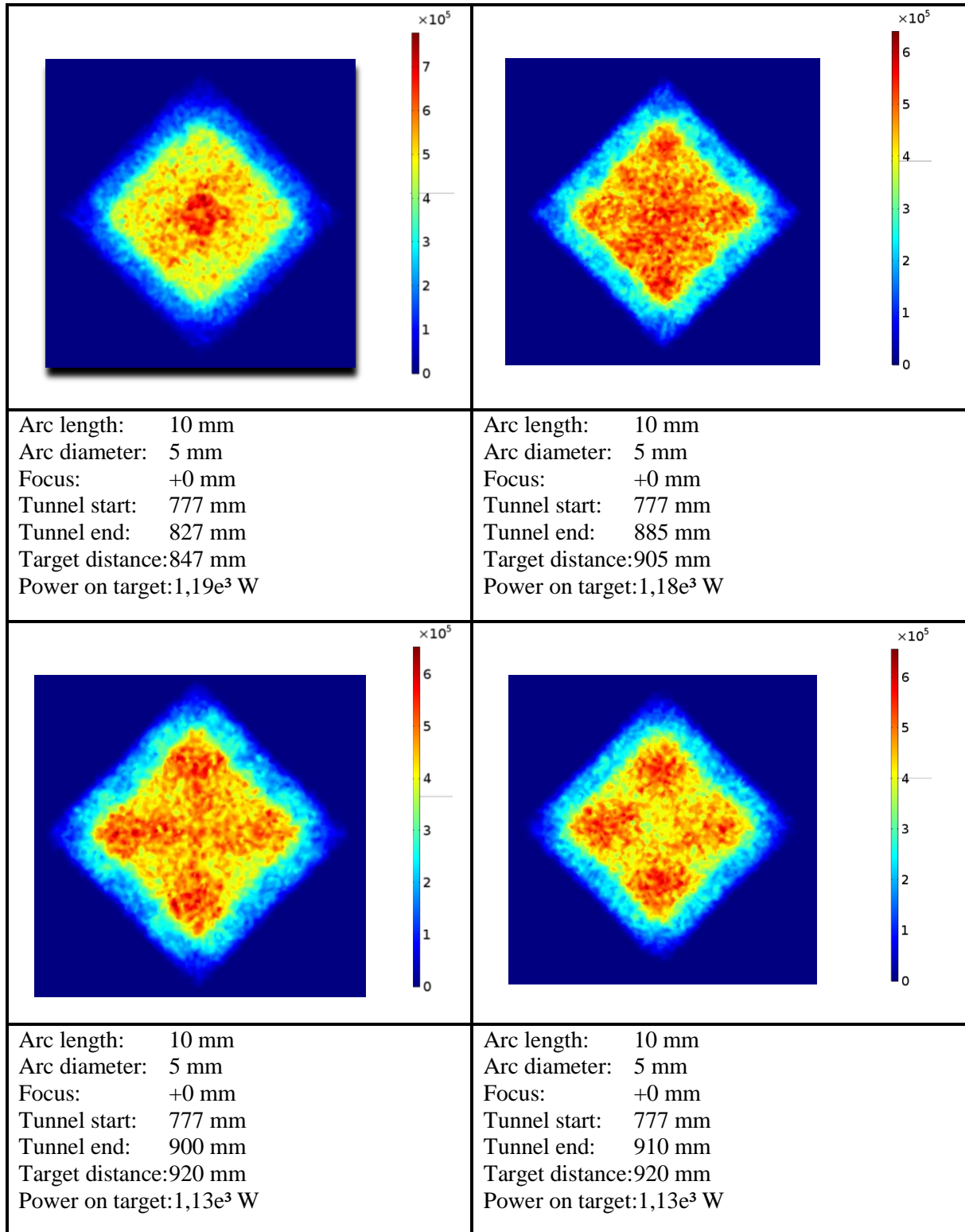


Figure 36: Ray tracing simulation using all lamps with a 45° rotated light guide tunnel varying tunnel length and target distance.

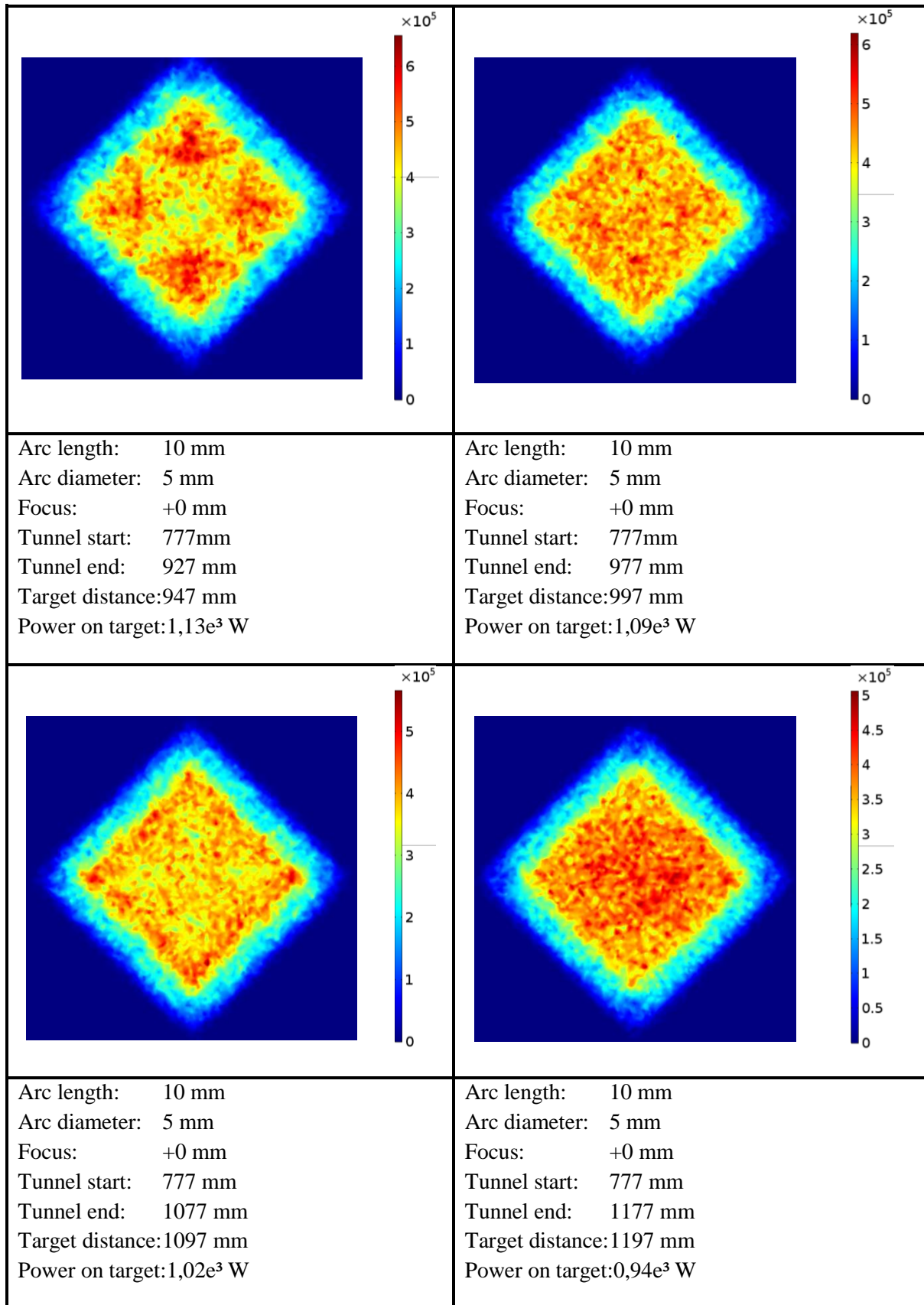


Figure 37: Ray tracing simulation using all lamps with a 45° rotated light guide tunnel varying tunnel length and target distance.

Figure 38 depicts the simulation of four reflectors with the real geometry manufactured reflectors that were obtained by 3D scanning of them. The result shows a flat distribution as needed for the HFSS. A very high amount of the light is focused into the tunnel resulting in high amount of radiative flux on the target plane. About 20 percent of the released radiative power is hitting the target plane.

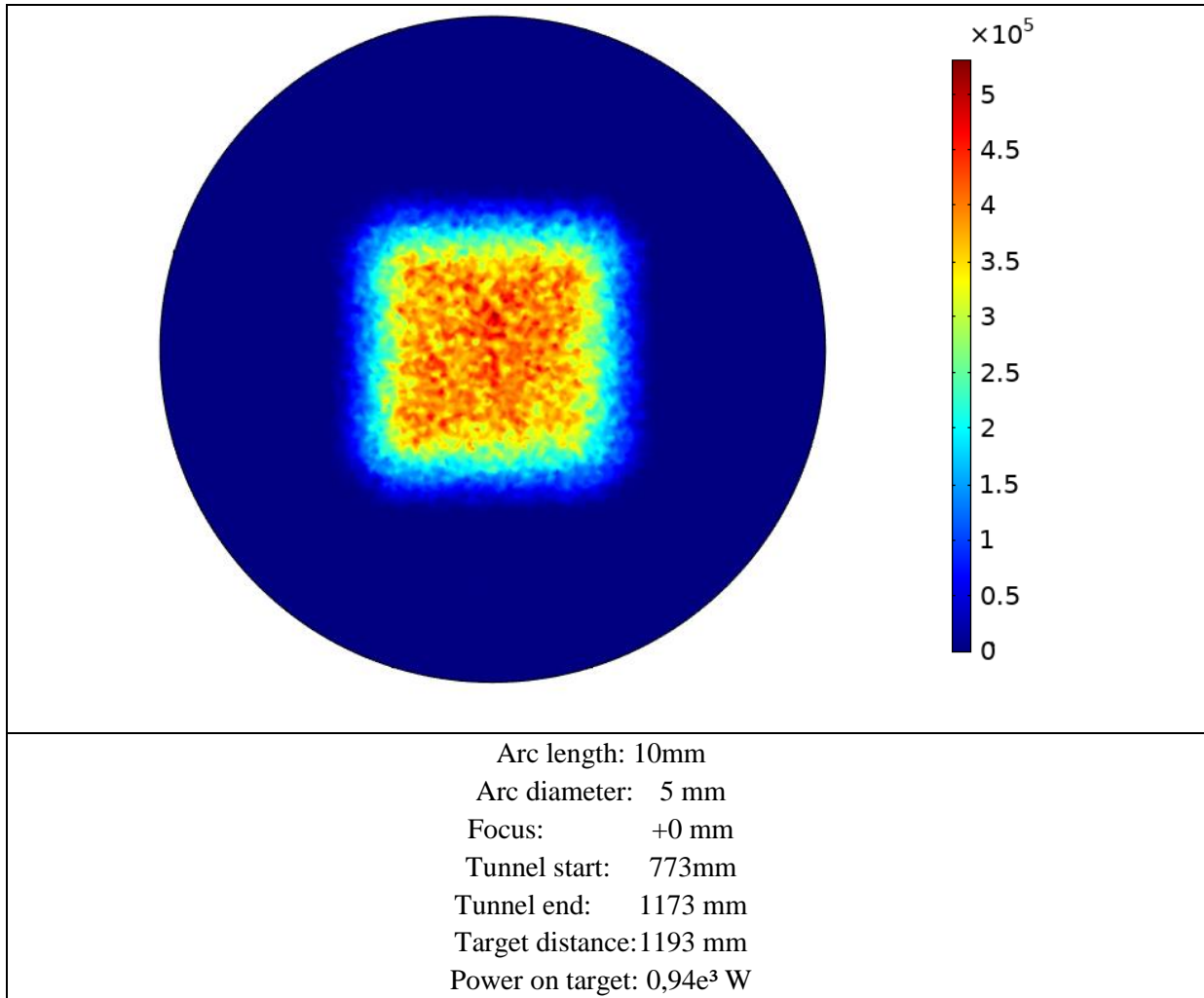


Figure 38: Ray tracing simulation light guide tunnel and as used reflector geometry of the 3D scanned reflector.

4.4 Ansys multiphysics

4.4.1 Air stream in casing

A computational fluid dynamic analysis has been set up to investigate the air stream through the casing. The temperature that is generated by the lamps must be cooled by forced convection. One of the easiest ways to achieve his was to use a fan that forces the air through the casing and out of the opening where the lamp sits. Finding the right fan is connected to finding out what pressure losses occur in the casing and throughout the hole. The opening only has a diameter of 26 mm which is already a challenge for most fans, but what makes the matter even more difficult is the fact that the lamp sits in the hole and blocks parts of it. The available area for the flow is only about 390 mm². The area available for the flow within the casing is about 5734 mm². This signifies a higher flow velocity in the casing. The flow speed within the casing can be seen in Figure 39. The overall pressure loss for the optimized system was calculated with about 24 Pa for an inlet flow speed of 2 m/s over a 60 mm diameter.

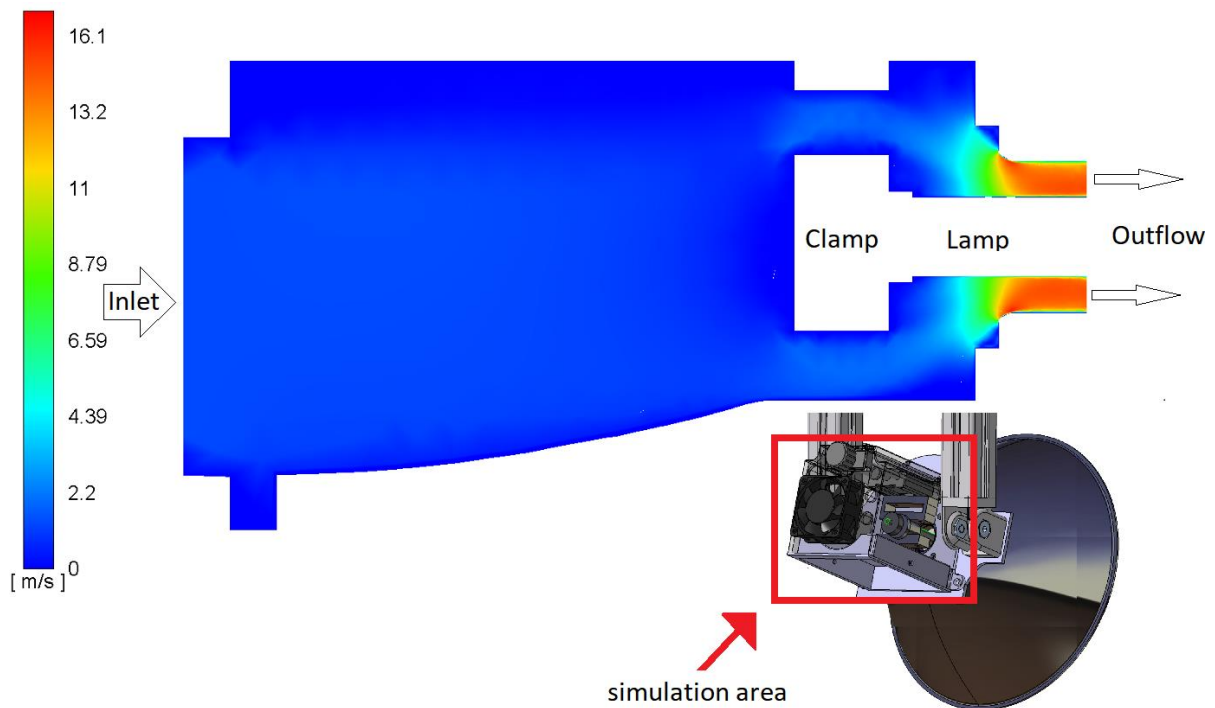


Figure 39: Casing simulation, velocity magnitude for air flow.

According to this simulated pressure loss a fan that can withstand the pressure drop of the system could be selected. The fan can be seen in Figure 58. To roughly validate, if the calculation was right and because a working forced convection is very important to get rid of the excess heat of the lamp, a prototype was built as seen in 7.4.

4.4.2 Temperature analysis of the clamp

The clamps are the parts that hold the lamp in position and some testing as shown later in chapter 7.1.2 revealed that the mounting points of the lamp become hot without forced cooling. Therefore, some investigations regarding the temperature distribution on the clamp have been conducted and during the process the final design for the clamp was worked out. This is especially important for the linear guide which consists of many plastic parts that cannot withstand temperatures of more than 90°C at maximum force load [35].

For the simulation a *thermal-transient analysis* was chosen. Since the heat flux from the lamp to the clamp is unknown, a temperature boundary condition on the clamp was chosen. This boundary condition sits on the area where the lamp socket, which holds one mounting end of the lamp, touches the clamp. All the other surfaces of the clamp except the upper side, which is the connection to the linear guide, have a convective boundary condition. The values for the boundary conditions were unknown but the idea was to optimize the part regarding temperature distribution on the top of the clamp and dissipate as much heat as possible. Therefore, the exact temperature values were not the goal of this simulation, but to lower the temperature on the top surface to reduce the risk of damage to the linear guide.

Table 7: Used data for simulation.

| | |
|----------------|-------------|
| Material | Aluminum |
| Temperature BC | 100°C |
| Convective BC | $100W/m^2K$ |

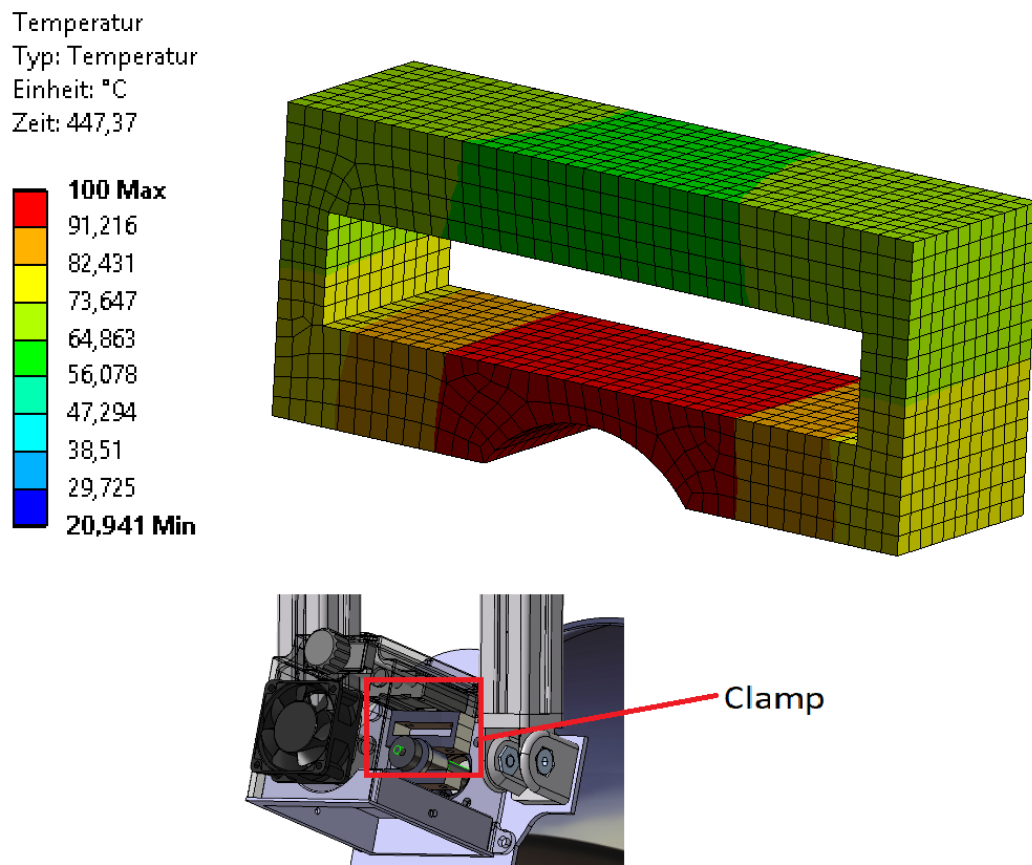


Figure 40: Thermal analysis of the clamp.

As a result, we got a temperature spread of about 35°C between the upper side and the place where the lamp is connected to the clamp. In 7.3 we tested the real temperatures of the clamp during a test run of the HFSS.

5 Component Selection

5.1 Lamps

The lamps are the source of light for the test set up. Several demands on the lamps are made and listed here.

- Costs
- Arc length
- Spectrum
- Mountability
- Power

Since the lamp market is very big only a small amount of different types of lamps were picked out before the utility analysis made.

The **costs** were considered, because lamps only have a limited lifespan until they must be replaced. To keep the recurring costs on a low level, this was a very important factor.

The **arc length** is of minor importance because of the test setup itself. If the HFSS should have a very high concentration factor this would be a very important part. In this HFSS the area that was illuminated was, compared to other HFSS, very big. The issue of the arc size is further discussed in 2.4.2.3

In case of the **spectrum**, there are no big tolerances allowed since the generated spectrum must be in the range of UV. If there is no UV light emitted, it was not accepted. Furthermore, the spectrum should fit well to the one of the sun, but here tolerances are allowed.

Mountability was an important part because of a faster installation and building time of the HFSS. Only one lamp type was available with a fitting socket, the others must be equipped with a self-built socket.

To simulate the sun with a high concentration factor, a certain amount of **power** is essential. Most of the lamps that did not make it to the utility analysis did not pass this step. Without high power lamps many small lamps are needed to obtain the amount of power needed on the specimen, but this would also mean that other components would have to be bought multiple times and that would raise the costs.

5.1.1 Lamp types utility analysis

Table 8: Utility analysis of different lamp types.

| | Importance Factor (IF) | Double ended Metal Halide | | Single ended Metal Halide | | Double ended Xenon Arc | | LED | |
|--------------|------------------------|---------------------------|-----------|---------------------------|-----------|------------------------|-----------|-----|-----------|
| | | | Total | | Total | | Total | | Total |
| Costs | 3 | 4 | 12 | 4 | 12 | 2 | 6 | 5 | 15 |
| Arc length | 1 | 2 | 2 | 2 | 2 | 5 | 5 | 4 | 4 |
| Spectrum | 3 | 3 | 9 | 0* | 0* | 3 | 9 | 4 | 12 |
| Mountability | 2 | 2 | 4 | 5 | 10 | 2 | 4 | 2 | 4 |
| Power | 3 | 5 | 15 | 5 | 15 | 5 | 15 | 1 | 3 |
| Sum | - | | 42 | | 39 | | 39 | | 38 |

*lamp production was discontinued during thesis (2018)

The chosen light sources are four *HMI 1200* double-ended metal-halide lamps with a color temp of 6000K. The arc gap is 10 mm long, the other dimensions can be seen in Figure 41 [36].

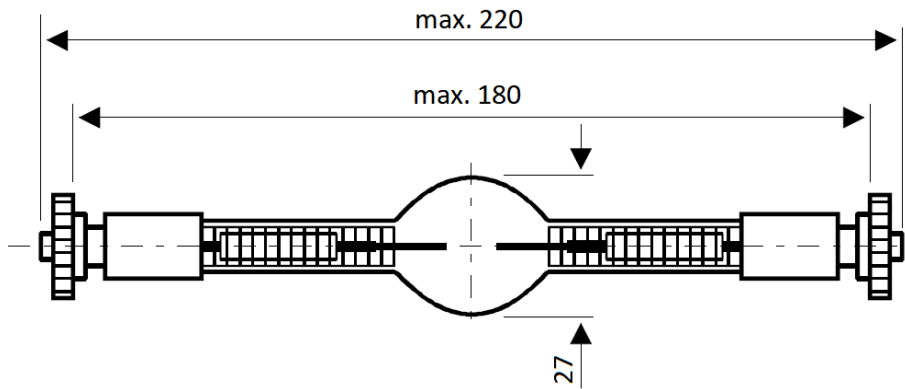


Figure 41: Osram HMI 1200 double ended metal-halide lamp [36].

5.2 Ballasts for metal-halide lamps

The ballasts are necessary because of the lamps that are used. Small lamps do not need ballasts, but high-power lamps need them to start and to operate. Different ways of trying to buy low cost ballast that are used to operate lamps for indoor gardening purposes did not deliver satisfying results. Therefore, other producers of ballasts are considered. Most of them are listed by the lamp producer but not all companies can still in business. During research, some cheaper Asian producers were considered too and one producer that was found who had a satisfying product is listed in Table 9.

5.2.1 Different producers

Table 9 shows some ballast producers who we contacted with our issue.

Table 9: List of ballast producers according to [37], [38], [39], [40].

| | IREM | Power Gems | ISLE Steuerungstechnik und Leistungselektronik GmbH | Ether Power Electronics |
|---------|---|---|--|---|
| Country | Italy | United Kingdom | Germany | China |
| Website | https://www.irem.it | https://powergems.com/ | www.isle-ilemanau.de | http://en.powerepe.com/ |
| Price* | + | + | ++ | +++ |

*subjective impression

Different quotations from all those companies were requested and *ISLE* and *Ether Power Electronics* (*EPE*) made the best two offers. Since price was the primary decisive factor, *EPE* was used as producer for the ballasts. The advantage of *ISLE* would have been the various adjustment parameters for the ballasts but included higher prices.

The chosen electronic ballast is from *EPE Ether Power Electronics* can supply the lamps with 100 percent power or a reduced power of 50 percent (not dimmable / only two power modes).

5.3 Reflectors

Most simulations are based on the shape variations of the reflectors. Different shapes result in different light guide properties. The properties of different shapes are indicated in 2.4. To get a useful reflector several computer simulations were performed to investigate one out of many useful shapes for the HFSS.

Producers of reflectors already have a range of different reflector shapes. Some of those reflectors have been investigated in the simulation to find a suitable shape for the HFSS.

The simulation results of the shapes of Asian reflector producers did not fulfill their purpose and therefore got rejected. This is not the fault of the producers because the reflectors are normally used as lampshades for households or industry with the main task of guiding as much light out of the reflector as possible, therefore focusing is not what these reflectors were built for.

The producers of reflectors for HFSS offer shapes. We have tested these shapes in the *COMSOL* simulation and their results were very good. This was expectable, since those reflectors are already optimized for HFSS and use high quality production processes to obtain a product with high average reflectance and high concentration factors. The disadvantages are that the reflectors are expensive and exceeded the cost limits set by us for this product.

Another attempt to fulfill the requirements of the reflector shape was to find a company that could produce the elliptical shape of the reflectors. The used process to form the reflectors was *metal spinning*. To produce the reflector a negative spinning-form of the reflector must be produced. This negative spinning-form is then clamped to the spinning machine. The final step is the metal spinning itself where a circular metal sheet is stretched over the spinning-form. The result is the final version of the reflector. The manufacturing of the negative spinning-form is very time-consuming which results in a high price for the form but can be compensated with the low costs of producing the reflectors. Since four reflectors are used in the HFSS, the costs of the form can be divided up to the four reflectors and therefore result in a desirable price.

Table 10 shows different reflector producers working with various manufacturing processes to produce the reflectors.

Table 10: List of reflector producers [41], [42], [43], [44].

| | Optiforms | Kaltbrunner in coop with Hegli und Gubler | Wilhelm Seidl Metalldrücker und Gürtler |
|----------------|---|--|---|
| Country | USA | Switzerland | Austria |
| Website | https://www.optiforms.com/ | https://www.kaltbrunner.ch/en/ http://www.hegkli-gubler.ch/ | https://www.metalldesign-wien.at/ |
| Processes Used | Electroforming | Metal spinning | Metal spinning |
| Coated | yes | yes | no |
| Price* | + | + | ++ |

*subjective impression

5.3.1 Material selection for the reflector

In 2.4 we investigated the properties of different materials but also knew that the high reflective coatings are expensive. Therefore, we decided to either use a pure aluminum surface or additionally put a thin anodic layer onto the surface.

6 Final Design of the GigiONE

6.1 The 3D concepts

Constructing the HFSS was done completely in Catia V5. Figure 42 shows the HFSS with four reflector units on the right side and the measurement table with the light guide tunnel and the compound table.

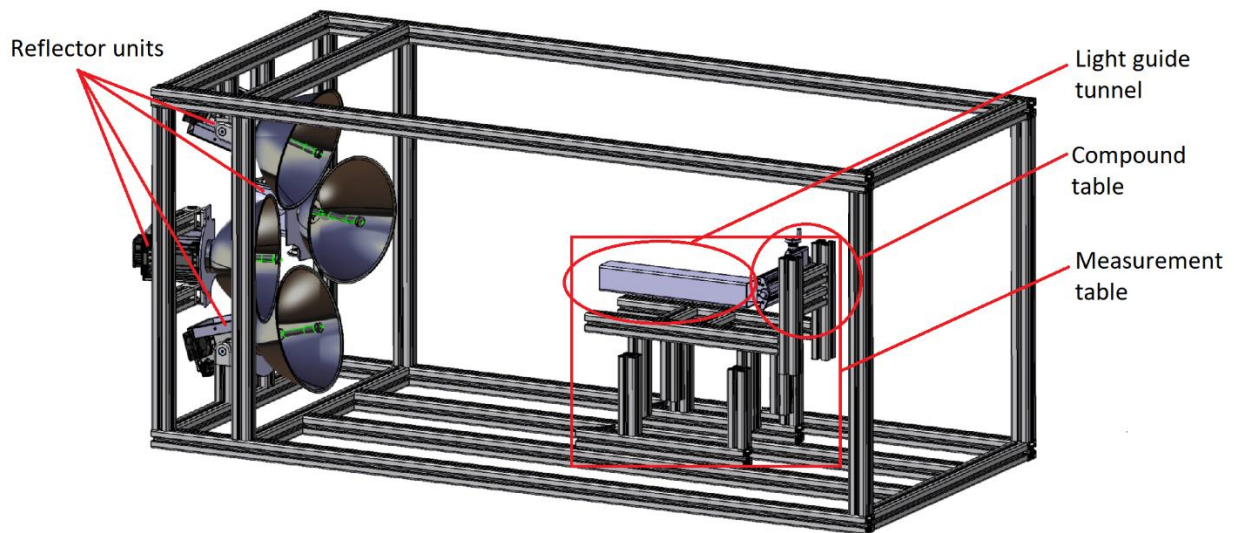


Figure 42: The 3D visualized HFSS facing the lamps to see components the sliding table.

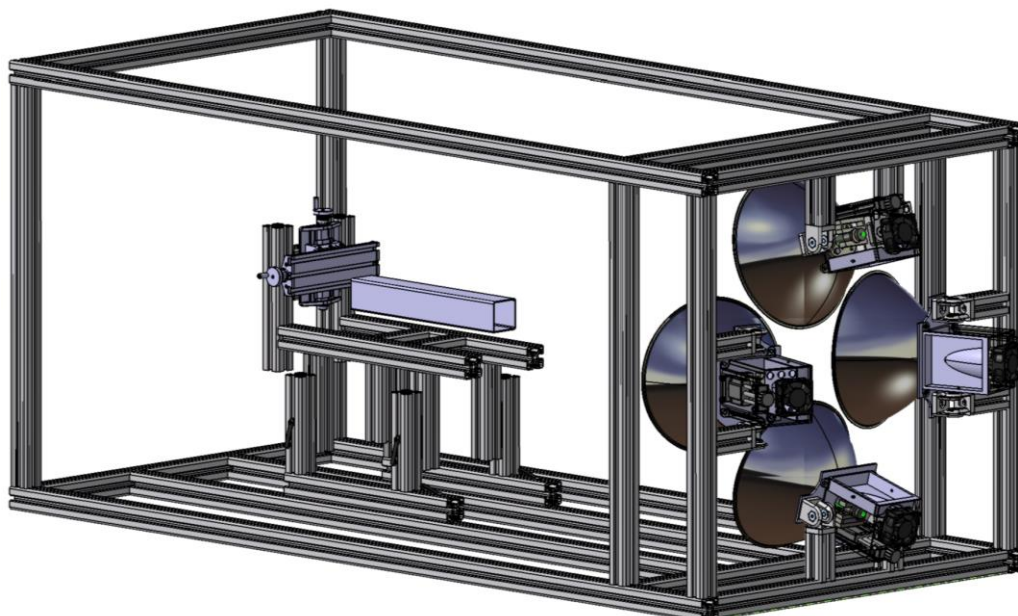


Figure 43: The 3D visualized HFSS facing the back of the reflectors units with the cooling fans.

Figure 44 and Figure 45 shows a detailed view of the reflector unit. In Figure 44 we can see the reflector front side, the *Osram HMI 1200* lamp and parts of the mounting plate. Figure 45 shows the backside of the reflector unit, the fan, the linear guide and the clamp can be seen inside of the transparent casing.

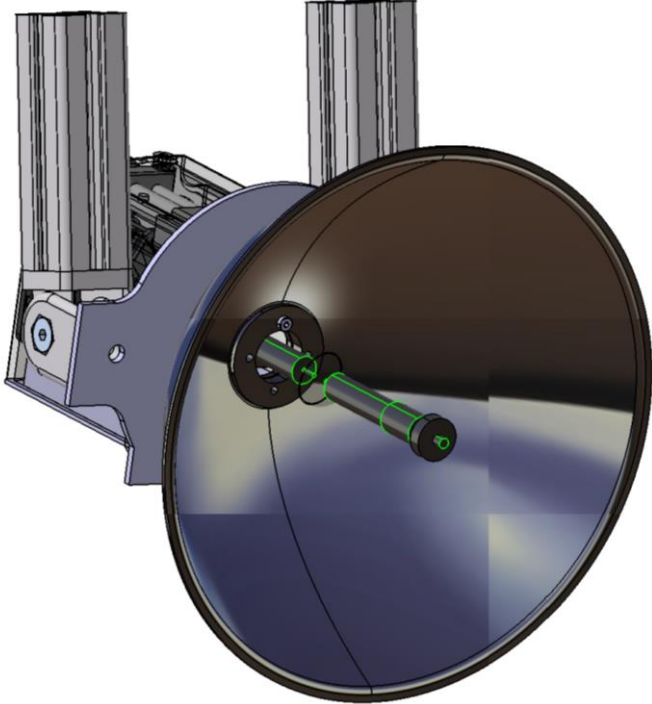


Figure 44: The 3D visualized lamp unit front side with lamp.

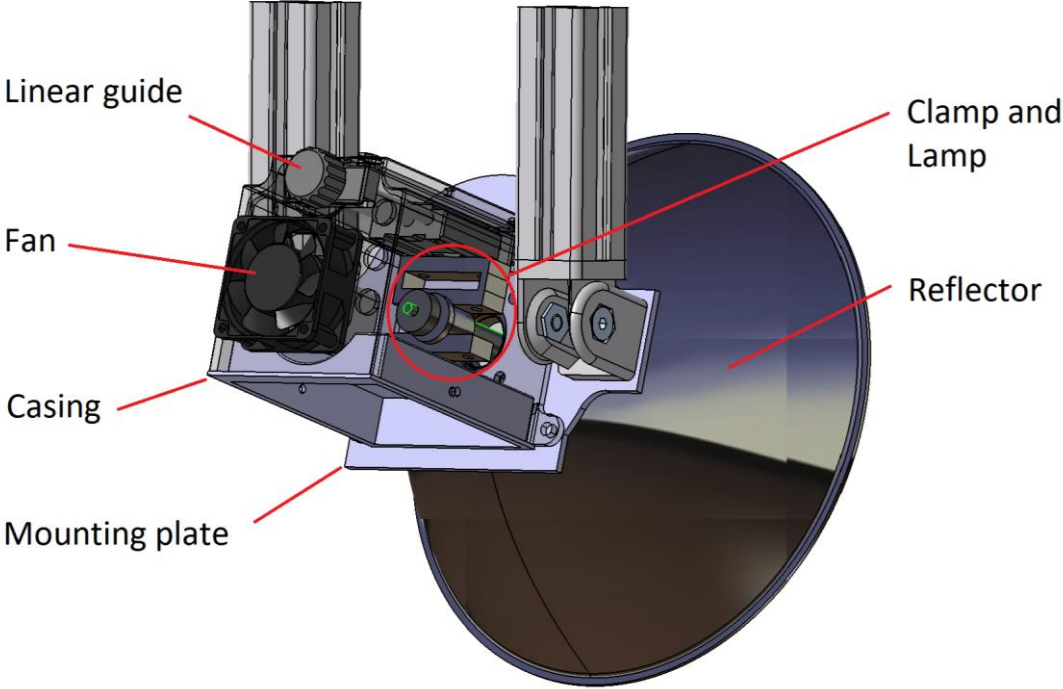


Figure 45: The 3D visualized lamp unit back side with fan, clamp and linear guide, the casing is transparent.

6.2 Safety considerations

The HFSS we built runs with UV emitting light sources. *Gerd Dibowski, Kai Esser* in “Hazards Caused by UV Rays of Xenon Light Based High Performance Solar Simulators” [45] discovered that critical levels of UV radiation are easily reached after a few seconds. The spectral measurements of the lamp in Table 15 also showed high UV emissions even with peaks in the UV. All team members got a sun burn when working too long in the exposed environment. Therefore, it is strongly advised to not enter the test room during a running experiment and if the room is entered then only with safety goggles that protect the eyes against UV light. To ensure that the safety goggles will block the UV light we even tested the goggles with our spectrograph. The test showed that the glasses reduced the intensity of the light behind the goggles and completely block the light below a wavelength of 400 nm. Furthermore, the skin should be protected with protective clothing to ensure that it is not getting damaged by the UV light (risk of severe sunburn and skin cancer).

6.3 System costs

The target of lowering the costs of the overall HFSS to a value of less than the cheapest found state of the art HFSSs presented in chapter 233 was reached. The costs of the different used and built parts can be found in Table 11.

Table 11: Costs of the assembled parts.

| | Quantity | Price per Unit [€] | Total Costs [€] |
|--------------------------------------|----------|--------------------|-----------------|
| Lamp | 4 | 80 | 320,00 |
| Ballast (incl. shipping (278,81)) | 4 | 316,68 | 1266,71 |
| Reflector | 4 | 189 | 945,00 |
| Reflector polishing | 4 | 100 | 400,00 |
| Mounting plate | 4 | - | 42,00 |
| igus® linear unit | 4 | 48,43 | 193,72 |
| ITEM® parts | - | - | 903,52 |
| ITEM® parts (own) | | - | 115,00 |
| Light guides | 3 | - | 84,00 |
| Papst® cooling fans | 4 | 36,15 | 144,6 |
| Additional items own production | | - | 299,99 |
| | | | 4714,44 |

7 Component Testing

7.1 Measurement of *Osram HMI 1200* metal-halide lamp

7.1.1 First testing

To see if the gravity has an influence on the lamps light arc a test was conducted to visualize possible deformations of the arc. The assumption was, that the lamps arc will deform.

7.1.1.1 Setup

The lamp axis was placed parallel to the ground surface as shown in Figure 46 and Figure 47.

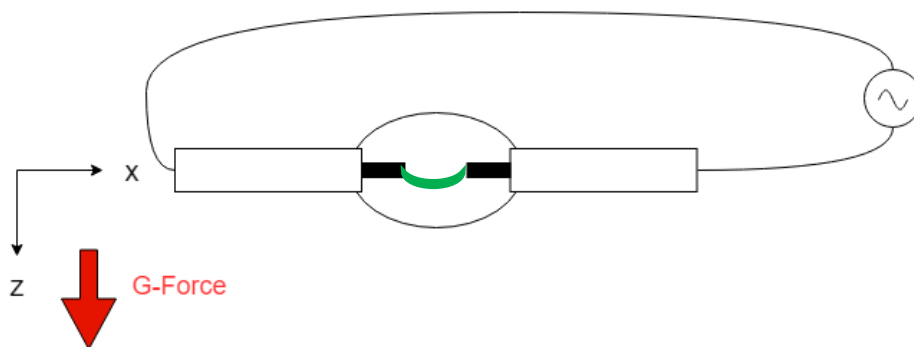


Figure 46: Lamp setup for arc visualization with expected arc deformation (green).

During operation the lamp releases a lot of light energy, which may cause critical heating of the camera and its components. The distance between lamp bulb surface and camera objective was around 300 mm.

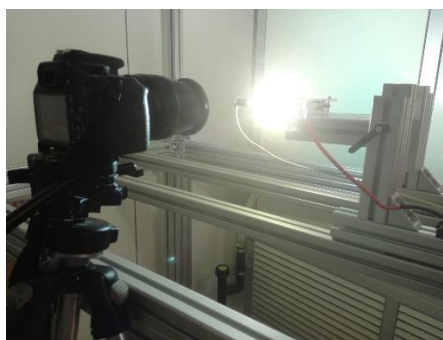


Figure 47: Camera positioning and Lamp positioning.

To reduce light power transmitted into the camera and avoid damage to the image sensor, as well as to have a clear view on the arc we placed a *ND1000* filter on the camera. The period of exposure was very short (1/4000 of a second) because of the bright light and to see the arc. The camera used for the test was a *Canon EOS 1200D*.








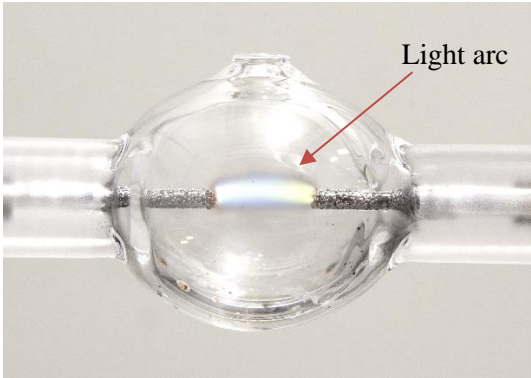
Figure 48: Used camera filter.

7.1.1.2 Arc of the lamp

The lamp should heat up till it reaches its operating temperature, this takes around 2 to 3 minutes. After the lamp heated up several pictures were taken to visualize the arc and its position. The glass bulb of the lamp has a little nipple on one side of the glass bulb which is possibly due to the production process. The nipple can be seen in Table 12 in the first picture, where also the position for the first test lamp can be seen. We positioned the lamp as the manufacturer advises the lamp to be positioned, with the glass nipple of the bulb pointing up. The following pictures are presented in the same sequence as they are taken.



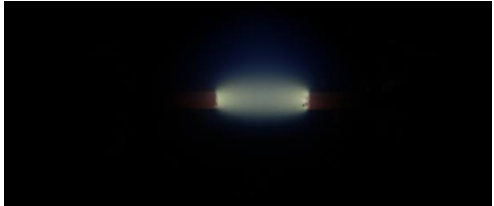

Table 12: Arc bending test.

| Information | Exposure time [sec] | Picture |
|------------------|---------------------|--|
| Bulb before test | 2.5 |  |
| Arc 1 | 1/4000 |  |
| Arc 2 | 1/1600 |  |
| Arc 3 | 1/800 |  |

| | | |
|---|-------|--|
| Arc 4 | 1/800 |  |
| Bulb and arc combined in photoshop for visualization purposes | 1/2 |  |

The analysis of the pictures showed that the arc is not bending down at all but does the exact opposite, it bends up. To see if the glass nipple has an influence on this phenomenon, we turned the lamp 180 degrees to have the nipple pointing to the ground to observe if the arc bends down.

Table 13: Arc bending test 2.

| Information | Exposure time [sec] | Picture |
|------------------|---------------------|--|
| Bulb before test | 1/6 |  <p data-bbox="1027 842 1358 875">Glass nipple pointing down</p> |
| Arc 1 | 1/640 |  |
| Arc 2 | 1/640 |  |
| Arc 3 | 1/640 |  |



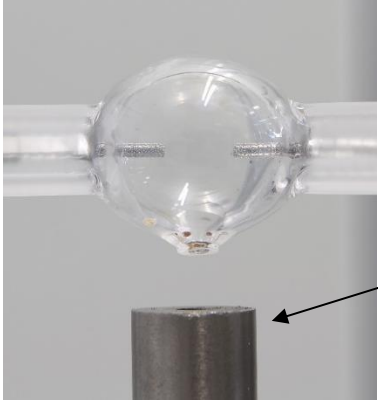
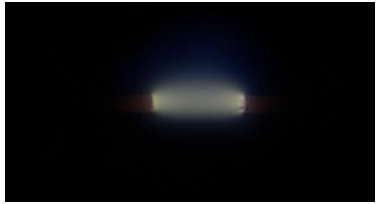





| | | |
|-------|-------|--|
| Arc 4 | 1/640 |  |
| Arc 5 | 1/640 |  |

Table 13 In Table 13 the first picture shows that the nipple of the lamps is pointing downwards but it seems as it does not influence the arc at all. The first pictures that were taken during heat up phase showed that the arc is not bending upwards, but the last pictures showed that after some waiting period the lamp arc is bending up again. This also corroborated our first thoughts that the arc is influenced by a strong *internal convection* due to the very hot plasma arc and the (compared to the arc) cold outer glass. This very high temperature differences may lead to density gradients within the bulb and forces the gas to rotate. This rotation forces the arc to bend upwards.

The third part of the test contained a neodymium magnet to see if a magnetic field influences the arc of the lamp and may pull the arc down to the center.

Table 14: Arc bending test 3 with magnet.

| | Exposure time [sec] | Picture |
|------------------|---------------------|--|
| Bulb before test | 1/8 |  |
| Arc 1 | 1/640 |  |
| Arc 2 | 1/640 |  |
| Arc 3 | 1/640 |  |

| | | |
|---------------------------|-------|---|
| Arc 4 | 1/640 |  |
| Arc 5 | 1/640 |  |
| Arc 6 (removed magnet) | 1/640 |  |

At the beginning of the test in Table 14 no difference to the second test of Table 13 was recognizable but after some minutes where the arc would normally bend up the same way as in Table 13, the phenomena did not occur again. Therefore, we saw that we can influence the arc with a magnetic field. To see if this was caused by the magnet we removed the magnet for the final pictures and clearly saw that the arc is bending up again.

The magnetic field that we used was about 0,012 Tesla in the arc volume and the distance between the surface of the magnet and the arc volume was about 25 mm. This was measured with a Teslameter model 904T by *Magnetic Instrumentation Inc.*

7.1.2 Second testing

7.1.2.1 Setup

For the tests the *HMI 1200* lamp was placed five meters away from the spectrograph a *Starline AvaSpec-2048* from *Avantes* as shown in Figure 49. This was necessary because of the high light emission that was produced by the *HMI 1200* lamp which otherwise would have resulted in measurements out of the measurement range of the spectrograph. The lamp was fixed in a rigid lamp holder that was placed on the ground Figure 50.

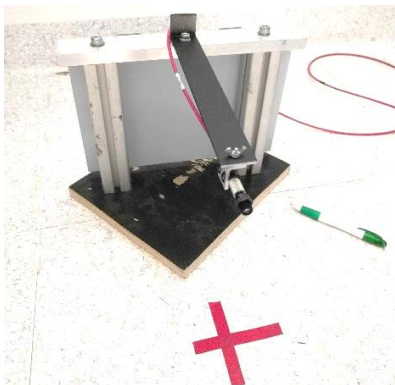


Figure 49: Spectrograph

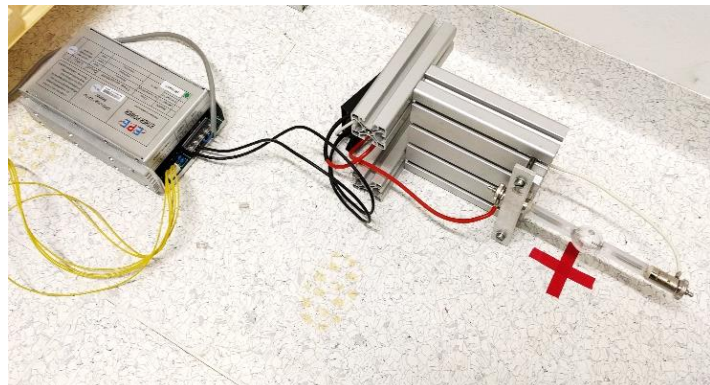
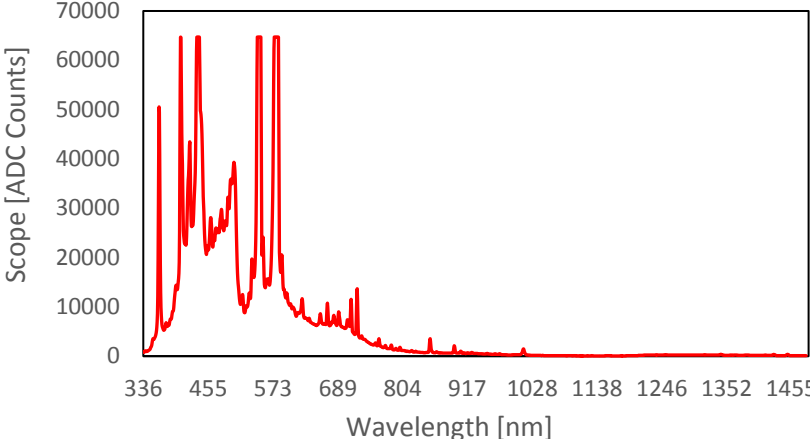
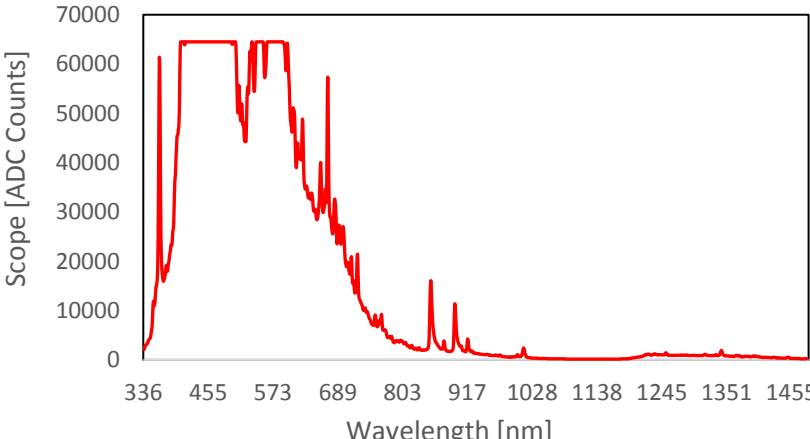
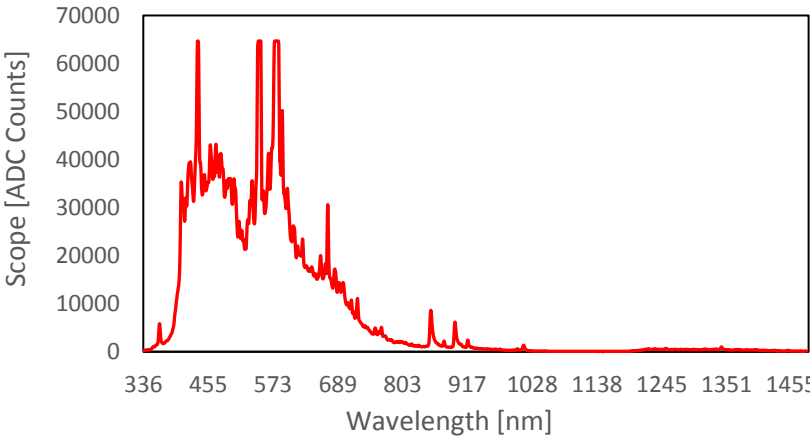


Figure 50: Lamp in lamp holder.

7.1.2.2 Results

We tested the lamps in the two different power modes. One power mode is 50 percent and the other one is 100 percent. As the results show some peaks in the shorter wavelength region occur. The peaks can be seen more clearly when the lamp is operated at lower power than when it is operated at high power. This means that a higher lamp power has a beneficial input for our needed spectrum, because it reduces the peaks and gives us a closer match to the solar spectrum. The second graph showed us that even the 5-meter distance between the *HMI 1200* lamp and the spectrograph was not enough to reduce the light intensity to a measurable range. Therefore, we chose to indirectly measure the 100 percent mode to receive the spectrum. The results are summarized in Table 15.

Table 15: Light spectrum test.

| Test Setup | Graph |
|---|--|
| HMI 1200 Direct view 50% power |  |
| HMI 1200 Direct view 100% power |  |
| HMI 1200 indirect view 100% power |  |

7.2 Reflectivity of aluminum

The reflectivity of different panels of aluminum was tested to figure out how different surfaces and purity influences the reflectivity of the material. All the samples were provided by the Austrian company *AMAG* and had a purity of 99,5 percent and more. The surfaces of the test samples were very different from close to a mirror surface to very gray and rough.

7.2.1 Setup

This was part of the measurement process of 7.1.2.1 but was expanded by aluminum plates that acted as a mirror to reflect the light produced by the *HMI 1200* lamp. For measuring, the spectrograph was rotated 180 degrees and to directly face the aluminum plate. To have the same path length for the light (5m) as in 7.1.1.1 we placed the spectrograph and the metal plate holder as depicted in Figure 51. We placed them closer to the lamp to still have the 5 meter path length for the light.

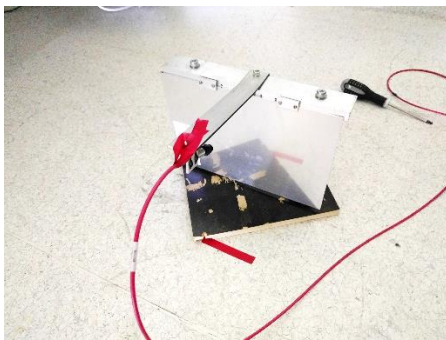


Figure 51: Plate holder and spectrograph.



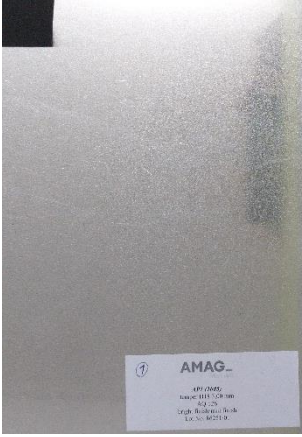

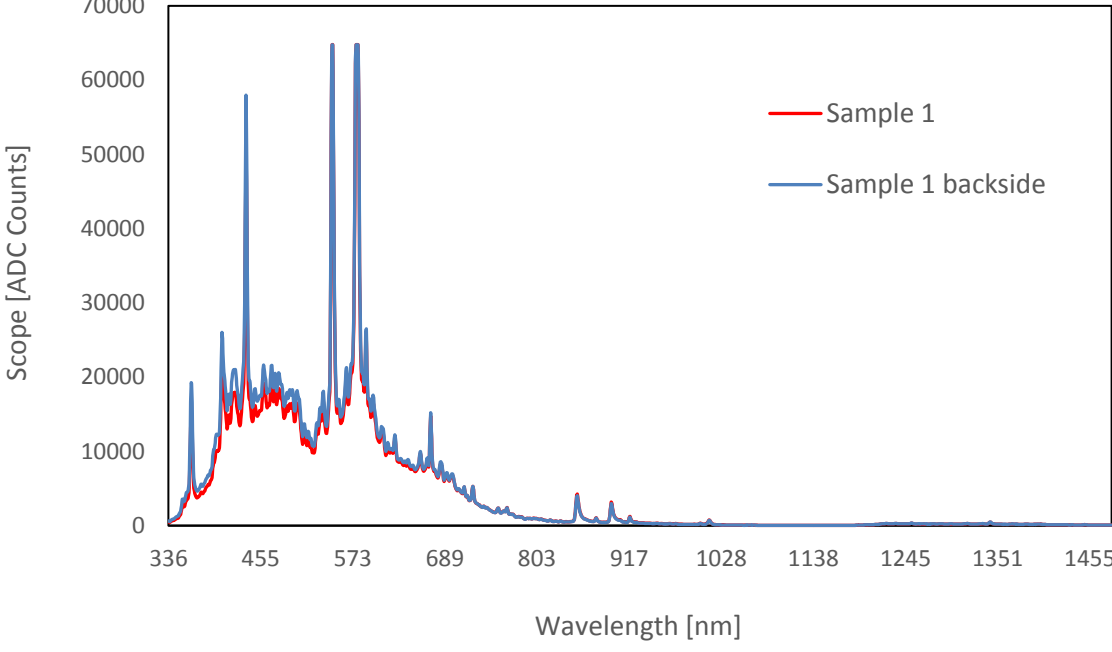
Figure 52: Plate holder in test mode.

7.2.2 Results

The results contain the reflected spectrum of the aluminum plates with the *HMI 1200* lamp as light source. Some of them were so specular that we had the same problem as in the test setup for the lamp spectrum in 7.1.2.2. Therefore, we sometimes had to manipulate the setup to get the desired results. Furthermore, we put a scale from gray (1) to mirror (10) in the results to validate the surface which gave us the possibility to get a sense for diffuse and specular reflectance.

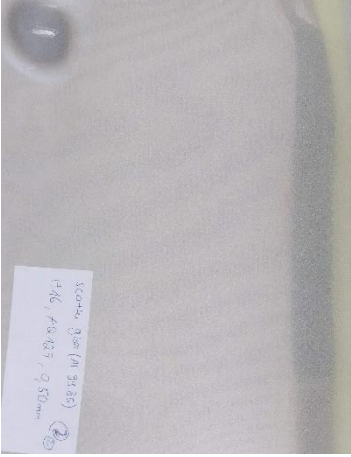

In Table 16 sample 1 is depicted. Here the results of the two sides got a spectrum that nearly matches. Since it was the first sample we think the test had some uncertainties and therefore the light intensity of both results was very low.

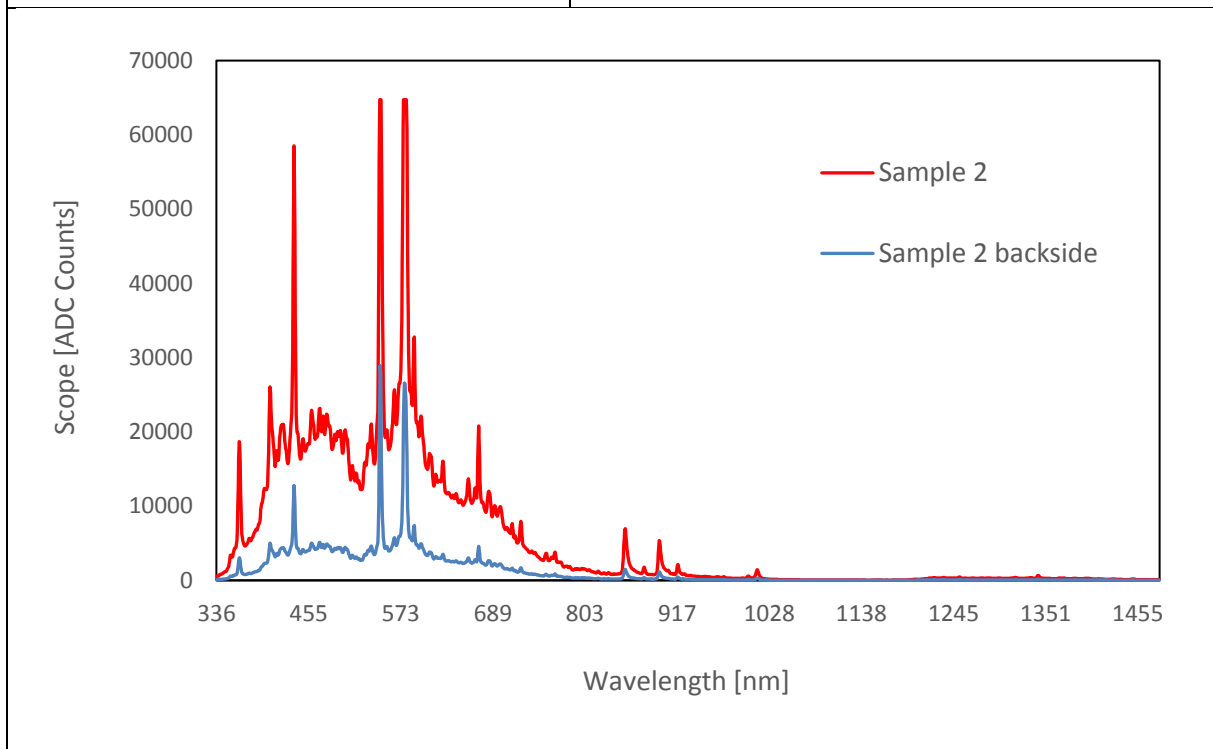
Table 16: Reflectivity test sample 1.

| Sample 1 | Sample 1 backside |
|--|--|
|  |  |
| <p style="text-align: center;">Al 99,85 Gray-Mirror-Scale: 4</p> | <p style="text-align: center;">Al 99,85 Gray-Mirror-Scale: 7</p> |
|  | |

In Table 17 sample 2 is depicted. Here the results of both sides differ in light intensity, but the spectrum was also very similar. The light intensity difference between the front and the back side is probably due to the different surface.

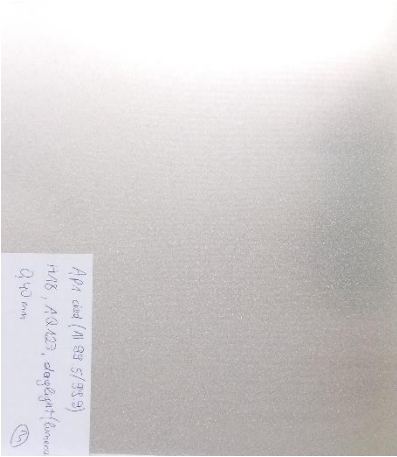

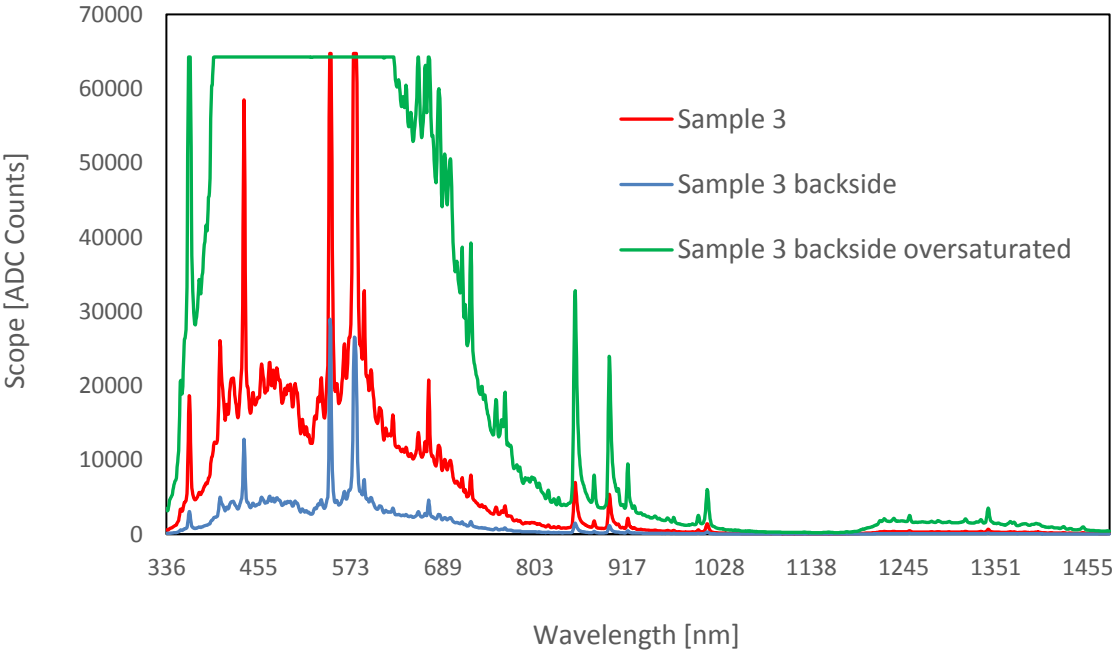
Table 17: Reflectivity test sample 2.

| Sample 2 | Sample 2 backside |
|---|--|
|  |  |
| <p style="text-align: center;">Al 99,85 Gray-Mirror-Scale: 4</p> | <p style="text-align: center;">Al 99,85 Gray-Mirror-Scale: 2</p> |



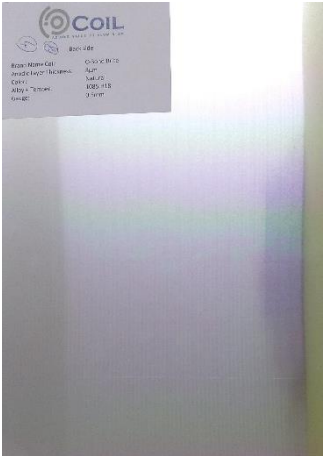

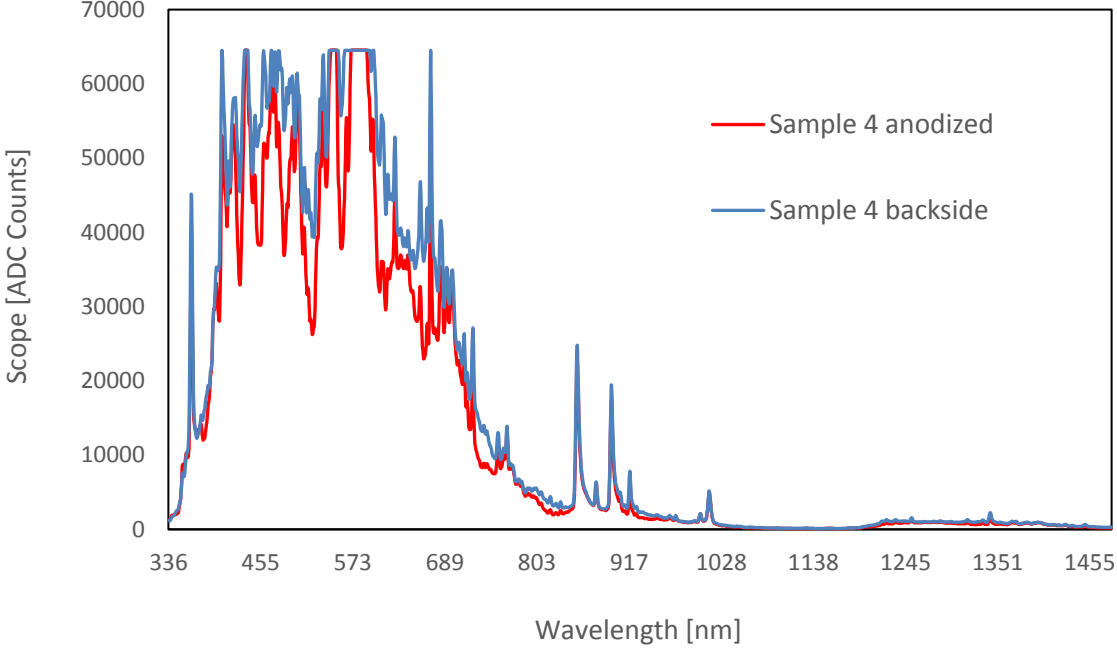
In Table 18 sample 3 is depicted. Here the results of both sides differ in light intensity, but the spectrum was also very similar. The backside was so specular that the results went above the upper threshold of the sensor. To still get a result we modified the test by turning the sensor slightly to the side. The light intensity difference between the front and the back side is probably due to the different surface.

Table 18: Reflectivity test sample 3

| Sample 3 | Sample 3 backside |
|--|---|
|  |  |
| <p style="text-align: center;">Al 99,5/99,9 Gray-Mirror-Scale:2</p> | <p style="text-align: center;">Al 99,5/99,9 Gray-Mirror-Scale: 6</p> |
|  | |

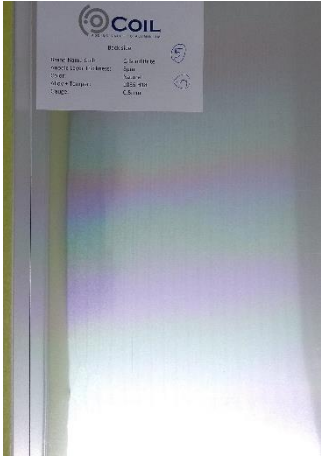

In Table 19 sample 4 is depicted. This sample has an anodized frontside and an untreated backside. The results of both sides differ in case of the spectrum, but the light intensity was in the same range.

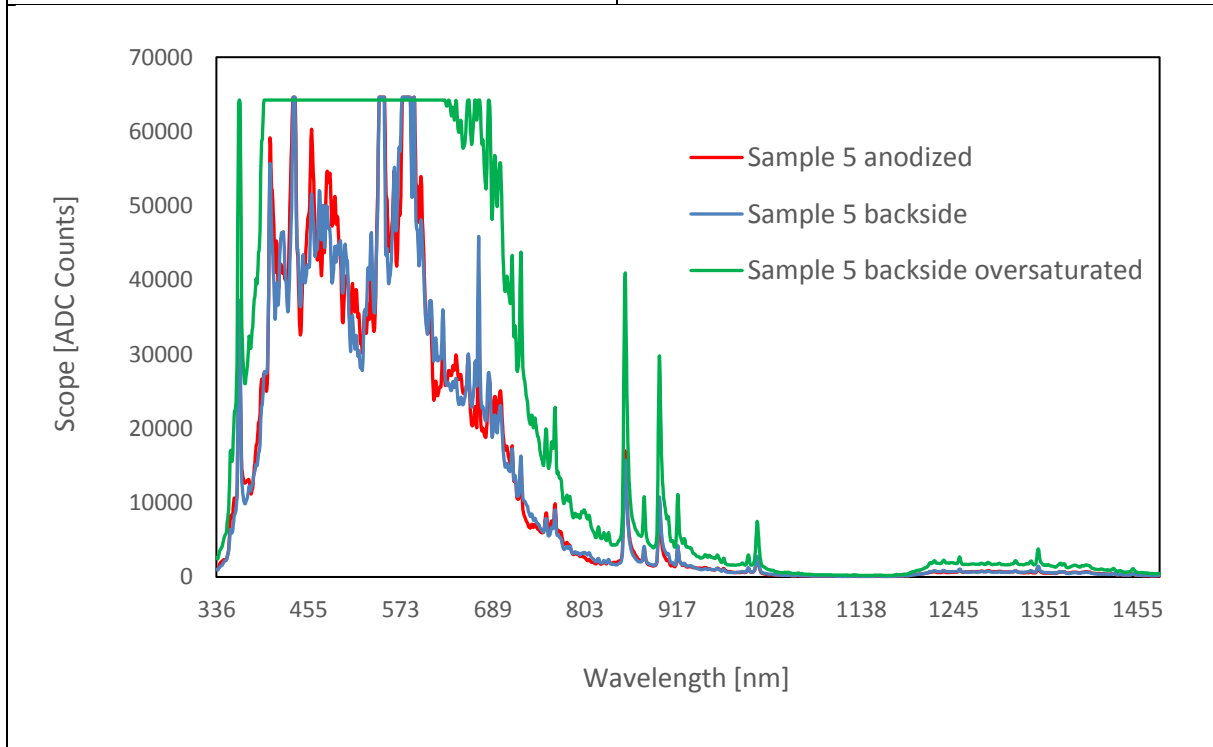
Table 19: Reflectivity test sample 4.

| Sample 4 anodized | Sample 4 backside |
|--|--|
|  |  |
| <p>Al 99,85 Anodic layer of 5µm Gray-Mirror-Scale: 4</p> | <p>Al 99,85 - Gray-Mirror-Scale: 6</p> |
|  | |

In Table 20 Table 17 sample 5 is depicted. This sample has an anodized frontside and an untreated backside. The results of both sides differ in spectrum and in terms of light intensity the backside was far better than the front side. To get a useful result we had to modify the sensor arrangement to lower the light intensity.



Table 20: Reflectivity test sample 5.

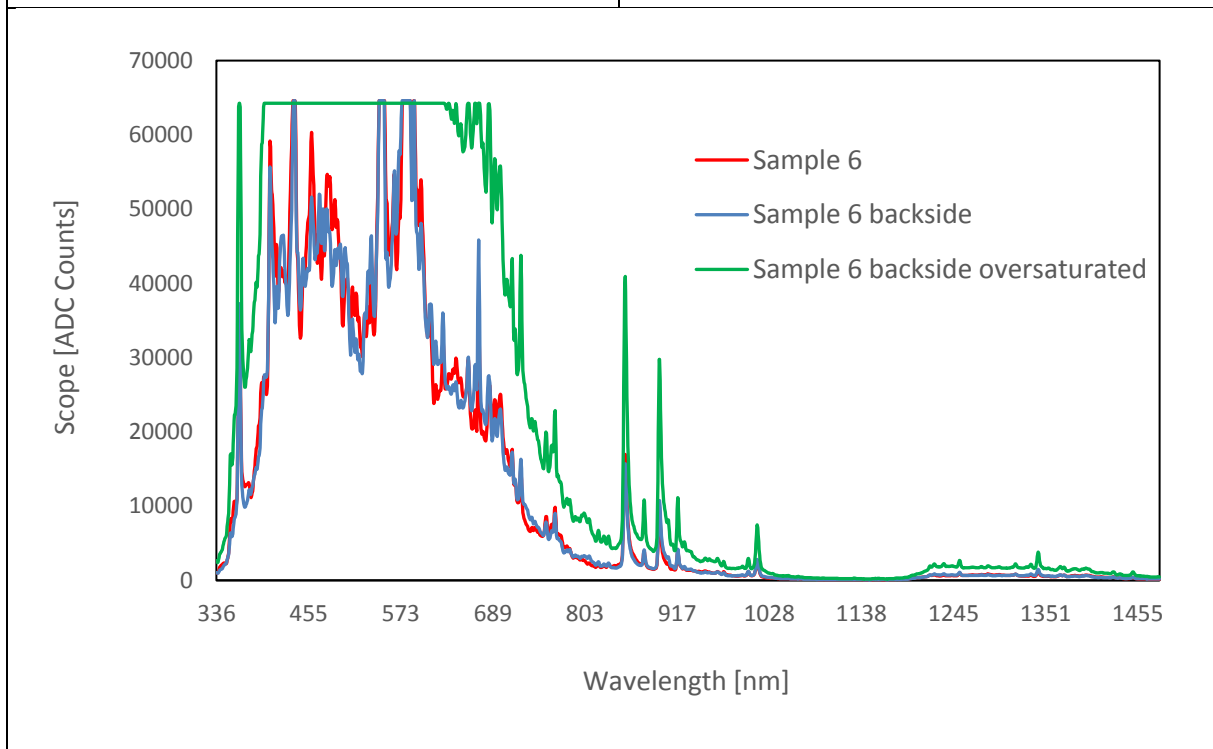
| Sample 5 anodized | Sample 5 backside |
|--|---|
|  |  |
| <p style="text-align: center;">Al 99,85 Anodic layer of 5µm Gray-Mirror-Scale: 3</p> | <p style="text-align: center;">Al 99,85 - Gray-Mirror-Scale: 6</p> |



In Table 21 sample 6 is depicted. Here the results of the two sides got a spectrum that nearly matches when the light intensity was reduced. The backside was too specular which resulted in an overflow for the sensor and therefore we modified the sensor by turning it a little bit to the side.

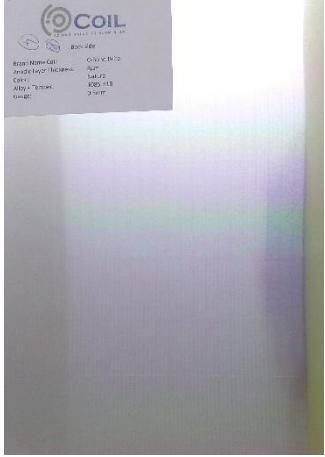
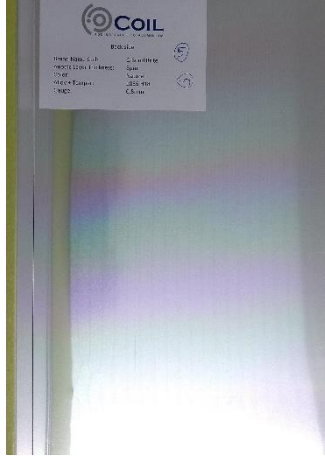
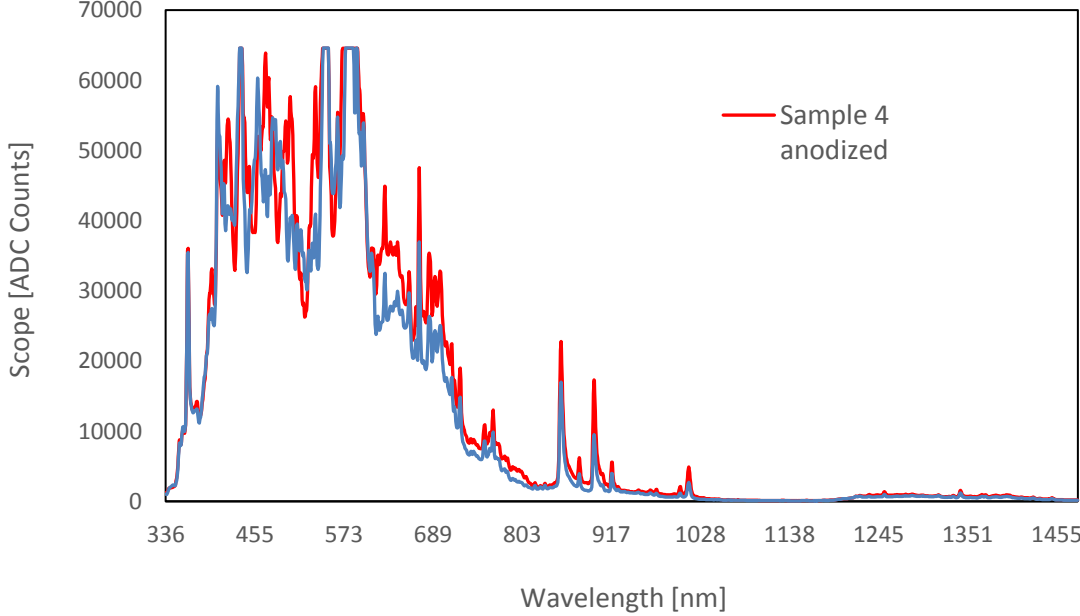
Table 21: Reflectivity test sample 6.

| Sample 6 | Sample 6 backside |
|---|--|
|  |  |
| <p style="text-align: center;">Al 99,85 Gray-Mirror-Scale: 4</p> | <p style="text-align: center;">Al 99,85 Gray-Mirror-Scale: 8</p> |



To compare both anodized samples we combined the results of both samples in Table 22. The result showed that sample 4 with the slightly better surface has some more specular wavelengths while others are the same as in sample 5.

Table 22: Reflectivity test anodized samples.

| Sample 4 anodized | Sample 5 anodized |
|--|--|
|  |  |
| <p style="text-align: center;">Al 99,85 Gray-Mirror-Scale: 4</p> | <p style="text-align: center;">Al 99,85 Gray-Mirror-Scale: 3</p> |
|  | |

7.3 Component temperature testing

Early phases of lamp testing demonstrated that the lamp generates a high amount of heat, especially the mounting points of the lamp were highly interesting for further design aspects. The mounting points showed high temperatures during the first lamp testing's. This could have led to problems with the used materials and components. To reduce the risk of temperature problems a CFD analysis was conducted to investigate the airstream through the casing (see section 4.4.1.).

Some components of the HFSS tend to get very hot especially those components which are directly radiated by the lamp. Therefore, a test under working conditions was conducted to find out what temperatures are reached by the components.

7.3.1 First setup temperature test

For the setup one reflector unit (Lamp unit 3) was equipped with temperature sensors (Ballast, Clamp, Mounting Plate and Reflector). For the data acquisition we used a multi-channel voltmeter *RIGOL M300*.

7.3.2 First results temperature test

The first part of the test was conducted with a running fan until we reached a stable condition. For the second part we switched the fans off to validate, if the fan air cooling system is effective. The results for both tests are combined in Figure 53. As the diagram shows the air cooling system is working well. The temperature increase after about 1300 seconds proves that the fan has an influence on the system. Also, the temperature of the clamp which was a critical component is cooled well since the temperature never went above 50°C. The mounting plate should not exceed 80°C for a longer period in order to harm the casing.

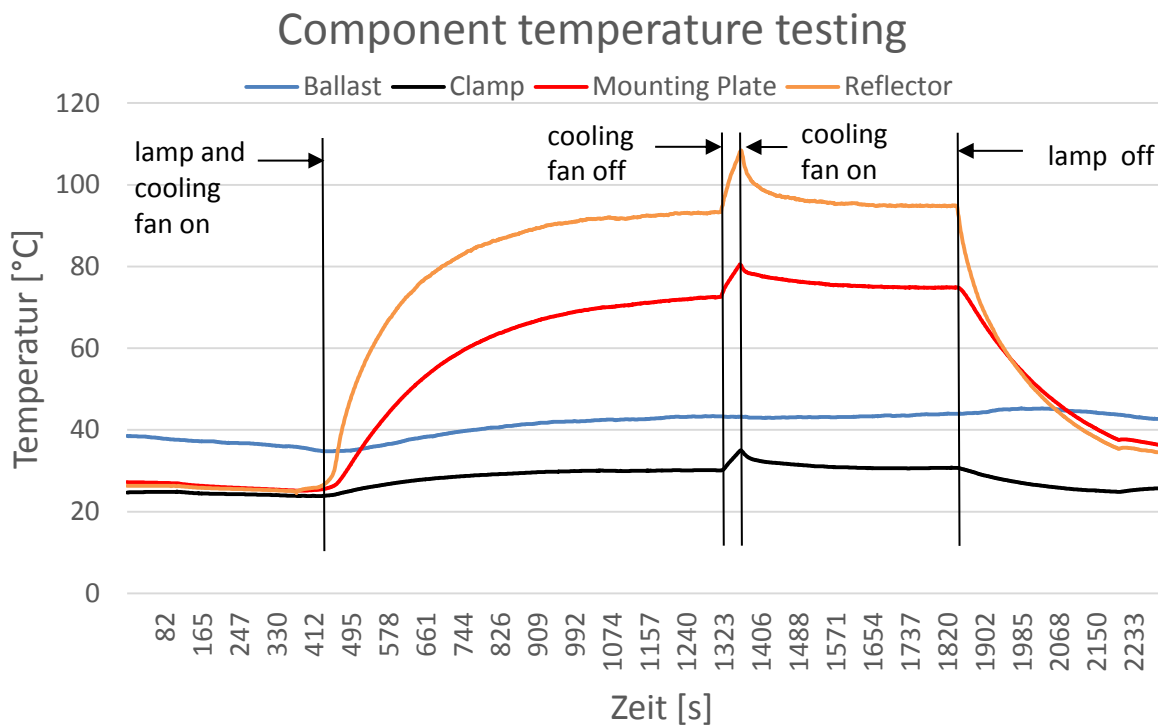


Figure 53: Component temperature test on lamp unit 3 with and without forced cooling.

7.3.3 Second setup temperature test

We conducted a second temperature test of the mounting plate and the reflector (Lamp unit 3). We did this to determine if the polishing of the reflector has an influence on the heat absorption of the reflector. For this test we did not use a cooling fan.

7.3.4 Second results temperature test

The diagram in Figure 54 shows the temperature during the second temperature test.

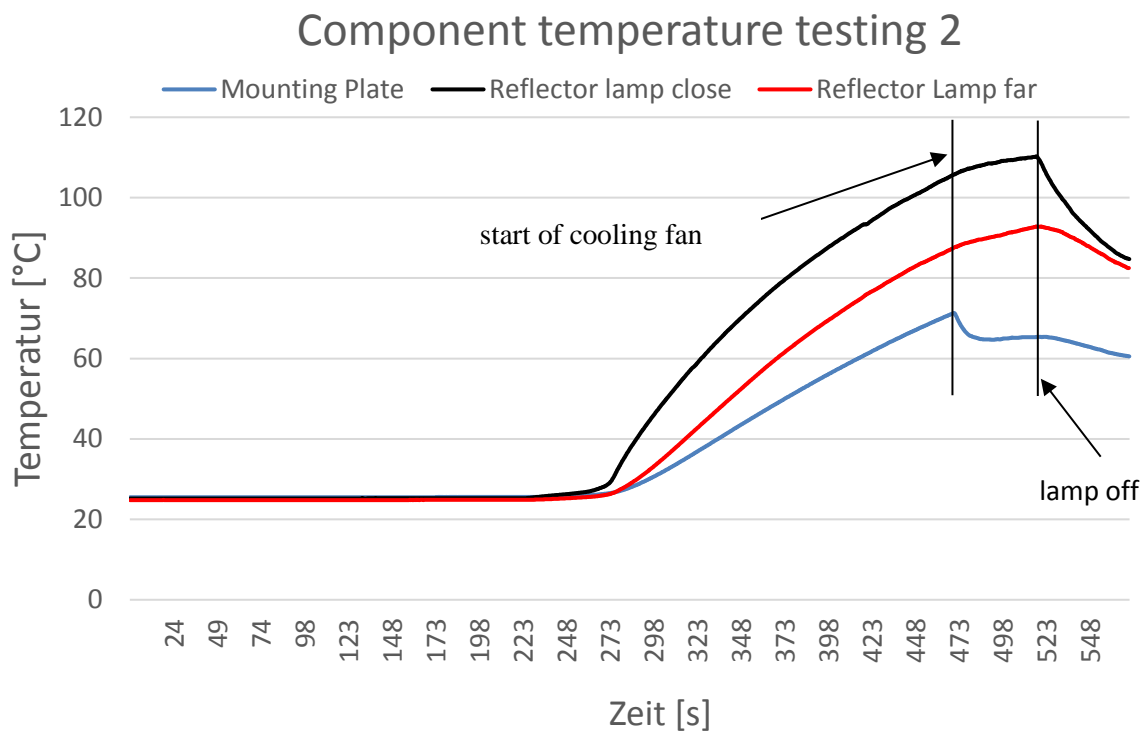


Figure 54: Component temperature test 2 for lamp unit 3 without forced cooling.

7.3.5 Third setup temperature test

For the third test we only tracked the temperature sensors on the mounting plates, while we conducted the final validation test. But unlike to the other tests we measured all 4 mounting plates at the same time. The fans were switched on during the test.

7.3.6 Third results temperature test

The diagram in Figure 55 shows the temperature during the third test. The lamps were shut down after about 300 seconds because we feared that the high flux distribution could damage the compound table. The different temperatures shown in Figure 55 are caused by different positions of the temperature sensors on the mounting plates.

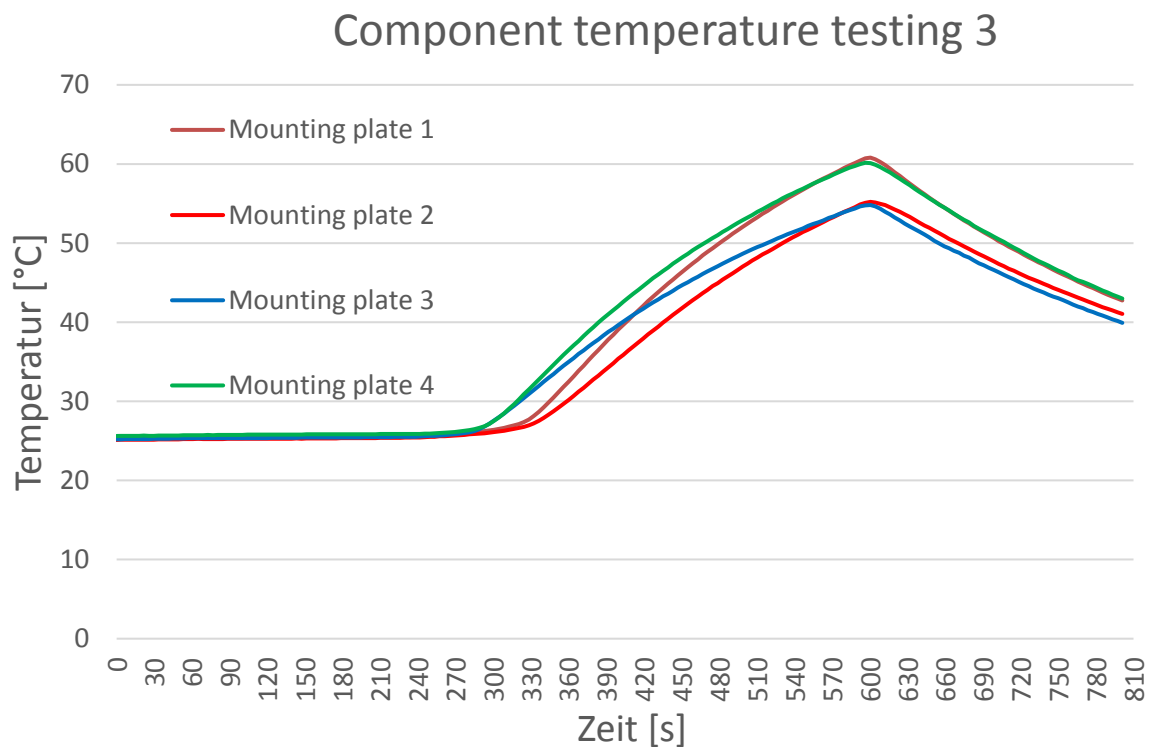


Figure 55: Temperature curves of the four mounting plates with polished reflectors.

7.4 Air stream test of the casing

In 4.4.1 we simulated the air stream through the casing to optimize the geometry of the manufactured parts. To validate if the simulation result was correct and because the air stream is used to cool critical parts we decided to build a small prototype (Figure 56, Figure 57 and Figure 58) of the casing and use the ordered fan to find out if the fan can produce enough pressure to keep the cooling stream upright.

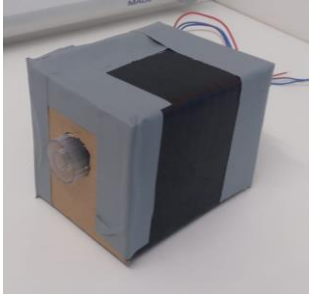


Figure 56: Casing prototype reflector side.

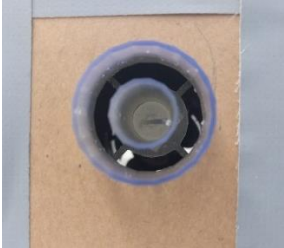


Figure 57: Casing prototype reflector side (outflow).

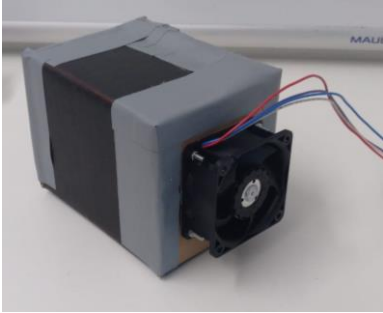


Figure 58: Casing prototype backside with fan.

The test showed that the fan was working very well and that we could start to manufacture the air stream critical parts.

8 Manufacturing and Assembly of Components

This section covers the design and manufacturing of custom made components for the HFSS and all relevant off-the-shelf components were described in this section.

8.1 Clamp unit

The clamp as depicted in Figure 59, had been designed and produced at the *Institute of Electrical Measurement and Measurement Signal Processing (EMT)*. It is mounted on the linear guide as depicted on Figure 71 and allows a fast switching between positioning-laser and lamp without a complex dismantling process. The clamp also holds the Lamp socket in position and transmits the translation of the linear guide movement to the lamp. The clamp was also designed under the aspect that the lamp is producing a lot of heat. Therefore, some thermal simulations were conducted in 4.4.2 and the geometry was adapted to have a beneficial design regarding temperature distribution and producibility.



Figure 59: Lamp socket (left), clamp (middle) and the assembly (right).

8.2 Lamp socket

Since the lamps must be replaced from time to time a socket which is mounted with the clamps was designed and produced by EMT. When this occurs, the new lamp should be placed in the same position as the lamp before, so it does not influence the measurement. Therefore, this socket also acts as a mechanical stop. The lamp itself has two knurled nuts on each end. These are normally used to fix the electric connection with the lamps. But we enhanced the purpose of the knurled nuts to also fasten the lamps in the lamp socket and therefore allow an easy and quick exchange of the lamps. The lamp socket can be seen in Figure 59.

One could think that using a standard lamp socket is an option, but this was not possible because this part does not exist. Therefore, the production of our own lamp socket was necessary, and we implemented some beneficial features.

8.3 Frame with measuring table

The frame and the table were completely constructed out of ITEM® parts and can be seen in Figure 60 and Figure 61. The frame measures 1750 mm in length, 780 mm in width and 780 mm in height. The measuring table is moveable in height and along approximately 60 percent of the overall length of the frame. In addition, a not necessarily needed lower frame was added to easily move the whole test bench to another location and to have a comfortable working height.



Figure 60: Frame with parts of the moveable table during assembly.



Figure 61: Moveable measurement table with the light guide.

8.4 Lamp unit casing

The casing as seen in Figure 62 and Figure 63 contains the fan, the linear guide and the parts that carry the lamp. It is 3D printed and designed by us. In this part the easy access to the lamp is also part of the design idea. The holes in the back are mainly for electric wiring and the fan. On the other side there is a square opening. This opening is sized that big because the mounting plate gets hot. We tried to reduce the temperature stress from the mounting plate to the casing by making the distance between the hot areas of the mounting plate to the casing as far as possible. On the bottom (in Figure 62 it is the top) we have a big hole which is the maintenance opening to get access to the lamp and the wiring inside of the casing. This opening can be closed by a cover which is also necessary to guide the cooling stream in the correct position. The flow simulation can be seen in 4.4.1.

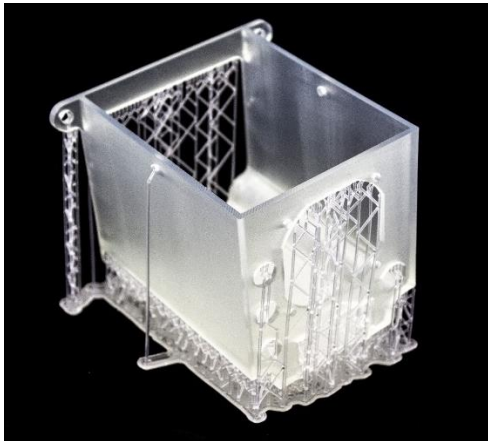


Figure 62: 3D printed casing part.

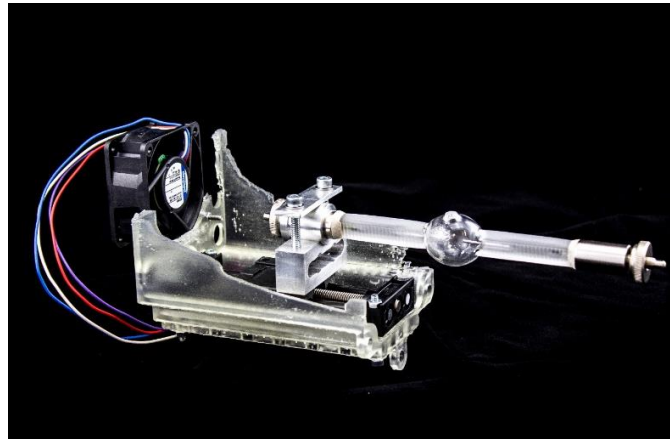


Figure 63: Parts assembled in cross-sectioned casing.

8.5 Mounting plates

The mounting plates have the purpose to connect the reflector and the casing with all the components inside. Furthermore, it is also the connection to the frame. The mounting plates are made of aluminum and they are manufactured by laser cutting from an external company. The plates are 4 mm thick, the shape can be seen in Figure 64. The hole in the center is the aperture for the lamp. The four holes close to the center are the attachment points for the reflectors. The five holes along the edge are the connection points between casing and the mounting plate. The two slightly bigger holes on the right and left side are the mounting points of the reflector units, to attach them on the frame.

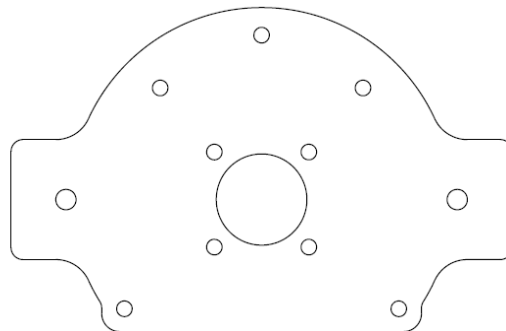


Figure 64: Shape of the mounting plate.

8.6 Reflector

The reflector is the part, which required most development effort. Finding the right material was described in section 2.5 and was important because of the need of the UV spectrum for testing multijunction cells. The final shape of the reflector was a combination of the simulation results and the space that was available in the test room. The surface of the reflector was untreated for the first test and got polished before the second test due to unwanted high diffuse reflectivity. The reflector has a thickness of 2 mm and the used material is 1050 aluminum alloy. The reflectors were manufactured with the process of metal spinning whereby a previously manufactured form was necessary. Figure 65 shows the drawing of the final reflector form. Figure 66 and Figure 67 show the final unpolished and polished reflector as it is built-in in the HFSS.

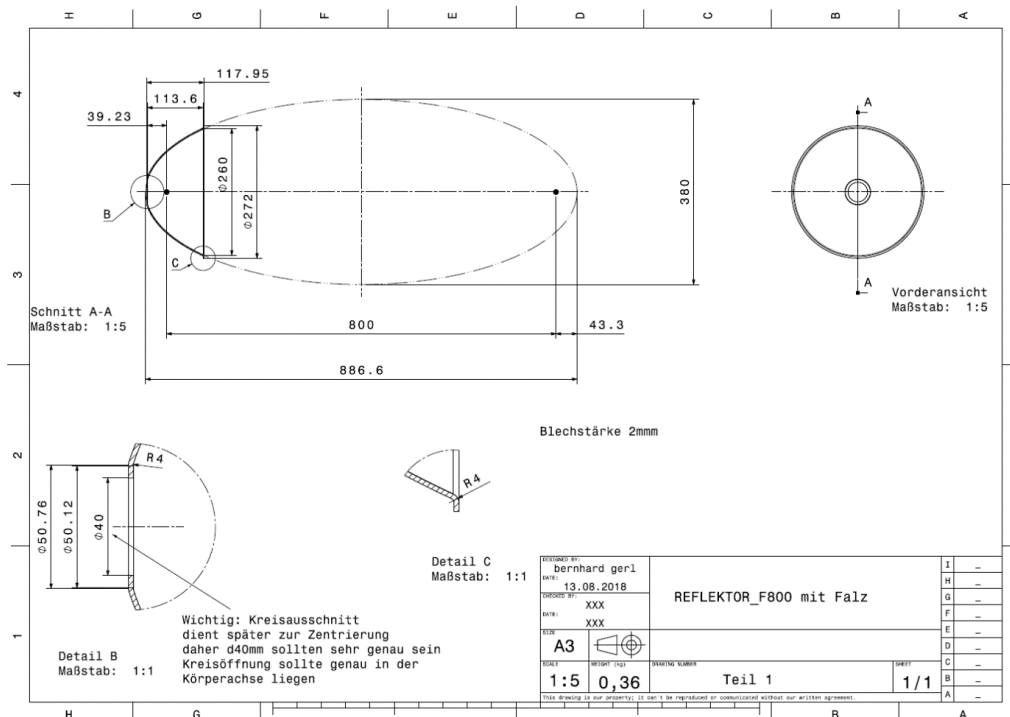


Figure 65: Reflector drawing



Figure 66: Reflector after metal spinning.



Figure 67: Reflector after polishing.

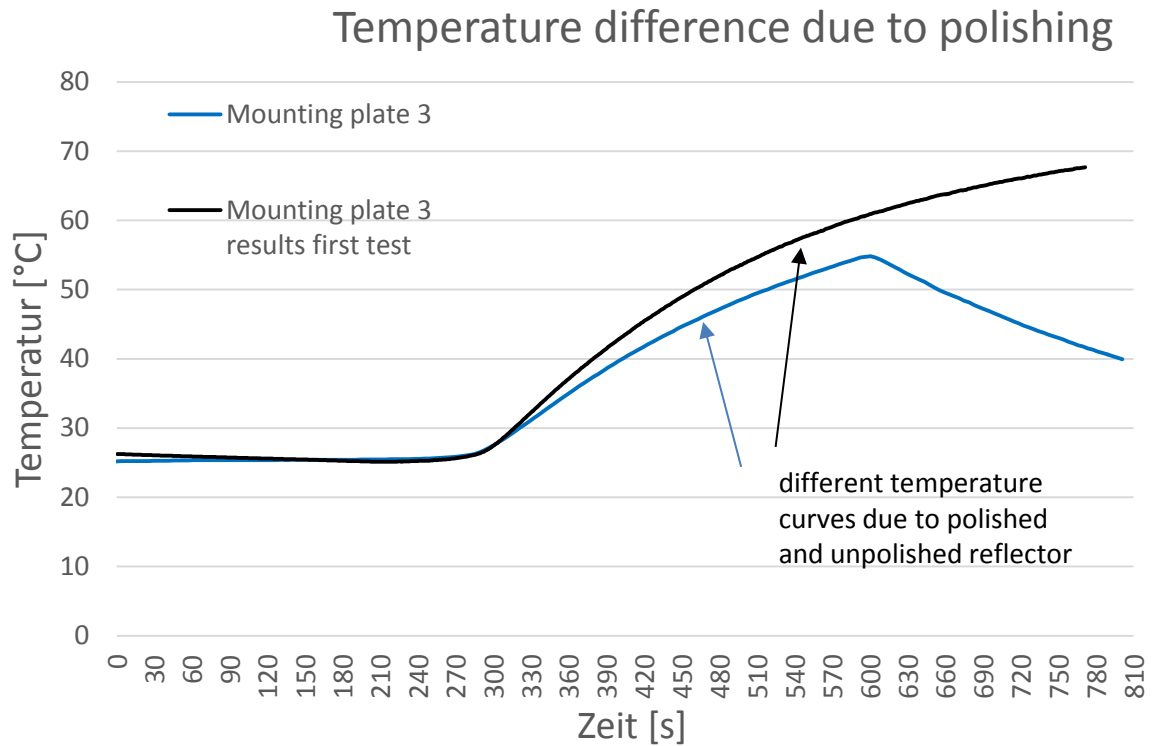


Figure 68: Temperature of mounting plate 3 with polished reflectors and temperature of mounting plate 3 of the first test with unpolished reflector.

In the diagram of Figure 68 the results of the first temperature test and third temperature test are compared. There was a clearly visible spread for mounting plate 3 between those two tests, which indicates that the polishing of the reflector has a positive influence regarding less absorption of the reflector.

8.6.1 Reflector 3D scanning

The four reflectors are assumed to have the same shape with minor differences regarding the fabrication accuracy. Since we did not know if the shape we got that was correct, we scanned the reflectors with a 3D scanner. The result of the scan was overlapped with the 2D drawings of the reflector to validate if the shape would be correct. Figure 69 depicts the results. Orange is the 3D scan and the black line is the original shape of the reflector drawing. As one can see the shape of the reflector is very precise.

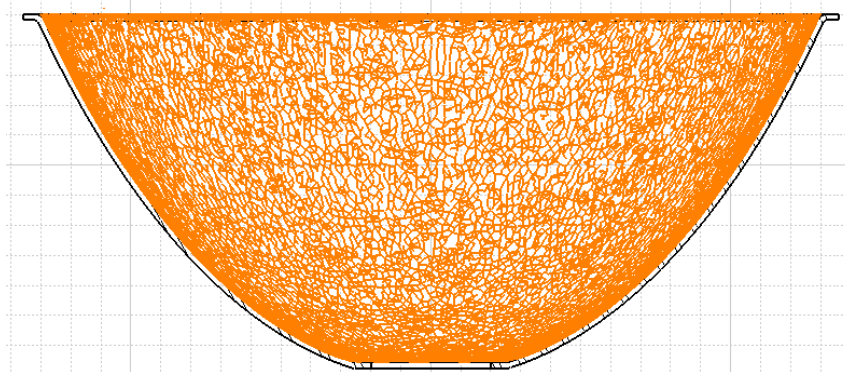


Figure 69: Overlapped pictures of the 3D scan and the original reflector drawing.

8.7 Tunnel

The tunnel also called the light guide is available in 3 sizes and was assembled at EMT, but the angle profiles and mirrors were manufactured externally. The background of the size and length of the mirror is discussed more detailed in 4.3.2. The smallest light guide was glued together, which is a very time-consuming work. Therefore, the bigger tunnels are only fixated with double-faced tape which was a very fast way to assemble the tunnels.



Figure 70: Light guide tunnels in size 50, 70 and 100 mm.

8.8 Linear guide

The linear guides that can be seen in Figure 71 holds the clamp and connects it with the casing. Most of the single components of the linear guide are made of plastic. We chose this part because of safety reasons to have an electrical insulation in case of a failure. Furthermore, we limited the linear guide with stoppers to avoid short circuits or collisions of the lamp with the reflector.



Figure 71: Linear guide with mounted clamp and lamp holder.

8.9 Fan

We used four *Papst 60x60mm high pressure fans* to cool the lamps with constant air flow. [46] For safety reasons we equipped the simulators with high quality fans because a fan failure would be critical, resulting in costs and time-consuming repair works.

8.10 The HFSS

The assembly took place completely at EMT. The assembled HFSS can be seen in Figure 72. The reflector unit is depicted in Figure 73.



Figure 72: The assembled HFSS with measurement table and light guide tunnel.



Figure 73: The assembled reflector unit.

9 Final Validation and Verification

9.1 First commissioning test of the solar simulator

The validation of the HFSS was also part of this thesis. Therefore, a *Hukseflux SBG01* heat flux meter [47] was assembled on a compound table to automatically measure the heat flux of a predefined field. Since we wanted a pillbox distribution we placed a tunnel in front of the sensor to test, if the simulations regarding distribution in *COMSOL* were correct. The measurement area is visualized in Figure 74.

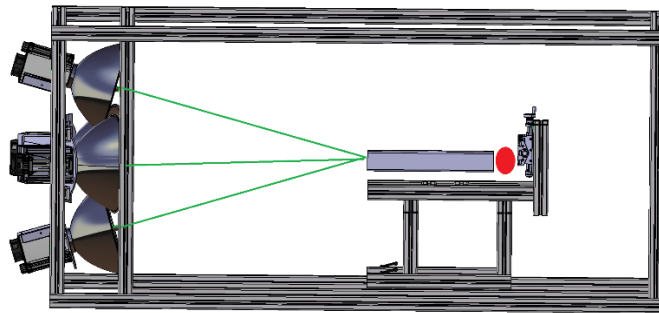


Figure 74: First test set up with measurement area in red.

First test setup

For the first test the smallest of the three light guide tunnels was placed onto the measuring table. The height of the table was adjusted to put the tunnel in the center of the HFSS where all the focal points of the reflectors meet. The edge of one end of the tunnel was set 20 mm behind the focal points and on the other end of the tunnel the *Hukseflux* sensor was placed 20 mm behind the rear end of the light guide tunnel. Figure 75 shows the first test, the light was so bright that the measurement table is not visible anymore.

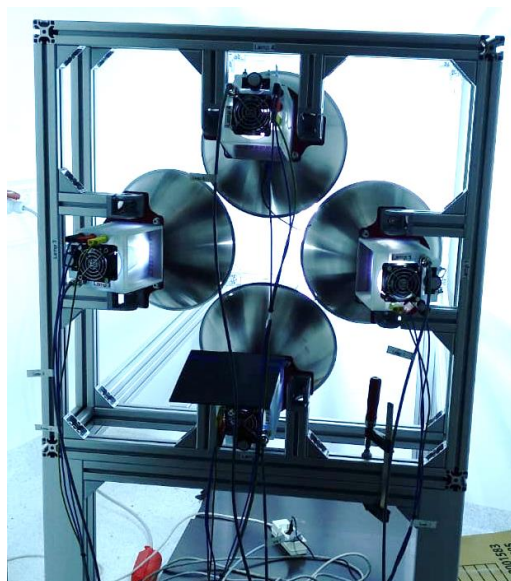


Figure 75: The first commissioning test with unpolished reflectors.

9.1.1 Results of the first test

All four lamps were activated during the test and as a result we measured a flat distribution after the light guide tunnel, just as the simulation showed us. The results of this can be seen in Figure 76 . Figure 76 also showed a problem regarding the reflectance of the reflectors, because they did not reflect much of the light into the tunnel due to big portions of diffuse reflectance. This meant only about 16-17 suns could be measured by the sensor compared to an intended irradiation of at least 60 suns.

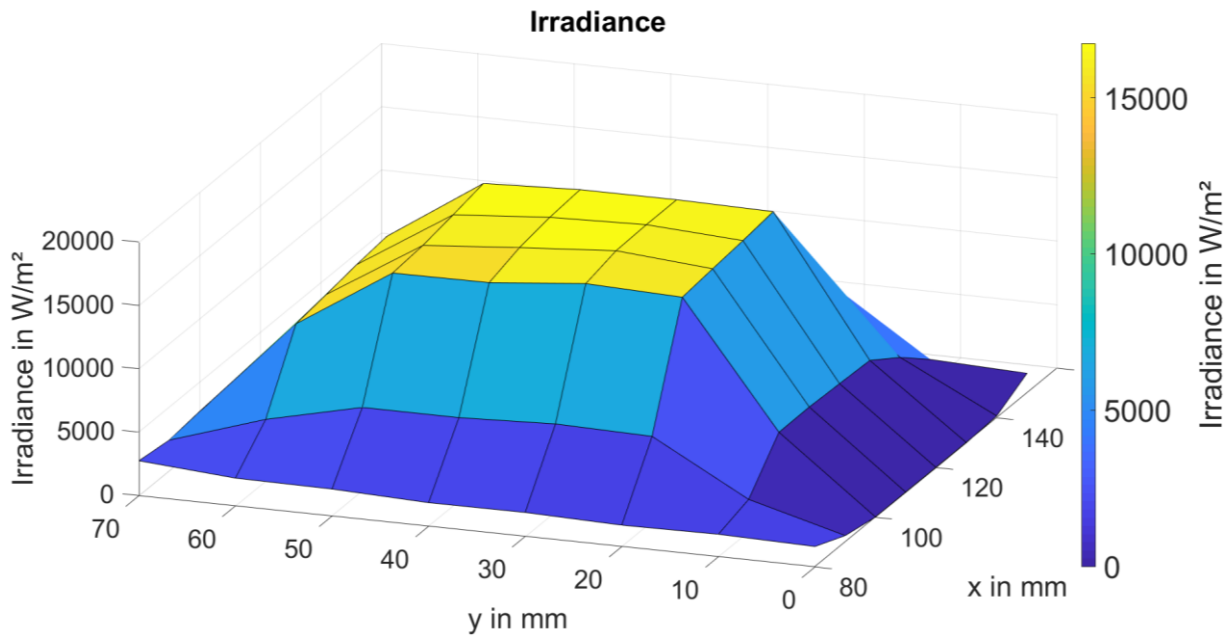


Figure 76: Irradiance distribution of the first test with a light guide tunnel used.

9.2 Second testing of the solar simulator

The second test already had some modifications on the used parts. The reflectors got polished to reduce diffuse reflection and to get a more specular reflection to increase the efficiency of the HFSS. Furthermore, we implemented some safety equipment to avoid unwanted contact that would result in a short circuit. To avoid the short circuit, we equipped the linear guides with stoppers to avoid unwanted contacts. The measurement area is visualized in Figure 77.

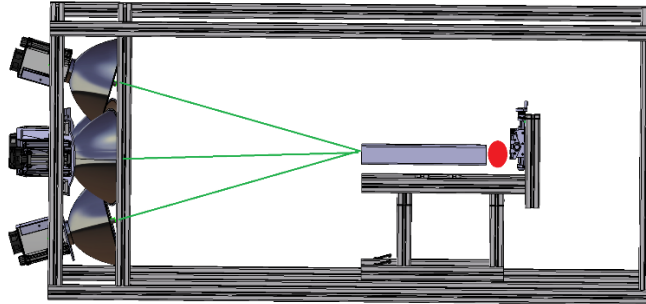


Figure 77: Second test set up with measurement area in red.

9.2.1 Second test setup

For the second test set up, we mounted the polished reflectors (compare section 8.6) and put the tunnel at an estimated focus position of the reflectors. Then we configured the compound table with the Hukseflux sensor and started the experiment.

9.2.2 Results of the second test

The second test already started different regarding illumination of the room we immediately recognized that the polishing caused a high reduction of diffuse reflectance and an increase of specular reflectance. The first test was conducted without much pre-adjustment to the components. Further adjustments will increase the transmitted power. As a result, we got a very similar distribution as in the first irradiance test, but with a high increase of intensity. The test showed an intensity of about 70-80 suns on the test target.

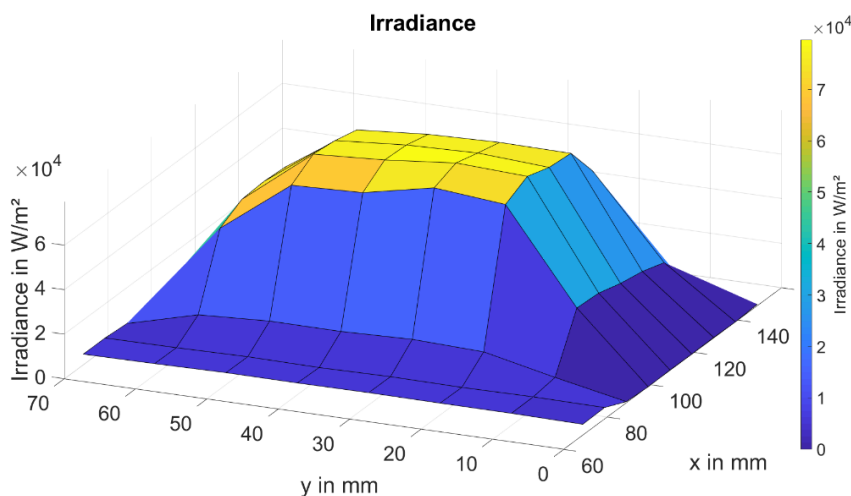


Figure 78: Irradiance distribution of the second test with a light guide tunnel used.

9.3 Testing the flux distribution in the focal point plane

We wanted to measure the behavior of the solar simulator in the focal plane. No additional parts were assembled during the second and this test, but we moved the lamps along the reflector axis to focus the light flux into the second focal point. For the measurement we removed the light guide tunnel and put the Hukseflux sensor plane in the area where we expected the focal plane. We tested four different conditions:

- 1 lamp with 50 percent power
- 1 lamp with 100 percent power
- 4 lamps with 50 percent power
- 4 lamps with 100 percent power

Before the compound table moved over the measurement field we waited till the lamp flux settled which is always necessary after switching on the power and change the power mode between 50 and 100 percent. The measurement area is visualized in Figure 79.

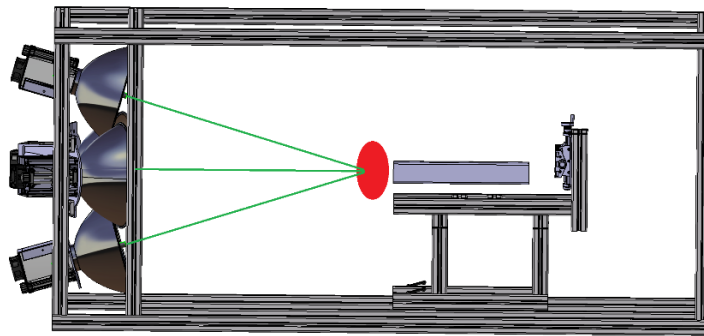


Figure 79: Testing of the peak flux in the measurement area red.

9.3.1 Irradiance for 1 lamp (Lamp 1) at 50 percent power

The measured peak flux for this set up was about 40-50 suns and gave us a distribution as depicted in Figure 80.

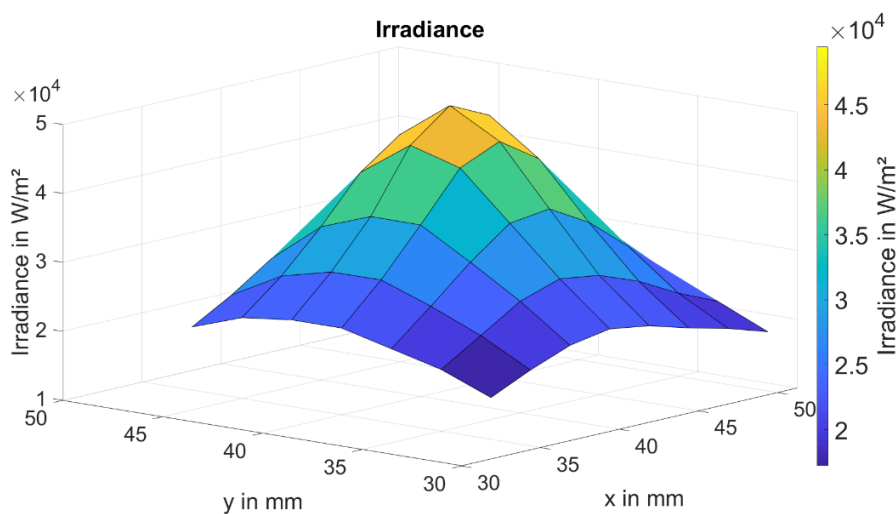


Figure 80: Gaussian irradiance distribution for 1 lamp at 50 percent power.

9.3.2 Irradiance for 1 lamp (Lamp 1) at 100 percent power

The measured peak flux for this set up was about 90 suns (increase of 100%) and gave us a distribution as depicted in Figure 81. The distribution was much flatter than the one in Figure 80, which was odd because the only parameter that was modified was the power mode.

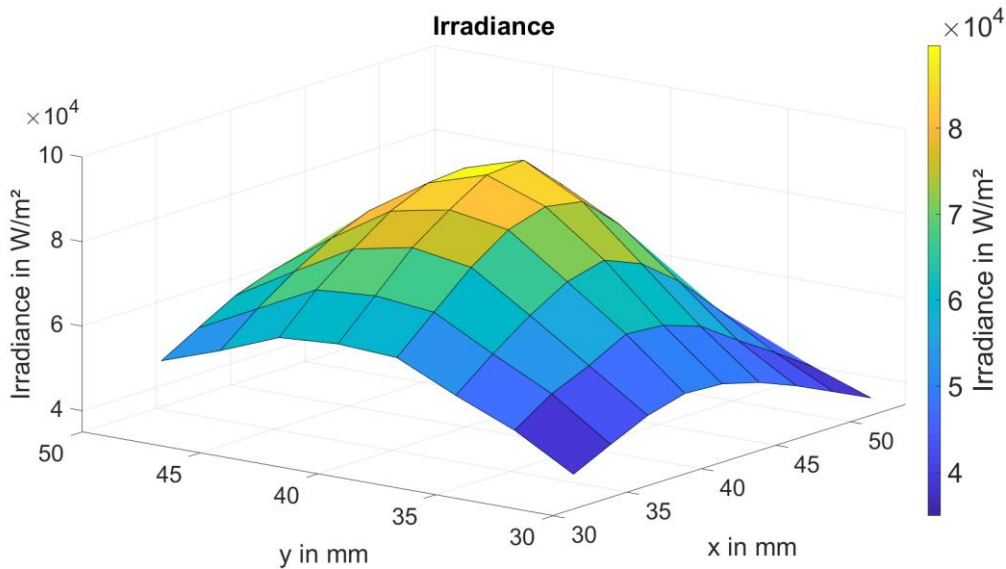


Figure 81: Gaussian irradiance distribution for 1 lamp at 100 percent power.

9.3.3 Irradiance for 4 lamps at 50 percent power

The measured peak flux for this set up was about 120-130 suns. The flatter distribution in Figure 82 compared to Figure 80 is probably caused due to the different positioned focal points of the different lamps. When the focal points are aligned more precise the distribution may get steeper.

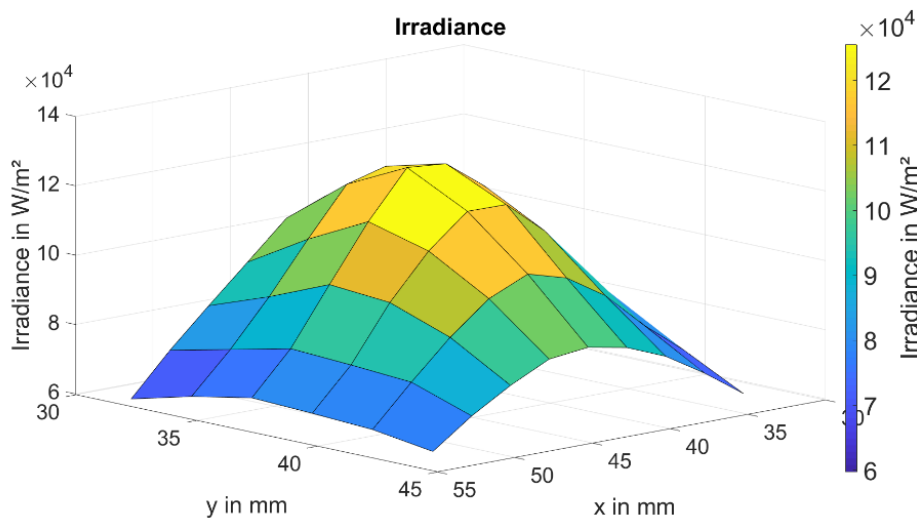


Figure 82: Gaussian irradiance distribution for 4 lamps at 50 percent power.

9.3.4 Irradiance for 4 lamps at 100 percent power

The measured peak flux for this set up was about 290 suns. Figure 83 showed compared to Figure 82 a more than twice as high maximum value (increase of 132%) was reached with all lamps on full power.

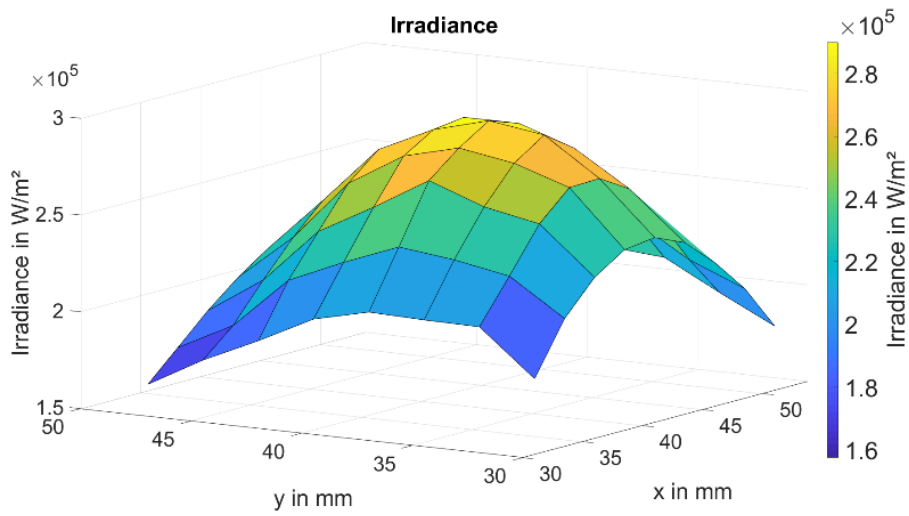


Figure 83: Gaussian irradiance distribution for 4 lamps at 100 percent power.

10 Conclusion, Summary and Outlook

10.1 Conclusion

A low-cost High Flux Solar Simulator was built at total costs of less than 5000 €. This low price was achieved by extensive search for suitable components and a smart approach in the necessary manufacturing processes. The minimum requirement of 60 suns and a pillbox distribution across an 50x50 mm aperture was completely fulfilled. During first commissioning, the HFSS reached only 17 suns, without any fine-tuning, but in the second test run the flux distribution offered an irradiance value of 80 suns and very flat irradiation field, with only minor adjustments to the lamps and the reflector units. A first try of overlapping all the focal points in the same spot went very well and a maximum flux of 290 suns was achieved. Further improvements will may result in even higher values. The used cooling equipment works very well and as long as the fan is switched on no parts of the HFSS reflector unit will get to a critical temperature level. The status of the final assembled HFSS can be seen in Figure 84.



Figure 84: The final assembled HFSS.

10.2 Summary

In this thesis the process of constructing and building a small High Flux Solar Simulator (HFSS) for Concentrated Photovoltaic testing was documented.

The goal of building a low-cost test bench for concentrated solar power was fully achieved. The most expensive parts which consist of the reflectors, the lamps and the ballasts were replaced by cheaper manufacturing processes and off-the-shelf products. Other High Flux Solar Simulators often use xenon arc lamps while we used the cheaper metal halide lamps. The ballasts were sourced from China and were about 83-92 percent cheaper than European and North-American products. Most of the nowadays built High Flux Solar Simulator use specially made reflector with high reflective surfaces. The price of these reflectors is very high and using a metal halide lamp with its long arc compared to a xenon lamp with a short arc is reducing the advantage of this reflector enormously. Therefore, the custom approach of building our own reflector was the best idea to decrease costs.

The reached peak flux of the systems was about 290000 W/m^2 . Photovoltaic testing needs a pillbox distribution of light rays. This characteristic was achieved by implementing a square light guide tunnel into the system which mixes the light while traveling through the light guide tunnel. The simulation the ray tracing model regarding light intensity distribution showed very satisfying results. The executed test on the real High Flux Solar Simulator also showed a flat distribution as predicted by the simulation. Light guide tunnels for the High Flux Solar Simulator are available with apertures if 2500 mm^2 , 4900 mm^2 and 10000 mm^2 .

10.3 Outlook

Future improvements of the GigiONE HFSS include an aluminum bottom to reduce the risk of fire due to broken lamps and attaching of an emergency switch. Furthermore, it is being considered that the whole simulator gets packed into an aluminum shell to reduce the risk of light hazards to humans. The measurement and the cooling equipment should be placed and secured as the plan in Figure 85 shows.

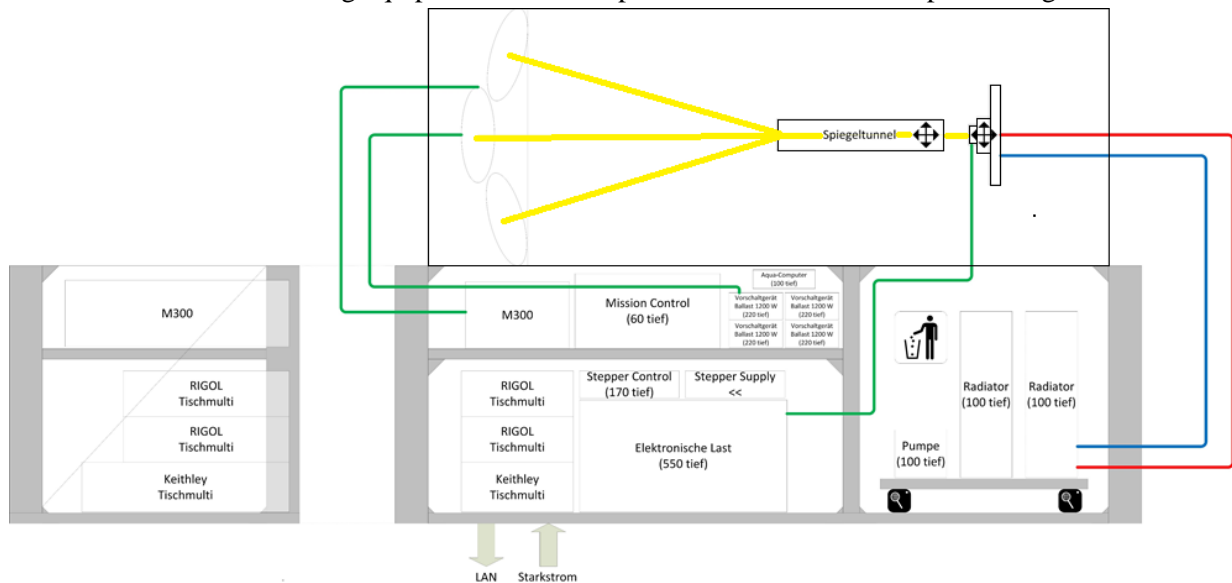


Figure 85: Plan of the equipment positioning.

The light guide tunnels already proved that they work well to achieve a pillbox distribution. It still should be considered to exchange them with more precise manufactured polished aluminum mirrors to increase the UV flux for the test sample. Furthermore, it should be considered that the tunnel is not square as it should be, because some issues in the ordering process resulted in slightly wrong dimensions of the mirror plates.

A fast exchange platform for the tunnel (attachment) would be highly beneficial to the simulator, because different shapes and sizes with whom the distribution of the parabolic through on the receiver tube could therefore be approximated. To achieve this without always constructing and building a whole new light guide would lower the expenditures and increase performance.

Another possible task for the HFSS are aging processes due to the strong UV emittance of the used lamps. Therefore, a UV translucent glass that blocks infrared and visible light must be implemented to the system otherwise the high temperatures would destroy the samples that are supposed to be aged. Aging samples can be plastic parts or liquids where the UV resistance is unknown.

List of Figures

| | |
|--|----|
| Figure 1: How a distillation process works. | 8 |
| Figure 2: Schematics of the self-sufficient NEWSUN desalination plant [3]. | 10 |
| Figure 3: Typical performance over temperature for an AZUR SPACE CPV cell according [5]. | 10 |
| Figure 4: Direct normal solar irradiation modified [6]. | 11 |
| Figure 5: Population density of the world fort the year 2015 modified [7]. | 11 |
| Figure 6: Areas of physical and economic water scarcity according to [8]. | 12 |
| Figure 7: Spectral distribution of downward-propagating short wavelength solar radiation [9]. | 13 |
| Figure 8: Spectral response of triple-junction cells from Azur Space according to [10]. | 13 |
| Figure 9: Geometrical concentration ratio described on a parabolic through mirror. | 14 |
| Figure 10: Gaussian(left) and flat, desired distribution (right) [12]. | 14 |
| Figure 11: Sun and earth configuration. | 15 |
| Figure 12: Air mass values according to [13]. | 17 |
| Figure 13: Direct and global radiation according to [13]. | 17 |
| Figure 14: Focusing Fresnel lens [15]. | 18 |
| Figure 15: Elliptical reflector with two focal points according to [16]. | 19 |
| Figure 16: Parabolic Reflector with one focal point according to [16]. | 19 |
| Figure 17: Elliptical reflector with focus widening due to arc length according to [18]. | 20 |
| Figure 18: Size of arc image at the secondary focal plane for an arc length of 9 mm and 23 mm and a focal length of 1585 mm and 3000 mm [18]. | 20 |
| Figure 19: Reflectance of metallic surfaces [20]. | 21 |
| Figure 20: Reflectance of aluminum at different temperatures [24]. | 22 |
| Figure 21: Arrangement of 75 kW lamp and reflector [31]. | 25 |
| Figure 22: Arrangement of several reflector and lamp units [32]. | 25 |
| Figure 23: Spectrum of xenon arc lamp [34]. | 26 |
| Figure 24: Spectrum of metal-halide lamp [34]. | 26 |
| Figure 25: Spectrum of argon arc lamp [34]. | 26 |
| Figure 26: HFSS parts with elliptical axis. | 27 |
| Figure 27: Reflector unit parts. | 28 |
| Figure 28: Arc diameter variation in simulation. | 29 |
| Figure 29: Geometric layout without tunnel. | 30 |
| Figure 30: Geometric layout with tunnel. | 30 |
| Figure 31: Ray tracing simulation using all lamps without light guide tunnel varying distance and arc position. | 31 |
| Figure 32: Ray tracing simulation using all lamps without light guide tunnel varying distance and arc position. | 32 |
| Figure 33: Ray tracing simulation using two lamps with light guide tunnel varying tunnel length and target distance. | 33 |
| Figure 34: Ray tracing simulation using all lamps with light guide tunnel varying tunnel length and target distance. | 34 |
| Figure 35: Ray tracing simulation using all lamps with light guide tunnel varying tunnel length and target distance. | 35 |

| | |
|---|----|
| Figure 36: Ray tracing simulation using all lamps with a 45° rotated light guide tunnel varying tunnel length and target distance. | 36 |
| Figure 37: Ray tracing simulation using all lamps with a 45° rotated light guide tunnel varying tunnel length and target distance. | 37 |
| Figure 38: Ray tracing simulation light guide tunnel and as used reflector geometry of the 3D scanned reflector. | 38 |
| Figure 39: Casing simulation, velocity magnitude for air flow. | 39 |
| Figure 40: Thermal analysis of the clamp. | 41 |
| Figure 41: Osram HMI 1200 double ended metal-halide lamp [36]. | 43 |
| Figure 42: The 3D visualized HFSS facing the lamps to see components the sliding table. | 46 |
| Figure 43: The 3D visualized HFSS facing the back of the reflectors units with the cooling fans. | 46 |
| Figure 44: The 3D visualized lamp unit front side with lamp. | 47 |
| Figure 45: The 3D visualized lamp unit back side with fan, clamp and linear guide, the casing is transparent. | 47 |
| Figure 46: Lamp setup for arc visualization with expected arc deformation (green). | 49 |
| Figure 47: Camera positioning and Lamp positioning. | 49 |
| Figure 48: Used camera filter. | 50 |
| Figure 49: Spectrograph | 57 |
| Figure 50: Lamp in lamp holder. | 57 |
| Figure 51: Plate holder and spectrograph. | 59 |
| Figure 52: Plate holder in test mode. | 59 |
| Figure 53: Component temperature test on lamp unit 3 with and without forced cooling. | 67 |
| Figure 54: Component temperature test 2 for lamp unit 3 without forced cooling. | 68 |
| Figure 55: Temperature curves of the four mounting plates with polished reflectors | 69 |
| Figure 56: Casing prototype reflector side. | 70 |
| Figure 57: Casing prototype reflector side (outflow). | 70 |
| Figure 58: Casing prototype backside with fan. | 70 |
| Figure 59: Lamp socket (left), clamp (middle) and the assembly (right). | 71 |
| Figure 60: Frame with parts of the moveable table during assembly. | 72 |
| Figure 61: Moveable measurement table with the light guide. | 72 |
| Figure 62: 3D printed casing part. | 73 |
| Figure 63: Parts assembled in cross-sectioned casing. | 73 |
| Figure 64: Shape of the mounting plate. | 73 |
| Figure 65: Reflector drawing | 74 |
| Figure 66: Reflector after metal spinning. | 74 |
| Figure 67: Reflector after polishing. | 74 |
| Figure 68: Temperature of mounting plate 3 with polished reflectors and temperature of mounting plate 3 of the first test with unpolished reflector. | 75 |
| Figure 69: Overlapped pictures of the 3D scan and the original reflector drawing. | 75 |
| Figure 70: Light guide tunnels in size 50, 70 and 100 mm. | 76 |
| Figure 71: Linear guide with mounted clamp and lamp holder. | 76 |
| Figure 72: The assembled HFSS with measurement table and light guide tunnel. | 77 |
| Figure 73: The assembled reflector unit. | 77 |
| Figure 74: First test set up with measurement area in red. | 78 |
| Figure 75: The first commissioning test with unpolished reflectors. | 78 |
| Figure 76: Irradiance distribution of the first test with a light guide tunnel used. | 79 |
| Figure 77: Second test set up with measurement area in red. | 80 |

| | |
|--|----|
| Figure 78: Irradiance distribution of the second test with a light guide tunnel used. | 80 |
| Figure 79: Testing of the peak flux in the measurement are red. | 81 |
| Figure 80: Gaussian irradiance distribution for 1 lamp at 50 percent power. | 81 |
| Figure 81: Gaussian irradiance distribution for 1 lamp at 100 percent power. | 82 |
| Figure 82: Gaussian irradiance distribution for 4 lamps at 50 percent power. | 82 |
| Figure 83: Gaussian irradiance distribution for 4 lamps at 100 percent power. | 83 |
| Figure 84: The final assembled HFSS. | 84 |
| Figure 85: Plan of the equipment positioning. | 85 |

List of Tables

| | |
|---|----|
| Table 1: Energy consumption of different desalination processes according to [4]..... | 9 |
| Table 2: Standard power densities according to [14]. | 16 |
| Table 3: Solar simulators with costs, available on the market. | 23 |
| Table 4: List of high flux solar simulators since 2015. | 24 |
| Table 5: HFSS with expenses..... | 24 |
| Table 6: Targets for the final HFSS. | 27 |
| Table 7: Used data for simulation. | 40 |
| Table 8: Utility analysis of different lamp types. | 43 |
| Table 9: List of ballast producers according to [37], [38], [39], [40]..... | 44 |
| Table 10: List of reflector producers [41], [42], [43], [44]. | 45 |
| Table 11: Costs of the assembled parts. | 48 |
| Table 12: Arc bending test. | 51 |
| Table 13: Arc bending test 2. | 53 |
| Table 14: Arc bending test 3 with magnet..... | 55 |
| Table 15: Light spectrum test. | 58 |
| Table 16: Reflectivity test sample 1. | 60 |
| Table 17: Reflectivity test sample 2. | 61 |
| Table 18: Reflectivity test sample 3 | 62 |
| Table 19: Reflectivity test sample 4. | 63 |
| Table 20: Reflectivity test sample 5. | 64 |
| Table 21: Reflectivity test sample 6. | 65 |
| Table 22: Reflectivity test anodized samples. | 66 |

Bibliography

- [1] UNESCO on behalf of UN-Water, "WATERThe United Nations World Water Development Report 2018 NATURE-BASED SOLUTIONS FOR WATER," Paris, 2018.
- [2] UNESCO on behalf of UN-Water, "The United Nations World Water Development Report 2017 WASTEWATER THE UNTAPPED RESOURCE," Paris,, 2017.
- [3] H. W. Armin Buchroithner, "NEWSUN - Nexus of Electricity and Water Supply for Urban Needs," Die Österreichische Forschungsförderungsgesellschaft FFG , Wien, 2017.
- [4] J. E. Miller, "Review of Water Resources and Desalination Technologies," United States, 2003.
- [5] AZUR SPACE Solar Power GmbH, "-CPV Solar Cells - AZUR SPACE Solar Power GmbH," [Online]. Available: <http://www.azurspace.com/index.php/en/products/products-cpv/cpv-solar-cells>. [Accessed 18 12 2018].
- [6] Solargis © 2017 The World Bank, "Solar resource maps of World," Solargis s.r.o, [Online]. Available: <https://solargis.com/maps-and-gis-data/download/world>. [Accessed 14 10 2018].
- [7] Center for International Earth Science Information Network - CIESIN - Columbia University, "NASA SEDAC," NASA Socioeconomic Data and Applications Center (SEDAC), 2017. [Online]. Available: <http://sedac.ciesin.columbia.edu>. [Accessed 14 10 2018].
- [8] International Water Management Institute, Comprehensive Assessment of Water Management in Agriculture., London: Earthscan, 2007.
- [9] Frank P. Incropera and David P. DeWitt, Fundamentals of Heat and Mass Transfer, vol. 5, New York: John Wiley & Sons, Inc., 2002.
- [10] AZUR SPACE Solar Power GmbH, "Azurspace," [Online]. Available: <http://www.azurspace.com/index.php/en/products/products-cpv/cpv-solar-cells>. [Accessed 15 10 2018].
- [11] The Pennsylvania State University, "Utility Solar Power and Concentration," The Pennsylvania State University, [Online]. Available: <https://www.e-education.psu.edu/eme812/node/8>. [Accessed 15 10 2018].
- [12] I. A. (. a. G. D. (DLR), "R12.5 Solar Simulator Evaluation Report," 2011.
- [13] SCIENCETECH, "Sciencetech Inc.," [Online]. Available: www.sciencetech-inc.com. [Accessed 27 2 2018].

- [14] Newport Corporation, "Newport Corporation," Newport Corporation, [Online]. Available: www.newport.com. [Accessed 14 12 2018].
- [15] A. D. a. F. Kühnlenz, "Optical Design Using Fresnel Lenses," *Optik & Photonik*, vol. 2, no. 4.
- [16] Newport Corporation, "Oriel Sol3A Class AAA Solar Simulators," Newport Corporation, [Online]. Available: <https://www.newport.com/f/class-aaa-solar-simulators>. [Accessed 9 10 2018].
- [17] W. Wang*, L. Aichmayera, B. Laumerta, T. Franssona, "Design and validation of a low-cost high-flux solar simulator using Fresnel lens concentrators".*Energy Procedia*.
- [18] BEN M EKMAN, THE DESIGN, CONSTRUCTION AND PERFORMANCE OF A NOVEL SOLAR SIMULATOR AND HYBRID REACTOR.
- [19] D. M. Mattox, Handbook of Physical Vapor Deposition (PVD) Processing (Second Edition), 2010.
- [20] Edmund Optics Inc., "Metallic Mirror Coatings," [Online]. Available: <https://www.edmundoptics.com/resources/application-notes/optics/metallic-mirror-coatings/>. [Accessed 20 12 2018].
- [21] C. J. Séraphin, "Literaturrecherche über aktuelle Einsatzbereiche von eloxierten Aluminium-Legierungen," 2014.
- [22] Charles C. He and Thomas M. Heslin, "Preventing Cracking of Anodized Coatings," 1995.
- [23] J. E. JANSSEN, R. H. TORBORG, J. R. LUCK, F. N. SCHMIDT, "NORMAL SPECTRAL REFLECTANCE OF ANODIZED COATINGS ON ALUMINUM, MAGNESIUM, TITANIUM AND BERYLLIUM," HONEYWELL RESEARCH CENTER HOPKINS, MINNESOTA, 1961.
- [24] Ernie W. Spisz, Albert J. Weigand, Robert L. Bowman, and John R. Jack, "SOLAR ABSORPTANCES AND SPECTRAL REFLECTANCES OF !" METALD FOR TEMPERATURES RANGING FROM 200 TO 500 K," 1969.
- [25] infinityPV ApS, "ISOSun," infinityPV ApS, [Online]. Available: <https://infinitypv.com/products/hardware/solar-simulator/isosun>. [Accessed 16 12 2018].
- [26] Photo Emission Tech, Inc., "Photo Emission Tech – Solar Simulator, Simulator Solar, Light Source, Full Spectrum Light, Solar Simulation Systems, IV Measurement System - Solar Simualtor Model SS400AAA," Photo Emission Tech, Inc., [Online]. Available: <http://www.photoemission.com/SS400A.html>. [Accessed 16 12 2018].
- [27] Sciencetech Inc., "Low Cost Solar Simulator," Sciencetech Inc., [Online]. Available: <http://www.sciencetech-inc.com/all-products/solarsimulators/continuous-solar/small-area-lens-based-solar-simulators.html>. [Accessed 16 12 2018].
- [28] Deutsches Zentrum für Luft- und Raumfahrt e. V. (DLR), "electronic library," Deutsches Zentrum für Luft- und Raumfahrt e. V. (DLR), [Online]. Available:

- <http://elib.dlr.de/115336/2/170928%20KW%20Synlight%20SolarPACES2017.pdf>. [Accessed 16 12 2018].
- [29] Daniel S. Codd, Andrew Carlson, Jennifer Rees, Alexander H. Slocum, "A low cost high flux solar simulator," *Solar Energy*, pp. 2202-2212, 12 2010.
- [30] J. Y. C. K. H. Antoine Boubault, "DESIGN AND CHARACTERIZATION OF A 7.2 KW SOLAR SIMULATOR," *J. Sol. Energy Eng.*, 2015.
- [31] D. Hirsch, P. v. Zedtwitz, T. Osinga, J. Kinamore, A. Steinfeld, "A New 75 kW High-Flux Solar," *Journal of Solar Energy Engineering*, 2 2003.
- [32] Jörg Petrasch, Patrick Coray, Anton Meier, Max Brack, Peter Häberling, Daniel Willemin and Aldo Steinfeld, "A Novel 50kW 11,000 suns High-Flux Solar Simulator Based on an Array of Xenon Arc Lamps," *J. Sol. Energy Eng*, 25 8 2006.
- [33] W. Wang, "Simulate a 'Sun' for Solar Research," 2014.
- [34] G. L. S. H. Roman Bader, "High-flux Solar Simulator Technology," 2016.
- [35] igus® GmbH, "igus," [Online]. Available: <https://www.igus.at/>. [Accessed 03 12 2018].
- [36] OSRAM GmbH, "HMI HMI 1200W/DXS S | OSRAM PIA," [Online]. Available: https://www.osram.at/pia/ecat/HMI-HMI%20Metal%20Halide-Halogen-Metalllampen-Speziallampen/at/de/GPS01_1028434/PP_EUROPE_AT_eCat/ZMP_56252/. [Accessed 18 12 2018].
- [37] IREM SpA a socio unico, "IREM," [Online]. Available: <https://www.irem.it>. [Accessed 16 10 2018].
- [38] Powergems Limited, "POWER GEMS," [Online]. Available: <https://powergems.com/>. [Accessed 16 10 2018].
- [39] ISLE Steuerungstechnik und Leistungselektronik GmbH, "isle Steuerungstechnik und Leistungselektronik GmbH," [Online]. Available: <http://www.isle-ilmenu.de/>. [Accessed 16 10 2018].
- [40] Ether Power Electronics Technology Co.,Ltd, "EPE," [Online]. Available: <http://en.powerepe.com/>. [Accessed 16 10 2018].
- [41] Kaltbrunner AG, "Kaltbrunner AG - Ihr kompetenter Partner für hochwertige Beschichtungen," Kaltbrunner AG, [Online]. Available: <https://www.kaltbrunner.ch/en/>. [Accessed 17 12 2018].
- [42] HEGGLI & GUBLER AG, "Heggli Gubler Metalldrückerei AG," HEGGLI & GUBLER AG, [Online]. Available: <http://www.heggli-gubler.ch/>. [Accessed 17 12 2018].
- [43] Optiforms, Inc., "Precision Electroformed Metal Components for 2018," Optiforms, Inc., [Online]. Available: <https://www.optiforms.com/>. [Accessed 17 12 2018].

- [44] Wilhelm Seidl Metalldrücker und Gürtler, "Wilhelm Seidl Metalldrücker und Gürtler in Wien," Wilhelm Seidl Metalldrücker und Gürtler, [Online]. Available: <https://www.metalldesign-wien.at/>. [Accessed 17 12 2018].
- [45] Gerd Dibowski and Kai Esser, "Hazards Caused by UV Rays of Xenon Light Based High Performance Solar Simulators".
- [46] RS Components Ltd, "622/2H3P | ebm-papst Axiallüfter," [Online]. Available: <https://at.rs-online.com/web/p/axiallufter/8004293/?relevancy-data=636F3D3126696E3D4931384E53656172636847656E65726963266C753D6465266D6D3D6D61746368616C6C7061727469616C26706D3D5E2E2A2426706F3D31333326736E3D592673723D2673743D43415443485F414C4C5F44454641554C>. [Accessed 18 12 2018].
- [47] Hukseflux Thermal Sensors B.V., "SBG01 heat flux meter," [Online]. Available: <https://www.hukseflux.com/products/heat-flux-sensors/heat-flux-meters/sbg01-heat-flux-meter>. [Accessed 21 12 2018].
- [48] S. S. T. K. M. Katie Shanks, "Optics for concentrating photovoltaics: Trends, limits and opportunities for materials and design," *Renewable and Sustainable Energy Reviews*, 2016.
- [49] M. C. Samuel Pellicori, "Coating Materials for High Reflectors".
- [50] J. König, "Peak Oil und die Verwundbarkeit moderner Gesellschaften," 2012.
- [51] Schenck-ROTEC, "Spinning service," [Online]. Available: <https://schenck-rotec.com/services/balancing-and-spinning-service/spinning-service.html>. [Accessed 4 10 2018].
- [52] Schuster-Engineering GmbH, "Aktuelles," 2011. [Online]. Available: <http://schuster-sondermaschinen.de/6.html>. [Accessed 4 10 2018].
- [53] Moon, HyungBin et.al., "Forecasting electricity demand of electric vehicles by analyzing," *Transportation Research Part D: Transport and Environment*, no. Volume 62, pp. 64-79, 2018.
- [54] IIT Guwahati, "National Programme on Technology Enhanced Learning (NPTEL)," [Online]. Available: <http://nptel.ac.in/courses/108103009/module6/lec17/8.html>. [Accessed 25 05 2015].
- [55] CLIMATS, "PRECISION SOLAR SIMULATION," CLIMATS, [Online]. Available: <http://www.climats-tec.com/en/products/1055-customized-solutions/1128-materials-testing/162-precision-solar-simulation.html>. [Accessed 16 12 2018].